1-1-2010

# Particle Matter Measurements for Inspection/Maintenance Programs

Daniel Joseph Pope
*University of Denver*

# Particle Matter Measurements for Inspection/Maintenance Programs

---

A Thesis

Presented to

The Faculty of Natural Sciences and Mathematics

University of Denver

In Partial Fulfillment

of the Requirements for the Degree

Master of Science

By

Daniel Joseph Pope

November, 2009

Advisor: Dr. Donald H. Stedman

Author: Daniel J. Pope
Title: Particle Matter Measurements for I\M Programs
Advisor: Donald H. Stedman
Degree Date: November, 2009

## Abstract

Particle emissions from Heavy Duty Diesel Vehicles (HDDVs) are currently measured by opacity or dynamometer gravimetric analysis. The Electronic Tailpipe Particle Sensor (ETaPS) is an inexpensive measurement device purported to give real time response to particle mass and was proposed as a possible addition to Inspection/Maintenance (I/M) programs. There were three goals to this study. The first was to verify ETaPS response to particle mass of HDDV exhaust. Integrated ETaPS signal was plotted against filter weight from dynamometer gravimetric analysis and a correlation was found. The second goal was to find a correlation between ETaPS readings and the Remote Sensing Detector (RSD). These tests were invalidated due to interference from power lines greatly affecting the ETaPS signal. The final goal was to find a relationship between the RSD and the dynamometer gravimetric analysis. Comparisons were made from averaged RSD smoke data, and averaged gravimetric data for each HDDV undergoing both tests. A measurable difference was found for RSD smoke readings between Diesel Particle Filter (DPF) equipped vs. non-DPF and DPF bypassed HDDVs.

# Acknowledgements

I would like to thank the Environmental Systems Products Holdings Inc., the California Air Resources Board, and the University of Denver for the opportunity and financing for this study. I would also like to thank all the professors and grad students for everything I have learned at the University of Denver with the special mentions of Dr. Donald Stedman, Dr. Gary Bishop, and my co-worker Brent Schuchmann. And finally, I would like to thank my parents for supporting me in everything I have done.

## Table of Contents

# Chapter 1: Introduction

## 1.1 Project Goal

According to the original ETaPS Innovative Clean Air Technologies (ICAT) project proposal, the goal statement was: *"Trucks with particle emissions which are significantly higher than they should be, need to be identified and repaired. If the outcome of the ICAT experiment is as positive as we hope, then we can imagine determination of "probable cause" using RSD, for instance as the vehicle accelerates from a stop at a weigh station. The trucks so identified could then be quickly instrumented and subjected to a road load ETaPS investigation, the outcome of which could be used to trigger enforcement action and calculate mass emission credits upon repair (1)."*

This project aims to test the ability of the RSD to adequately flag high emitting heavy duty diesel vehicles (HDDV) for on road testing with the Electronic Tailpipe Particle Sensor (ETaPS). There is little literature on the ETaPS system, and for this reason, the instrument response to particle mass needed to be correlated to gravimetric filter data. This is because an instrument used in emissions testing programs needs to measure gravimetric data due to enforceable federal and state standards measured in these units *(2)*. The RSD response to the same high and low emitting vehicles was also tested.

## 1.2 Health Hazards of PM

Diesel exhaust (DE) is a mixture of many compounds composed of gaseous and particulate matter. The gas mixture is comprised of largely ambient nitrogen uninvolved

in normal combustion, excess oxygen unused in combustion, as well as the combustion products carbon dioxide and water vapor. Included in this mixture are reaction byproducts of nitrogen and sulfur compounds, carbon monoxide, as well as various hydrocarbons. Particulate matter resulting from diesel exhaust is comprised of carbon soot, adsorped organic compounds, and small quantities of other compounds such as nitrates, and sulfates *(3)*.

Diesel particulate matter (DPM) can be categorized into three sub groups of aerodynamic diameter; coarse, fine (<2.5μm), and ultra fine (<0.1μm). Overall these particles have large surface areas allowing them to adsorb other organics that may be present in the exhaust stream. Their small size makes them easily respired.

DPM resulting from on-road and off-road diesel exhaust was found to make up approximately 6% of the total nationwide Particle Matter (PM) inventory for particles measuring less than 2.5μm ($PM_{2.5}$). The average is ~23% if natural sources are excluded. Estimates run as high as 35% for urban areas *(3)*.

Health hazards arising from exposure to these particles come in three categories. In acute, or short term exposure, effects come in the form of irritation, light-headedness, nausea, or allergenic response. Chronic or long term, non-carcinogenic effects include long-term inflammation of the lungs. Chronic carcinogenic effects due to inhalation of exhaust particles have been determined to be likely. "There is considerable evidence demonstrating an association between DE exposure and increased lung cancer risk among workers in varied occupations where diesel engines historically have been used *(3)*."

It is therefore of interest to regulate the emission of DE particles. Several countries and American states have instituted thresholds for these particles, and have instituted a variety of ways of testing diesel vehicles and performing particle detection *(2)*.

## 1.3 Emissions Standards and Testing Programs

Emissions standards began in the U.S. in the '70s and '80s with ambient standards starting with measurement of total suspended particles (TSP). This was a broad designation covering particles ranging from 0.01μm to 100μm and average ambient concentration limits of 75μg/$m^3$ annually and 260μg/$m^3$ daily. This standard was later lowered to particle sizes less than 10μm, ($PM_{10}$), in 1987 with average ambient concentration limits of 50μg/$m^3$ annually and 150μg/$m^3$ daily. The current standard, enacted in 1997, is for 2.5μm particles at 35μg/$m^3$ daily *(3)*. An overview of international ambient and HDDV PM standards over time are tabulated in **Figure 1**and **Figure 2**.

**Ambient PM Standards on Three Continents**[a]

| | Canada | | | | U.S. | | | | E.U. | | | | Australia | | | |
|---|---|---|---|---|---|---|---|---|---|---|---|---|---|---|---|---|
| year initiated | size | annual [μg/m3] | daily [μg/m3] | exceedances | size | annual [μg/m3] | daily [μg/m3] | exceedances | size | annual [μg/m3] | daily [μg/m3] | exceedances | size | annual [μg/m3] | daily [μg/m3] | exceedances |
| 1970 | TSP | 70 | 120 | | | | | | | | | | | | | |
| 1971 | | | | | TSP | 75 | 260 | | | | | | | | | |
| 1980 | | | | | | | | | TSP | 80 | 250 | | | | | |
| 1987 | | | | | $PM_{10}$ | 50[g] | 150[g] | 1 | | | | | | | | |
| 1997 | | | | | $PM_{2.5}$ | 15 | 65 | 7.3[b] | | | | | | | | |
| 1998 | | | | | | | | | | | | | $PM_{10}$ | [f] | 50 | 5 |
| 1999 | | | | | | | | | $PM_{10}$ | 40 | 50 | 7 | $PM_{2.5}$[e] | 8 | 25 | |
| 2000 | $PM_{2.5}$ | [f] | 30 | 7.3[b] | | | | | | | | | | | | |
| 2006 | | | | | $PM_{2.5}$ | | 35 | | | | | | | | | |
| attainment target | | | 2010 | | | | 2010[c] | | | | 2010 | | | | 2008 | |

[a] Sources: 1999/30/EC, (*6*–*14*). [b] Permitted exceedances for $PM_{2.5}$ for U.S. and Canada are specified as follows: The three year average of the annual 98th percentile of the daily, 24-h (midnight to midnight) average concentrations may not exceed the standard. [c] U.S. States may propose to extend the $PM_{2.5}$ target year by up to 5 years (2015) [d]While the E.U. has no $PM_{2.5}$ standard, directive 1999/30/EC states in Article 5, section 3: "Action plans for $PM_{10}$ (...) shall also aim to reduce concentrations of $PM_{2.5}$." [e] The Australian daily $PM_{2.5}$ standard is still under review. [f] No standard set. [g] Due to a lack of evidence linking health problems to long-term exposure to coarse particle pollution, the U.S.EPA revoked the annual PM10 standard effective December 17, 2006. The daily standard is still in effect as of March 2007.

**Figure 1: International ambient standards since 1970.**

**Figure from reference** *(2)*.

**New HDV Diesel Engine PM Standards[a]**

| | U.S. and Canada[c] | | E.U. | | | Australia |
|---|---|---|---|---|---|---|
| applicable GVWR[b] | >8500 lbs. (3856 kg)[d] | | >3500 kg | | | >3500 kg |
| year implemented[b] | transient [g/kWh] | stationary [g/kWh] | title | transient [g/kWh] | stationary [g/kWh] | |
| 1988 | 0.80 | | | | | |
| 1991 | 0.34 | | | | | |
| 1992 | | | Euro1 | | 0.36[f] | |
| 1995 | | | | | | U.S. 1991 or Euro1 or Japan 1994 |
| 1996 | | | Euro2 | | 0.25 | |
| 1998 | 0.13 | 0.13 | | | | |
| 2000 | | | Euro3 | 0.16 | 0.10 | |
| 2002 | | | | | | U.S. 1998 or Euro3 |
| 2004 | 0.13 | 0.13 | | | | |
| 2005 | | | Euro4 | 0.03 | 0.02 | |
| 2006 | | | | | | |
| 2007 | 0.013 | 0.013 | | | | U.S. 2004 or Euro4 |
| 2008 | | | Euro5 | 0.03 | 0.02 | |
| 2010 | | | | | | U.S. 2007 or Euro5 |
| Test cycle | FTP[h] | SET[e,h] | | ETC[h] | ESC[g,h] | either U.S. or E.U. |

[a] Sources: 1999/96/EC, 2005/55/EC, (*16, 17*). [b] For E.U. and Australia, the standards are listed under the year that they are required for new models, understanding that existing models need to comply with the new standard only when their certification expires, usually the year after. [c] Canada has required U.S. vehicle standards since 2004. U.S. and Canada standards are based on model year. U.S/Canadian standards issued in g/bhp-hr (1 g/bhp-hr = 1.341 g/kWh). [d] For California, the HDV cutoff 14 000 lbs (6350 kg), below that, the standard is 0.12 g/mi for Tier 1 and LEV, and 0.06 g/mi for ULEV and SULEV. [e] SET applies to Consent Decree manufacturers 1998–2007, all manufacturers starting in 2007. [f] For Euro1, 0.36 applies to engines over 85 kW. Smaller engines meet 0.612 g/kWh. [g] Europe also has a load response (ELR) test. [h] Abbreviations: GVWR, gross vehicle weight rating; FTP, federal test procedure; SET, supplemental emission test; ETC, european transient cycle; ESC, european stationary cycle.

**Figure 2: International HDV standards since 1988.**

**Figure from reference *(2)*.**

Heavy duty vehicle inspection and maintenance (HDV I/M) programs have been implemented in a variety of ways. Differences occur in regulatory approaches that include rules regarding vehicle age, fleet size, or single owner exemptions. There are also differences in testing frequency and recruitment, the two main types being periodic vs. roadside.

Periodic testing is subdivided into three groups: centralized, decentralized, and fleet self-inspection. Centralized testing was implemented in Washington, Utah, Idaho, Illinois, and Arizona wherein one body conducts all HDV I/M tests *(2)*. Decentralized testing was employed in Colorado, New Jersey, Massachusetts, and New York. Here, independent testing stations performed inspections on HDVs. In fleet self-inspection, adherence to standards is maintained by individual fleet owners. Colorado, Illinois, New Jersey, and New York use this method as well, along with frequent auditing of self-inspected fleets.

Roadside testing has been valued as great way of cutting costs compared to periodic testing *(4, 5)*. One criticism of this type of testing is its ability to accurately represent total fleet contributions. Differences in fleet composition may vary between locations, therefore station setup and recruitment may have an effect on measurement. For instance, fleet traffic between the Mexico border, state borders, or harbor locations may vary greatly. However, the low cost of testing, high measurement counts per site, and little operator involvement allow for large coverage of possible testing sites, thereby reducing the effect of site bias.

## 1.4 Traditional Testing Instrument Methods

After recruitment to one of the above mention programs, a vehicle must be tested. Testing particulate matter is usually done by one of two methods. Opacity based testing or gravimetric analysis.

### 1.4.1 Opacity Testing

Most programs use an opacity based free acceleration smoke (FAS) test, more commonly known as snap-idle or snap acceleration test. The test employs a smoke opacity meter measuring across the exhaust pipe of the vehicle. This light source shines perpendicularly across the exhaust stream into a photocell or photodiode detector and data are collect continuously.

The vehicle is then put through a snap acceleration cycle by a professional test center driver. The vehicle's throttle is held in fully open position until maximum governed engine speed is reached plus an additional 4 seconds. The throttle is then released and the vehicle is allowed to return to idle speed. Idle speed is maintained from 5 to 45 seconds, allowing deceleration of the turbocharger, and then the cycle is repeated.

Opacity is measured in terms of transmittance, transmittance being the fraction of light reaching the detector of the total light emitted from the source, and opacity % is reported as 100 * (1 – T). The widespread use of FAS methods is mainly due to the ease of measurement and low cost of testing. It does not require a dynamometer or exhaust

dilution tunnel, and as will be detailed later, the cost of the alternative gravimetric method is very large in comparison. Cut points for the test are high enough that visual screening is an adequate method for recruiting vehicles for instrument testing *(6)*.

FAS opacity based measurements are successful in identifying gross emitting vehicles that are in need of repair, however, setting the threshold for passing too low causes even well maintained vehicles to fail *(6, 7, 8)*. Opacity standards for California were set at 40% in 1991 and have not been lowered for this reason.

Opacity measurements have several other problems as well. One criticism against them is the comparison of the snap idle cycles to realistic driving conditions. The torque-speed patterns employed in a cycle may not represent vehicle emissions that may occur in a regular environment. This may be especially true for more modern vehicle equipped with electronic controls. Cycles may produce patterns that cause these modern computerized controls to adjust for reliability instead of performance or emissions control.

Another problem with opacity measurement is its sensitivity to environmental factors such as altitude, barometric pressure, air temperature, and humidity. "Testing has shown at-site ambient environmental conditions to be among the most influential testing factors that affect as measured snap-acceleration smoke results *(9)*." All of the aforementioned factors are combined into a single parameter of "dry air density" for final adjustment of the measured opacity. Unfortunately, each engine shows various degrees of sensitivity to changes in air density.

This makes any universal adjustment an approximation. The degree to which these factors can affect measurements is exemplified in **Figure 3**.

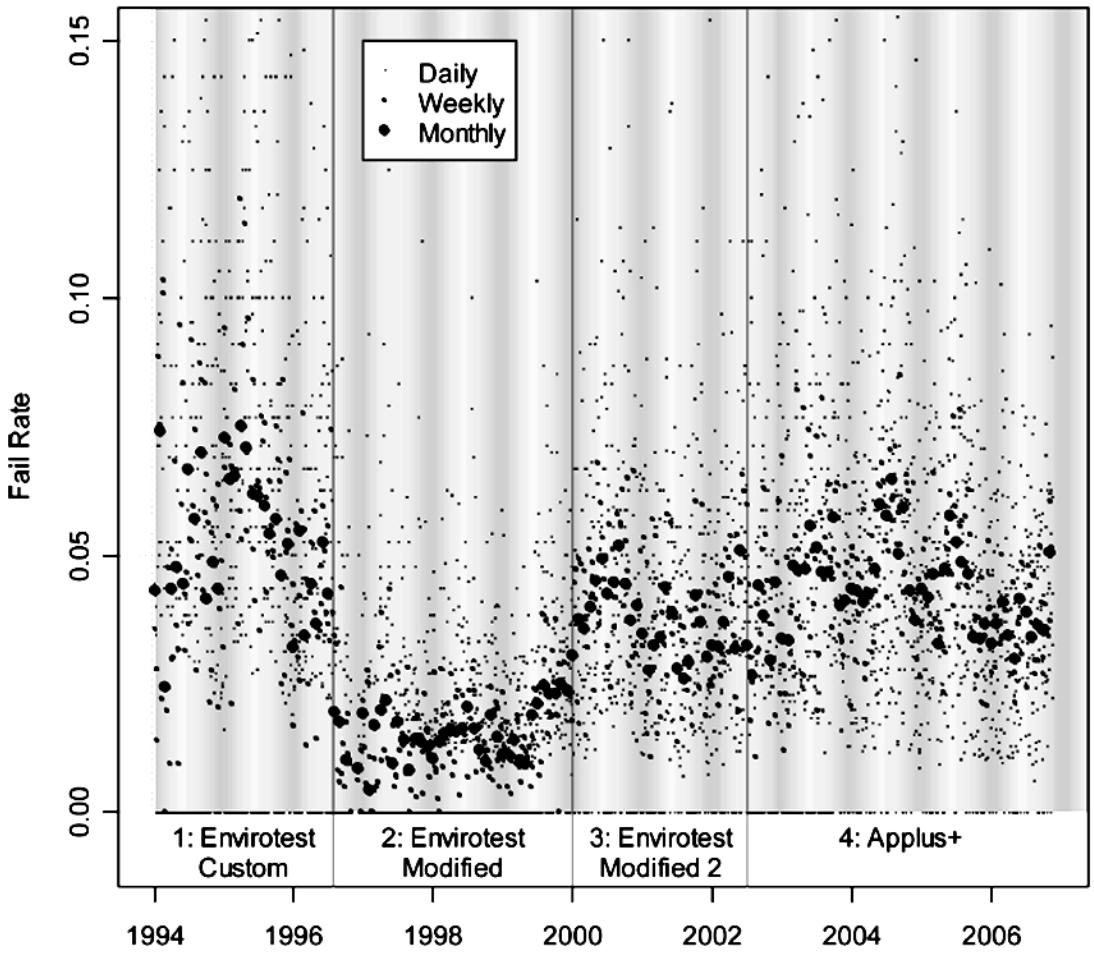


**Figure 3: Washington State HDV periodic inspection failure rate percentage over time. Each numbered bin represents a change in testing method. Dark gray vertical stripes represent winter months. Light grey vertical stripes represent summer months.**

**Figure from reference *(2)*.**

The chart is a scatter plot of fail rates in the Washington state HDV inspection program over time and is divided into four segments relating to different measurement regimes. Of note are the darkened vertical stripes relating to winter of each year. The authors claim a significant statistical difference between higher fail rates in the summer and lower fail rates in the winter.

But the most problematic issue for FAS is its poor correlation to PM. Opacity has been shown to share only slight trend with PM *(5)*. In more in depth studies PM was plotted vs. opacity for different duty cycles and does not always show a good correlation *(10, 11)*. **Figure 4**, **Figure 5**, and **Figure 6** demonstrate inconsistent results across different testing types. Correlations vary, and accuracy and precision are low.

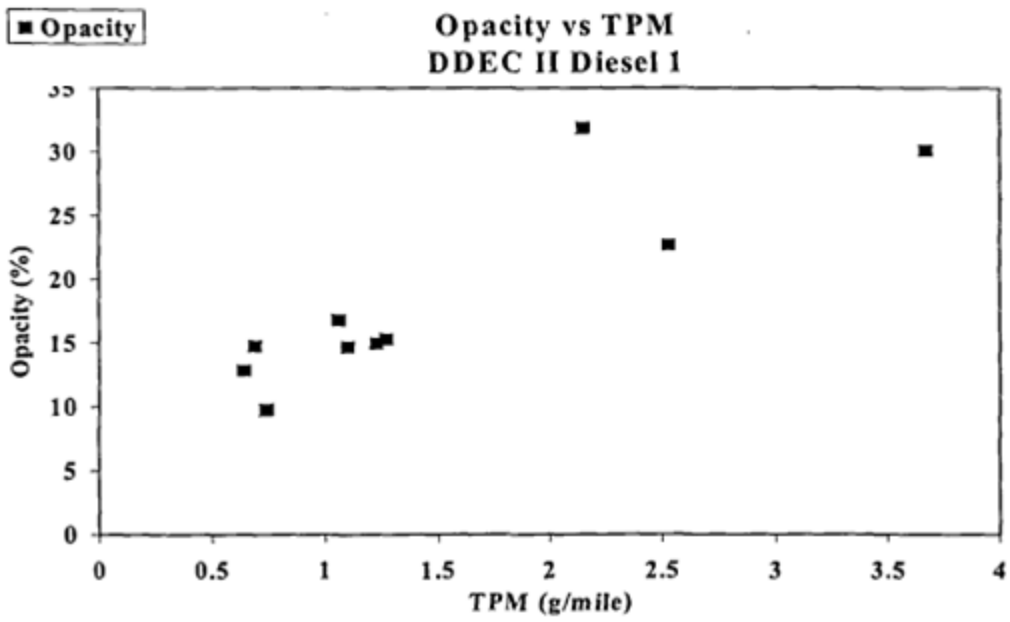


**Figure 4: Opacity vs. Total Particulate Matter (TPM) as measured by an opacity meter and gravimetric analysis from dynamometer testing for buses model years 1988 - 1993 powered by Detroit Diesel 6V-92TA DDEC II engines.**

**Figure from reference *(5).***

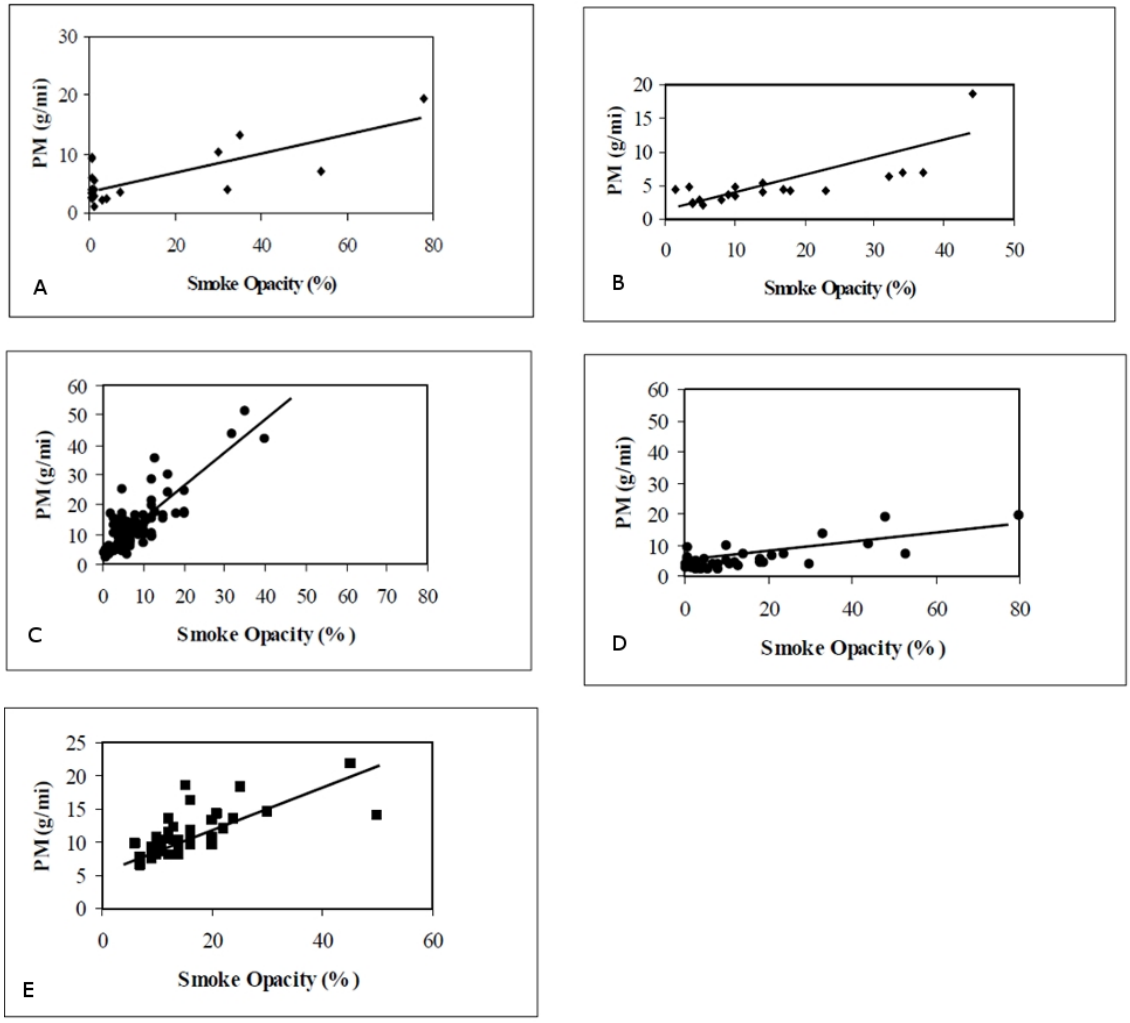


**Figure 5: Dynamometer gravimetric data vs. smoke opacity for several truck types and driving cycles.**

**A) 1985-1987 Buses Snap Idle**
**B) 1988-1990 Buses Snap Idle**
**C) Pre 1985 Buses Real world acceleration simulation**
**D) Post 1985 Buses Real world acceleration simulation**
**E) Pre 1985 Trucks Real world acceleration simulation**

**Figure from reference *(10).***

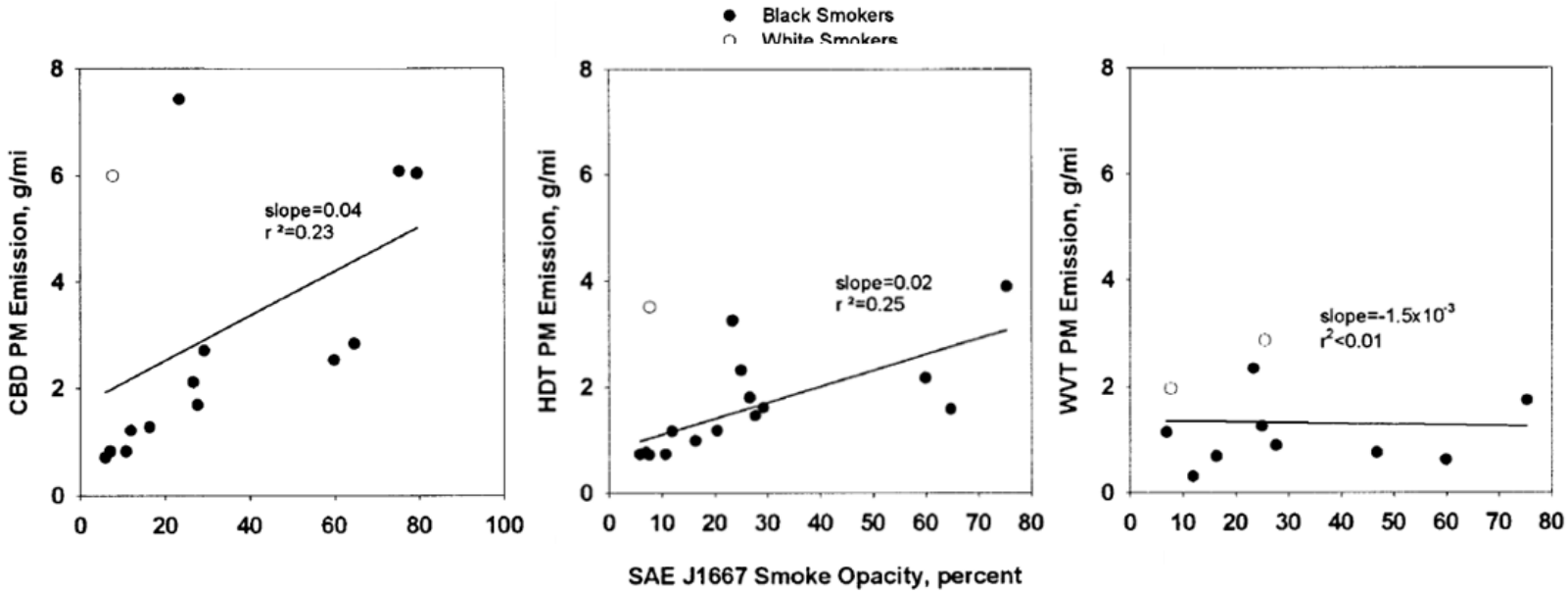


**Figure 6: Dynamometer gravimetric analysis for different driving cycles vs. smoke opacity as measured by the SAEJ1667 test. The cycles tested from left to right are the Central Business District cycle (CBD), Heavy Duty Transient (HDT), and West Virginia Transient (WVT).**

**Figure from reference *(11).***

### 1.4.2 Gravimetric Filter Method (GFM)

PM can be directly measured by weighing a total or known portion of particulate matter in an exhaust stream. Exhaust particles are collected on a filter while a vehicle runs on a chassis dynamometer. The filter is then weighed and a mass measurement is obtained.

A dynamometer works by simulating real world driving conditions while keeping a vehicle stationary. It is made of four major parts; rollers, hub adapters, flywheel assembly, and eddy current power absorbers. The rollers are free rotating drums on which the powered wheels of the vehicle rest. The hub adapters couple the drive axle of the engine with the flywheel assembly and eddy current power absorber. The flywheel assembly simulates the weight of the vehicle, and therefore the normal operating engine load. While coming up to speed, the vehicle engine must work to spin the heavy flywheel. The load put on the engine is similar to the load on the engine accelerating the weight of the vehicle up to that same speed. Eddy current power absorbers increase engine load in a manner that simulates wheel/road friction and air resistance.

Once a vehicle is connected to a dynamometer, it is taken through driving cycles representing different on-road driving modes. Examples of this include stop and go city driving, highway cruising, or heavy acceleration/braking.

While one of these cycles is being performed, exhaust gas is ported into a measurement chamber. The exhaust is first diluted with filtered air, and then ported to

different measurement devices. These may include $NO_x$, CO/ $CO_2$, or hydrocarbon analyzers, real time microbalance (e.g., Tapered Element Oscillating Microbalance (TEOM)), and filter. Before testing the filter is prepared in a clean room at constant temperature and humidity. When testing, it is moved into the dilution chamber, and a known fraction of the exhaust stream is passed through it.

The main benefit of performing gravimetric analysis by particle capture on filters is the direct measurement of particle mass in units compliant with state and federal standards. Problems with poor correlations are completely bypassed, although there may still be issues with absorption of water vapor or semi-volatile hydrocarbons. This allows for greater discrimination between pass/fail vehicles. Compare this to opacity measurements in which cut off points are set very high in order to not give false fails. Inaccuracy issues with opacity were at one time great enough to shut down the California program from 1993 to 1998 due to lawsuits (*8*).

Another benefit of GFM over opacity is its better representation of normal driving conditions (*12*). It has been noted, however, vehicle electronics may identify abnormal operation if not all wheels are rotating.

The major drawbacks against GFM are the time involved to perform measurements and the associated costs. One full cycle test can take up to 20-30 minutes. If several cycles are performed on one truck, and if you were to include preparation time, testing time can take up to a full day.

The second drawback is the prohibitive cost involved in testing a single truck *(13)*. Northeastern States for Coordinated Air Use Management (NESCAUM), for example, quotes an operating cost of $10,000 dollars per day for HDV testing. Average equipment costs are $300,000 and the test requires a skilled workforce for operation *(13)*. Of course, while these costs seem high, it is important to scale them against a comparable FAS program. California's program is runs at about $22 million per year *(143)*. Comparison is difficult however. State implementation programs (SIPs) are usually calculated in a cost per mass basis and due to the highly inaccurate nature of opacity measurements, total program costs are uncertain.

## 1.5 Alternative Sensor Methods

There are a number of instruments available for measuring various attributes of particulate matter in exhaust. The following summary of measurement devices, while no means comprehensive, was compiled to give an overview of available techniques.

**Nephelometer/ Laser Light Scattering / Mie Scattering**

One way to measure particle quantity is by measuring the scattering of light on an aerosol sample. Either a halogen light source or laser light source is used to illuminate a sample gas. A mirror set at 90º to the light source focuses scattered light from the aerosol onto a detector *(15)*.

**Condensation Particle Counter (CPC)**

A CPC, **Figure 7**, measures total particle count by a condensing process. Particles from sample air first enter a saturation chamber then pass to a condenser to undergo a condensing process. The saturation chamber is filled with some high vapor pressure liquid like butanol, alcohol, or water. The vapor then condenses around the particles in the sample air. In this manner, ultrafine particles can grow to approximately 10μm. At this size, particles are measurable by light scattering. The condensed particles are then moved to a measurement chamber. Laser light illuminates the sample and 90º scattered light is collected and used to determine particle concentration *(16)*. CPC's do not measure particle mass but are used in conjunction with other particle sensors.

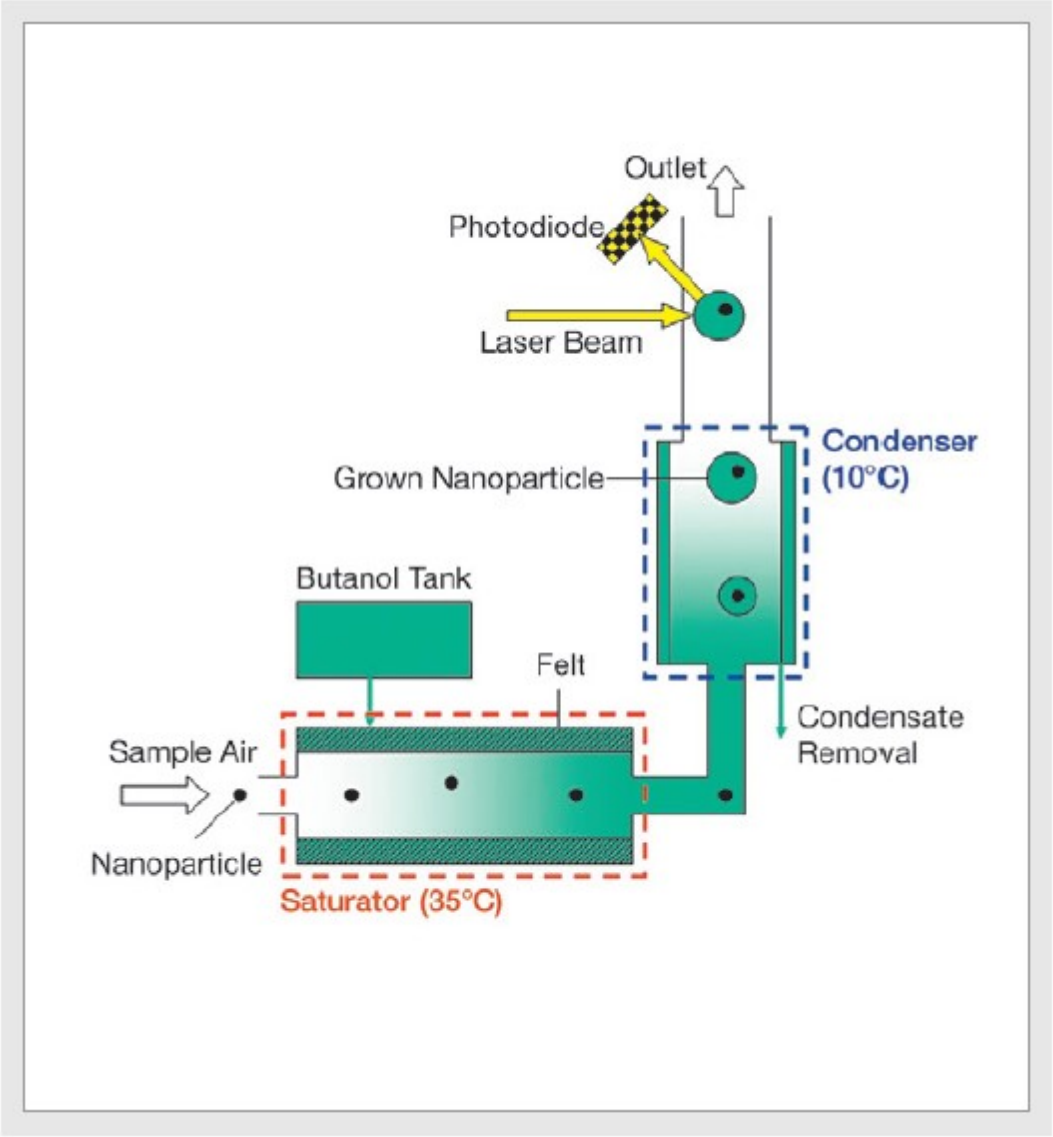


**Figure 7 Condensation Particle Counter (CPC) Block Diagram**

**Figure from reference *(16).***

**Impactor**

Impactors, **Figure 8**, are instruments designed to separate particles by size. They can be used in a single stage to exclude large particles from measurement, such as an initial separator for a $PM_{10}$ or $PM_{2.5}$ mass filter sampler, or multistage in order to separate particles for use in a distribution analysis method.

The theory behind its operation is the use of bends in airflow to make separations based on whether a particle has mass to either follow the direction of flow, or inertially resist flow direction and follow its initial path. Bends in airflow are created by an impactor plate in the flow stream. The flow moves around the plate carrying lighter particles with it. Heavier particles continue their path and impact on the plate. A series of plates**, Figure 9**, can be set up with greater and greater changes in the angle air flow. In this manner, a series of plates can collect a size distribution of particles. Errors in measurement may occur if heavier particles experience "bounce-back" off the impactor plates and continue down the air flow. This can be avoided by applying thin layers of oil to the plates. However, this may complicate final mass measurements *(17)*.

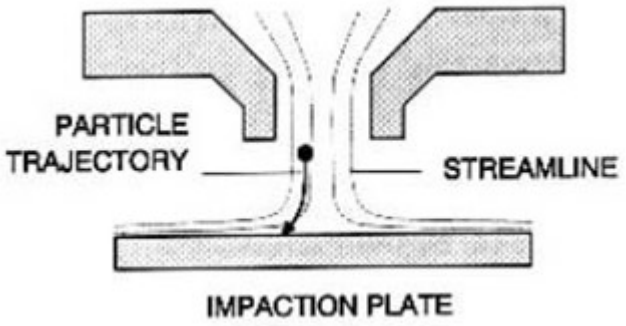


**Figure 8: Single impaction plate diagram.**

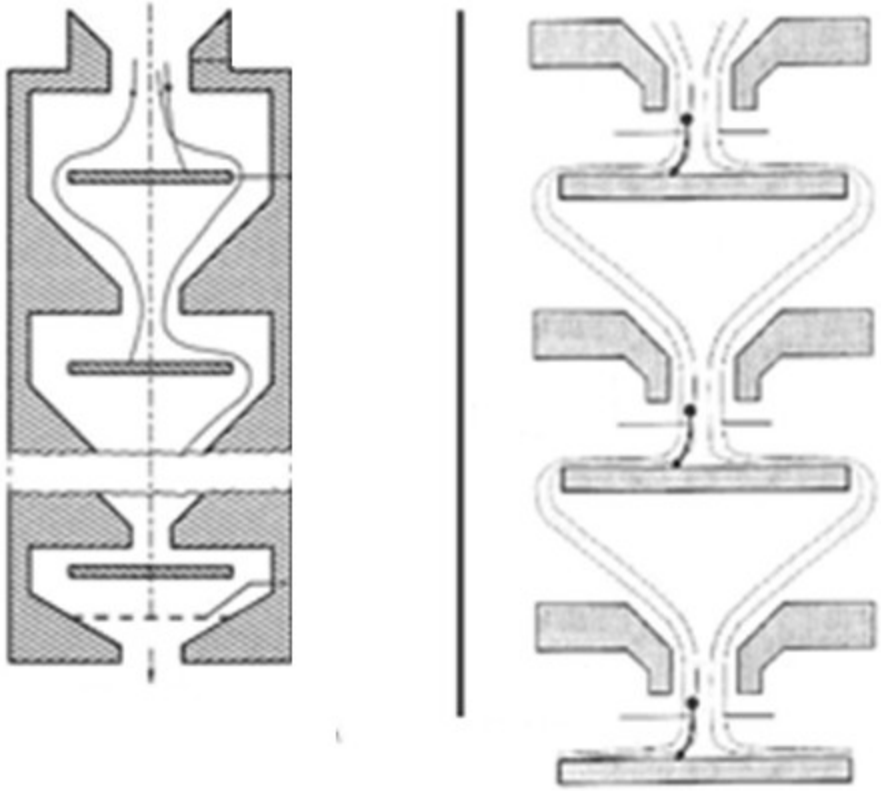

**Figure 9: Multiple impaction plate diagram.**

**Cyclones**

Cyclones, **Figure 10**, are not a measurement device, but are often used in conjunction with other instruments for the purpose of filter out larger particles. The devices use centrifugal force to remove the larger particles from the exhaust stream. Exhaust enters through a lower pressure inlet. The stream then circles the conical inlet tube creating a vortex. Smaller particles are able to follow the circular path of the exhaust stream and are carried on to a measurement device. Larger particles have too much inertia to follow this path and impact the side walls of the conical tube, thereby removing them from measurement *(18)*.

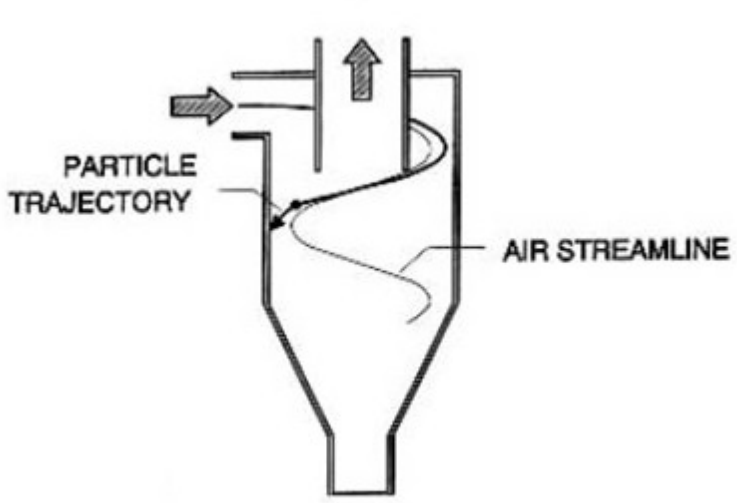


**Figure 10: Cyclone diagram.**

**Aerodynamic Particle Sizer (APS)**

The APS measures time of flight. This property is related to the aerodynamic equivalent diameter for certain sized particles. In practice, a stream of exhaust fraction passes through two acceleration nozzles. Time of flight is then measured for passage between two laser beams. Particles having small aerodynamic diameters are accelerated faster by the nozzles and pass more quickly between the beams. The particles are then counted, and a size distribution of the sample can be determined *(19)*.

**Electrical Aerosol Detector (EAD)**

The EAD, **Figure 11**, makes continuous measurements of aerosol diameter concentration. It does this by splitting a sample flow into two parts. One part of the sample is ported directly into a mixing chamber. The other sample is passed through filters to remove all exhaust particles. The filtered sample then passes through a corona and transports corona ions into the mixing chamber. The purpose of this is twofold. First, by ionizing exhaust particles indirectly, no soot particles are lost to the surface of the corona charger. Secondly the mixing process, known as "counter flow diffusion charging", places a defined charge state on the sample particles. The current flow is then measured by an electrometer. The signal can be converted to particle diameter by the linear relationship to the number of elementary units of charge on particles *(20, 21)*.

**Differential Mobility Analyzer (DMA)**

A DMA operates by measuring electrical mobility of particles and operates in a somewhat similar manner to an impactor. Particles travel through the devices, and only

those meeting certain size and charge thresholds follow a stream of  air through an oulet. The rest impact upon instrument surfaces.

An inlet at the top of the device lets in an exhaust flow.  Entering the inlet, the particles are exposed to an aerosol monocharger which electrically charges particles in the exhaust.  The sample stream then flows through a sheath between an outer and charged inner cylinder.  As the stream flows down the cylinders particles are attracted to the inner portion.  Particles with low mobility do not change much in their path and exit through a disposal outlet.  Particles with higher mobility collide with the inner cyclinder. Particles within a certain range of mobility escape through a sample outlet and can be measured by a second device which collects all arriving charged particles.  Mobility is varied over time by adjusting the inner cylinder charge.  In this way, a distribution of particle mobility is found *(22)*.

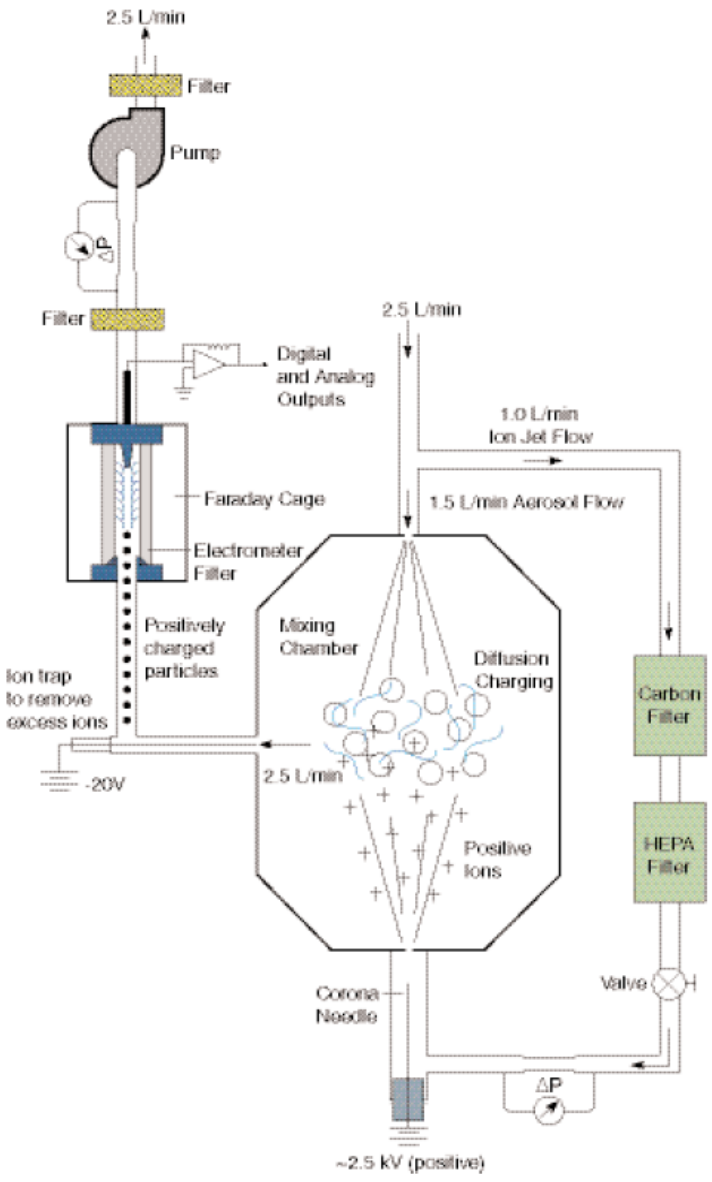


**Figure 11: Electrical Aerosol Detector (EAD) block diagram.**

**Figure from reference *(20).***

**Scanning Mobility Particle Sizer (SMPS)**

The SMPS, **Figure 12**, measures the distribution of particle sizes in a given exhaust stream. Due to the nature of its design, continuous measurements are not available. The device selectively measures one particle size range at a time and creates a distribution chart at the end of measurement. Several distributions of sample air can be measured to check assumptions about the uniformity of the sample air particle distribution over time.

The instrument works in several steps. The first process is to exclude particles over a certain size. This is done to remove particles outside the measurement range that might contribute to data inversion errors due to multiple charging. This accomplished by either a single stage impactor or a cyclone.

The second step is the separation of particles by their electrical mobility. This is done through the use of a differential mobility analyzer (DMA). In the DMA, particles with too negative or positive charge are either trapped on the inner electrode, or removed through an exhaust port. Particles within a certain mobility range pass through a narrow slit at the end of the DMA.

The particles are then counted using a CPC. The DMA moves through a range of different electrical mobilities, and each range is counted. These data are then used to construct a distribution chart.

PM calculations from SPMS data make assumptions about particle volume vs. particle size as determined by electrical mobility as well as particle density. Mass calculations can then reported as summations over detection time. The lowest response

time of this instrument is approximately 30s, and therefore continuous measurement of PM is not possible by this method. Exhaust measurements will necessarily be tied to engine operation during the range of the measurement *(23)*.

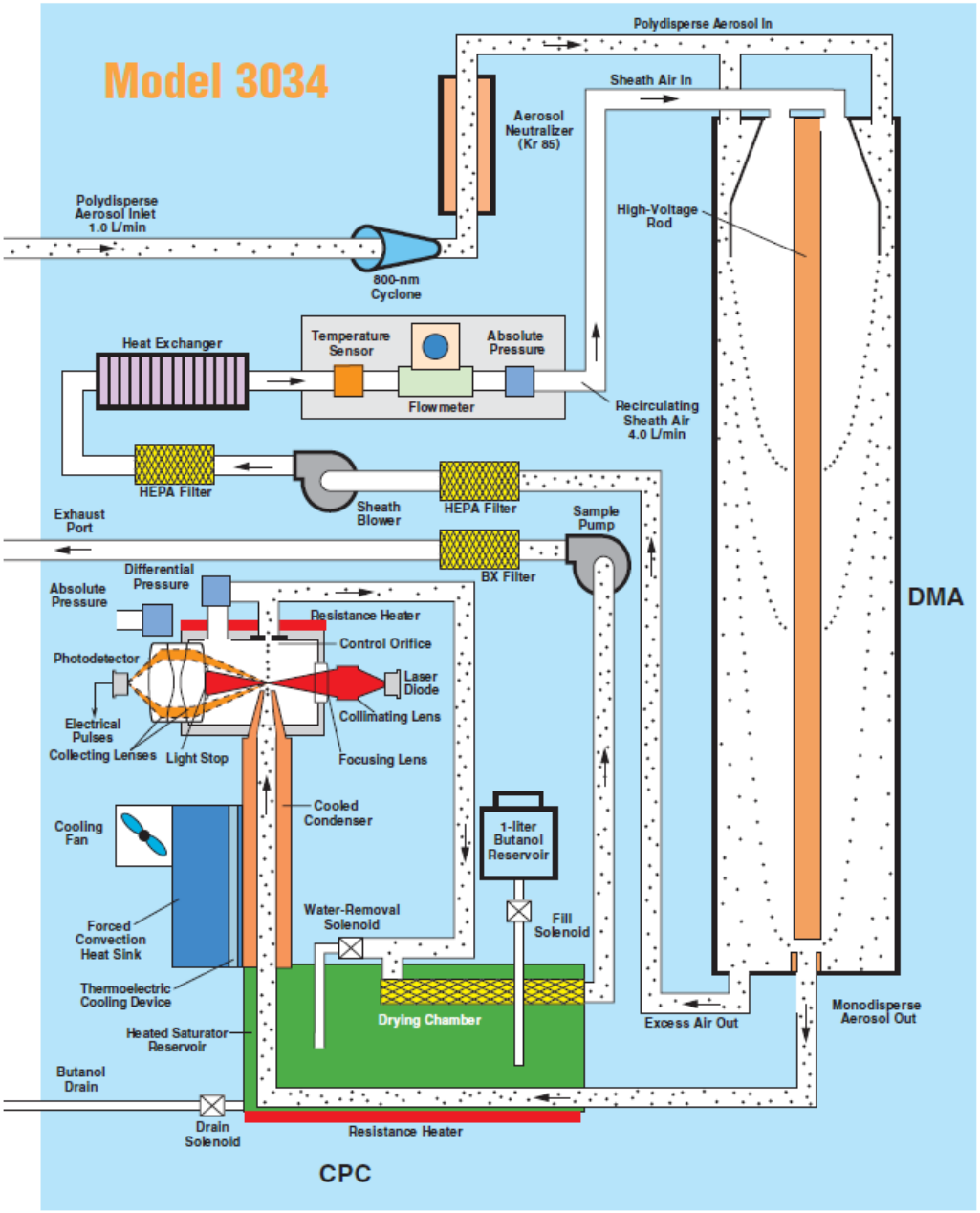


**Figure 12: Scanning Mobility Particle Sizer (SMPS) block diagram.**

**Figure from reference *(23).***

**Engine Exhaust Particle Sizer (EEPS)**

The EEPS, **Figure 13**, measures the particle size distribution of a given exhaust flow. Its function is somewhat comparable to an SMPS. Particles are charged and then separated based on their electrical mobility. Measurements of particles with different electrical mobilities can be accomplished simultaneously with multiple detectors.

The instrument continuously draws in a sample of the exhaust air. This air is moved through a chamber containing a corona charger where particles are positively charged. The particles then enter into the measurement chamber. The chamber consists of a high voltage positively charged electrode column surrounded by electrometers.

Sheath air flows from the corona chamber to the measurement chamber and around the high voltage electrode. The positive charge of the electrode repels the positively charged particles. These particles then deviate from their paths and onto the electrometers. Electrical mobility of the particle determines the amount of path deviation. In this way electrometers set at different points down the path of the measurement chamber collect a different range of electrically mobile particles.

This design allows for continuous measurement of particle size distribution, because there is an electrometer measuring each segment of the distribution. However, resolution is limited to the number of electrometers present in the device. This resolution is lower than SMPS, which is can readily be increased by reducing the effective slit size of the DMA *(24)*.

**Electric Low Pressure Impactor (ELPI)**

The ELPI operates in a similar manner to the EEPS. Particles of an exhaust stream are given a unipolar charge upon entering a corona charging chamber. From here the air sample flows into a low pressure impactor equipped with electrometers on each impactor plate. ELPI is able to measure size distribution continuously at rate of less than 5Hz, but has a lower detection limit of 3μm. It is also able to measure particle mass, but not continuously. When functioning in this manner, it behaves the same as a low pressure impactor *(19).*

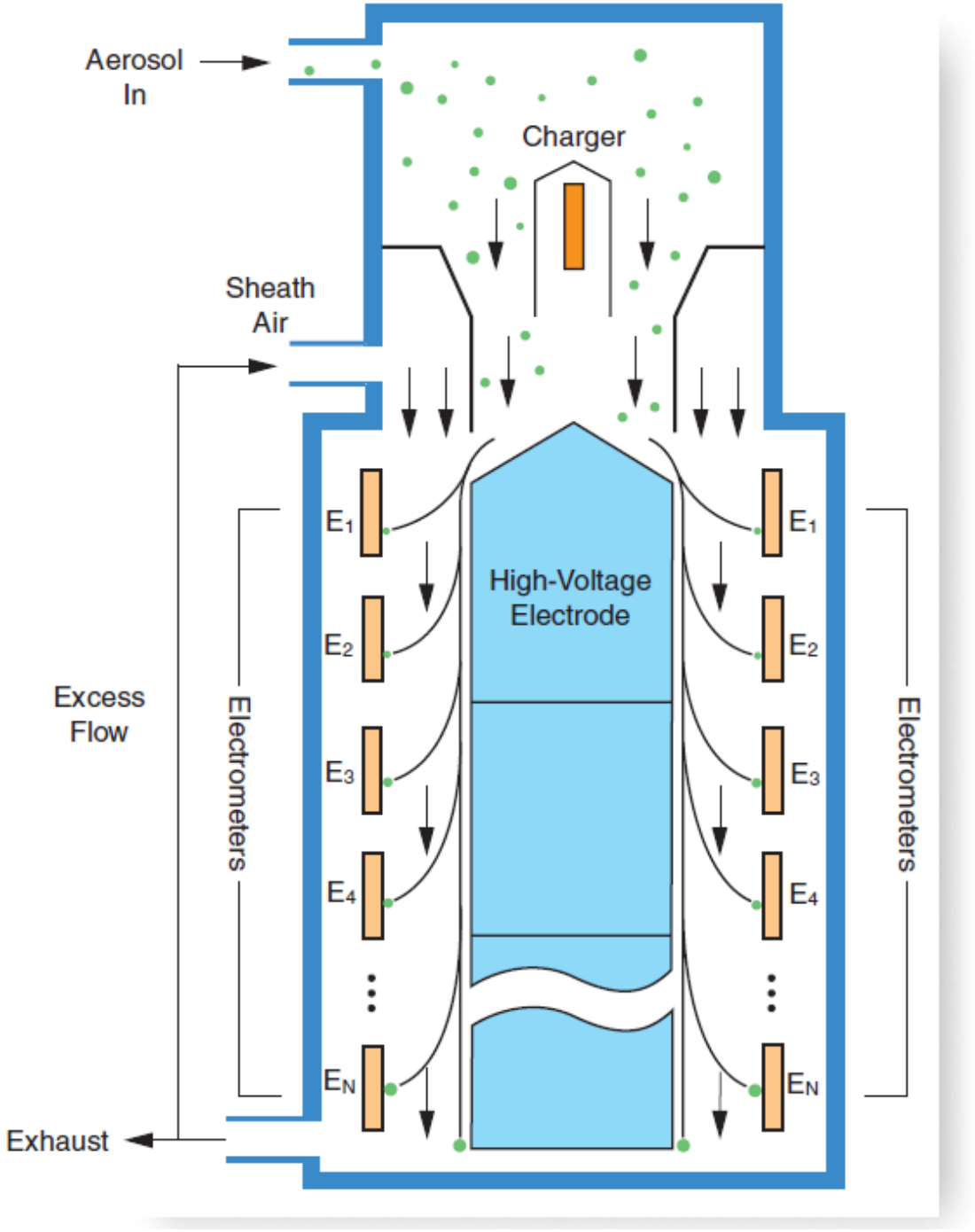


**Figure 13: Engine Exhaust Particle Sizer (EEPS) block diagram.**

**Figure from reference** (*24*).

**Laser Induced Incandescence (LII)**

LII, **Figure 14**, is a process that occurs when a sample of soot is energized by laser light. Energy absorbed from the laser cause the soot temperature to rise. The soot then loses this energy to its surroundings, increasing the overall temperature of the sample. If the absorbed energy is high enough, incandescence (black body radiation) will occur. Measuring this incandescence can yield information about soot volume fraction and primary soot particle size.

The instrument is practically limited by the requirement of a high intensity laser, attenuation of laser excitation and incandescence over longer path lengths or dense soot volume fractions, fluorescence interference from hydrocarbons, and large uncertainty *(25)*.

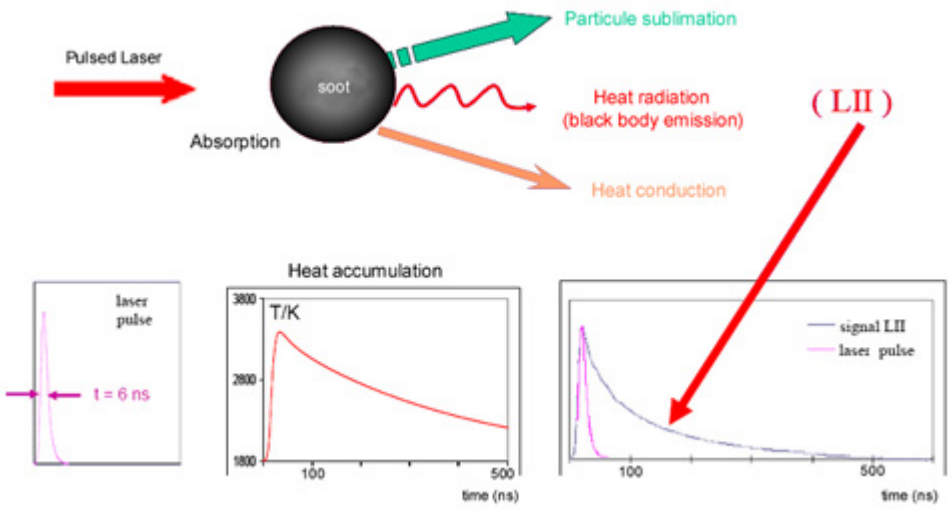


**Figure 14: Laser Induced Incandescence (LII) operational theory.**

**Figure from reference *(26).***

**Photo Emission Charging**

This process is done by energizing soot particles with ultraviolet radiation. Electron emission from these irradiated particles then occurs when the photon energy is higher than the work function of the particle surface. PM is then measured as a relation to electron emissions. However, these measurements can be influenced by absorbtion of the emitted electron by other material in the exhaust stream. This process is called back diffusion and can cause signal response to be lowered.

One type of photo emission charging instrument is the Photoelectric Aerosol Sensor (PAS). The PAS ionizes particles containing polycyclic aromatic hydrocarbons (PAHs) with an ultraviolet lamp. Charged particles are then collected by filter and measured with an electrometer *(27)*.

**Photo Acoustic Soot Sensor (PASS)**

The PASS measures acoustic resonance of a soot sample excited by modulated laser light. The sample is pumped through a resonator tube. The laser light shines into the tube. The soot becomes excited and quickly relaxes by non-radiative methods. By this method, the soot transfers heat to the surrounding gas. This causes a pressure wave. The laser is modulated with the tube's resonance frequency to create a standing acoustic wave. A microphone located at the maximum amplitude of this wave records a signal. This signal is proportional to absorption of the soot in chamber.

These measurements are taken as exhaust flow continuously flows through the resonator tube. Detection times of one second or frequencies of 1Hz allow a real time measurement of exhaust soot *(28)*.

**Beta Attenuation**

Beta Attenuation is a method to directly measure particle mass through the measurement of beta rays passing through a sample. Beta rays can then be detected by a scintillation detector.

In the first stage of measurement, the instrument is usually coupled with a cyclone or impactor in order to remove larger particles. A zero is then performed either by doing an initial measurement on a blank sample or by running a blank alongside the actual measurement. Beta radiation from a carbon-14 source is directed at the blank filter tape. Carbon-14 emits a constant stream of electrons on the sample over the course of an hour. The amount of beta radiation passing through the clean filter and reaching the detector is recorded as the zero level.

Sample air from an exhaust stream is pulled through a spot of clean filter tape. The spot of tape is then exposed to beta radiation for an hour and the number of particles reaching the detector is recorded. This zero is subtracted from the data and a mass can then be calculated by Lenard's Law.

The primary drawback of this method is the hour long detection time for a single portion of exhaust *(29)*.

**Quartz Crystal Microbalance**

Quartz crystals have the property of the piezoelectric effect. Applying voltage to the crystals results in physical changes. If alternating current is applied, the crystal will oscillate. Depositions of particles on the crystal vary the oscillation frequency. The change in mass of the crystal can then be calculated by Sauerbrey's equation *(30)*.

**Tapered Element Oscillating Microbalance (TEOM)**

The TEOM, **Figure 15**, is capable of direct measurements of particle mass. The basic operating principle behind the TEOM is the accumulation of particles on an oscillating element causing a measurable change in frequency.

The heart of the TEOM system is the hollow, tapered, cantilever system. This tapered element (TE) is oscillated at its natural frequency. A filter is applied to the hollow opening of the TE. A diluted exhaust stream is passed through the filter and through the hollow opening. As particles from the exhaust stream accumulate on the filter, the oscillating frequency of the TE changes.

Mass measurements are made at a rate of 5Hz. The measurements are made by determining the change in oscillation from the previous measurement. A mass/oscillation relationship can be made, and a continuous particle mass measurement can be made.

Deposition of water or volatile organic compounds (VOCs) on the TE can result in falsely high PM measurements. These compounds may also be removed from the filter if exhaust flow temperatures through the TE increase. This results in negative

readings from the TEOM. For this reason, continuous data may not correlate well with actual PM measurements. However, if the filter is free from water vapor and VOCs at the end of measurement, an integrated TEOMs mass measurement should cancel out the interfering positive and negative instrument responses leaving an accurate PM total *(17)*.

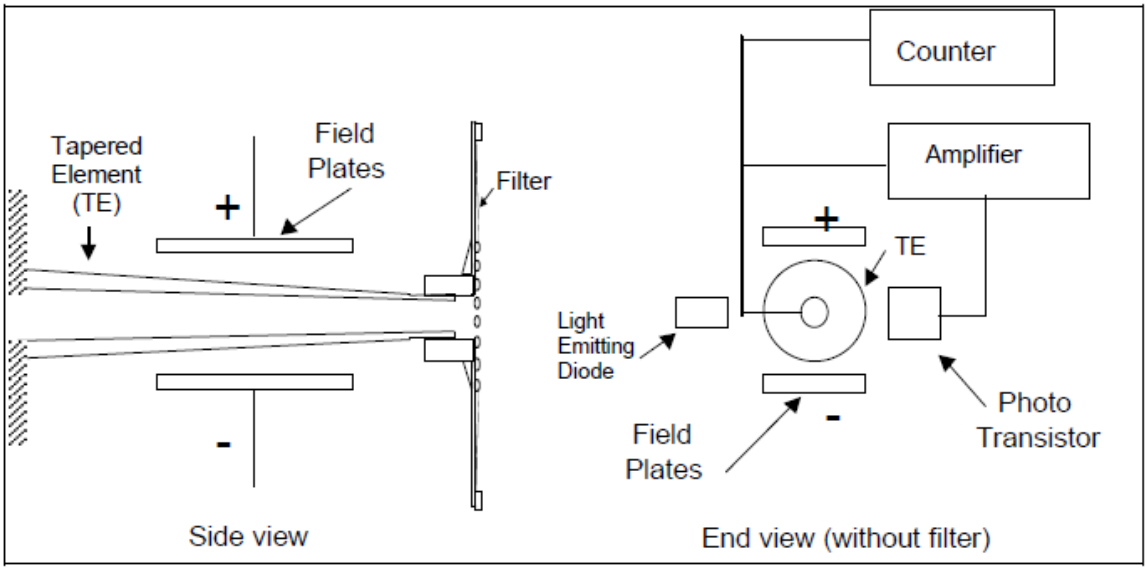


**Figure 15: Tapered Element Oscillating Microbalance (TEOM) block diagram.**

**Figure from reference *(17)*.**

## 1.6 Electronic Tailpipe Particle Sensor (ETaPS )

The ETaPS is another instrument that employs a corona for the purpose of diffusion charging. The function will be covered in more detail in a later chapter, but a quick overview is that exhaust flows through a perforated tip across the ETaPS corona charger. Exhaust then gathers charge based on its active surface area. The instrument then measures the current needed to maintain the corona voltage. This current is thought to correlate with particle surface area.

The focus of this study is to determine experimentally in real world conditions, the extent to which this measurement corresponds to particle mass, as measured by a gravimetric filter method on a dynamometer.

The instrument was chosen as a possible replacement, or screening tool, for dynamometer tests for a number of reasons. The first category that ETaPS is advantageous in is its cost and simplicity. The ETaPS instrument itself is approximately $3000. Test costs for PM measurement would be similar to an opacity measurement, and this procedure has the possibility of being performed on-road off-dynamometer for even greater cost efficiency. The simplicity of the instrument leads to other reductions in cost as well. The system is easy to setup and output data are not complicated, meaning less user training is required and the system does not need specialized technicians to be operable. The device is easily maintained, repaired, and needs infrequent cleaning. The system measures raw exhaust and therefore does not need the equipment necessary for dilution tunnels or filters. All these benefits may translate into reduced overall cost of I\M programs or expansion of coverage with no increase in total costs.

The second category ETaPS is well suited for is its direct measurement capability. Unlike many other measurement systems, ETaPS does not require dilution of exhaust or any sort of particle capture. The ETaPS can be placed directly in the exhaust stream of a vehicle for its measurements. Another advantage is its relatively small size and weight. Because of this, the ETaPS can be mounted to a moving vehicle and take real world measurements. This avoids problems of trying to simulate realistic driving conditions on a dynamometer. The ETaPS is also able to take continuous measurements allowing for a finer examination of vehicle driving modes resulting in different levels of emissions.

The last advantage of ETaPS is that it may be in a good position to continue as a standard measurement device if guidelines for emissions standards change. At the moment, particle emissions are defined by particle mass. However, health effects of particle emissions are also dependent on particle surface area, which the ETaPS potentially measures *(31)*. A shift in emissions standards in the future may mean very little change in I\M programs if ETaPS is an available measurement device.

While ETaPS has many advantages over other instruments, there are no peer-reviewed publications on it, and very few studies have been performed. The following figures show the results of correlations with other instruments. The results of these studies indicate a relationship between ETaPS signal and particle mass.

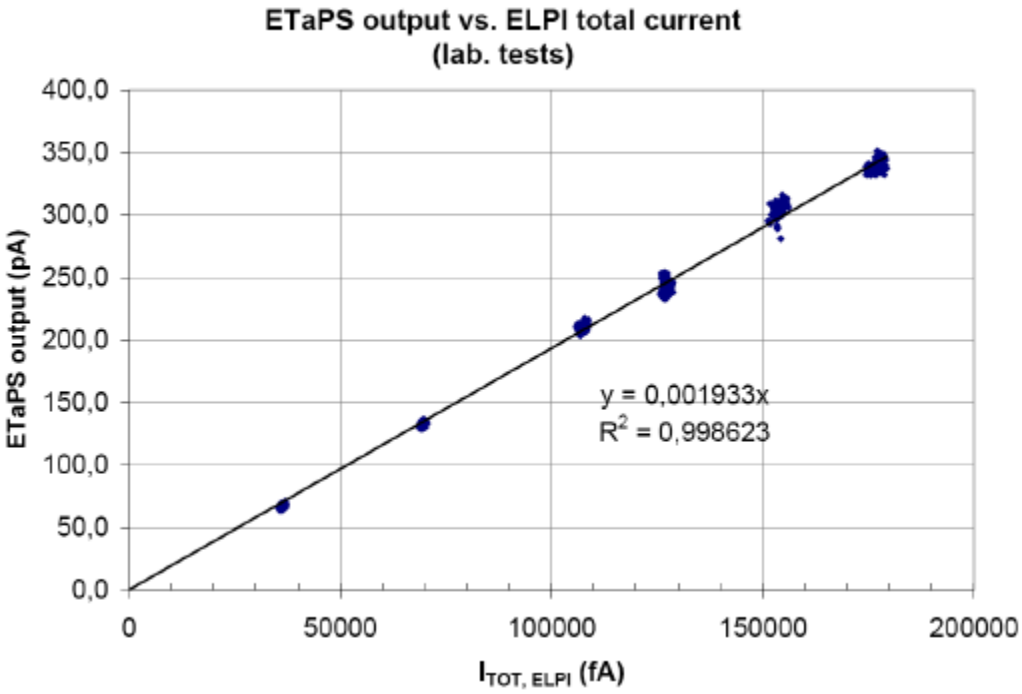


**Figure 16: ESP study comparing ETaPS vs. ELPI response.**

**Figure from reference *(32).***

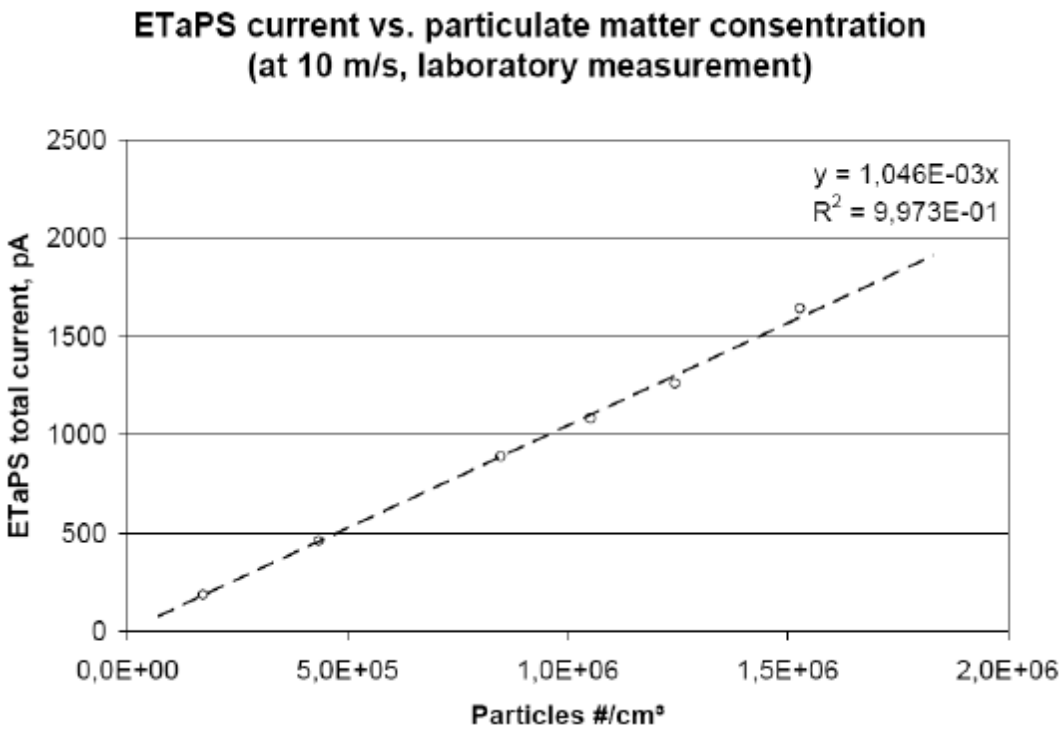


**Figure 17: ESP study comparing ETaPS vs. CPC.**

**Figure from reference *(32).***

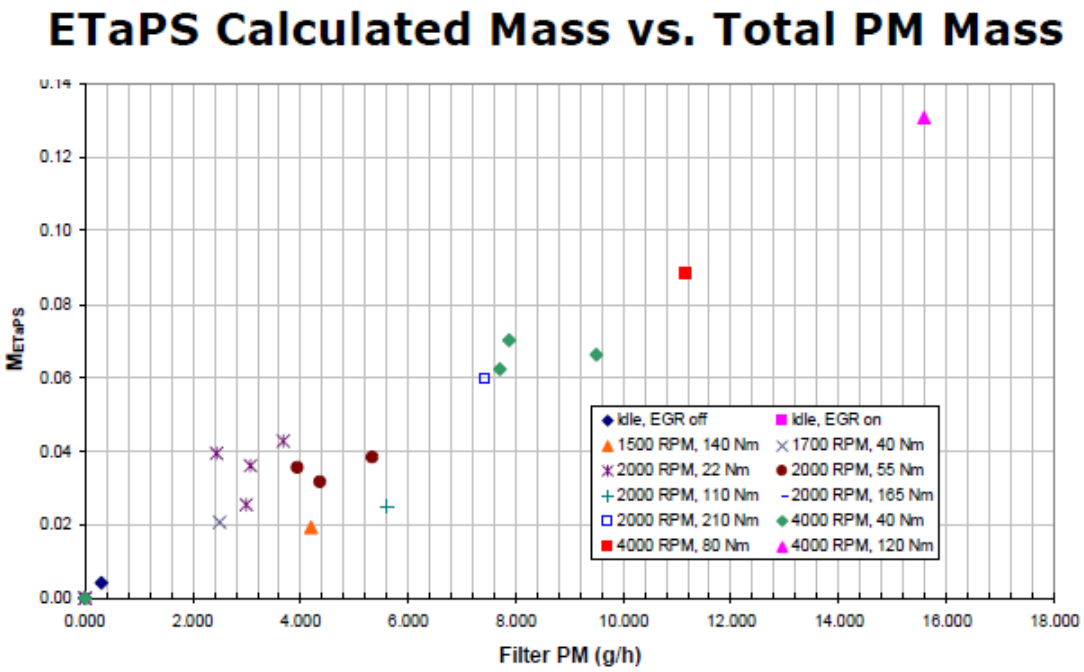


**Figure 18: ESP study comparing ETaPS calculated mass to filter weight.**

**Figure from reference *(32).***

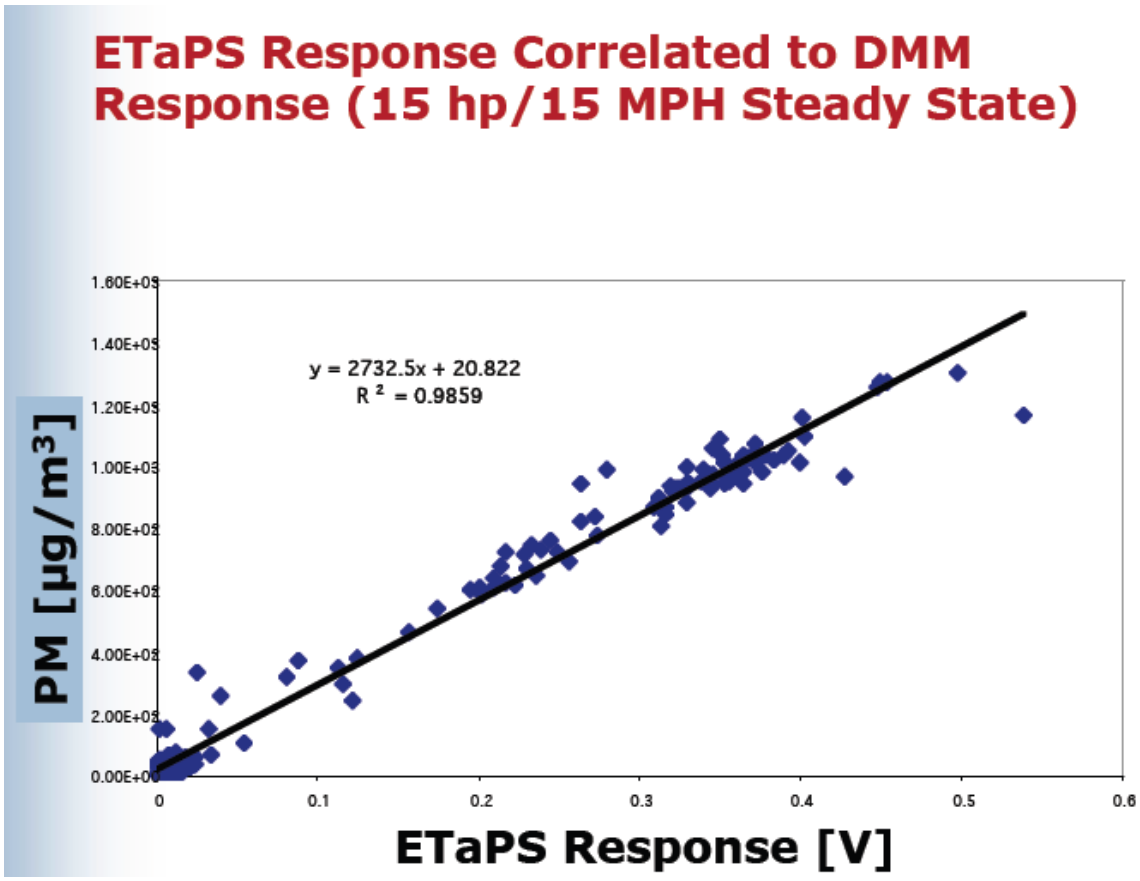


**Figure 19: ESP study of DMM vs. ETaPS response.**

**Figure from reference *(33).***

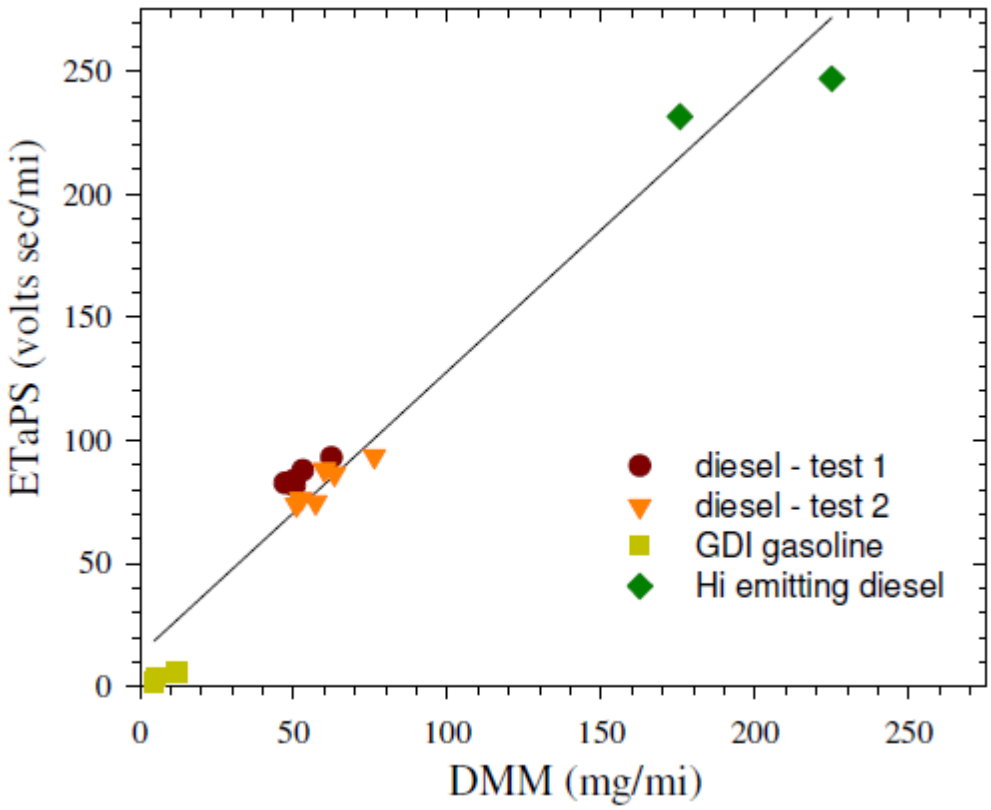


**Figure 20: Ford study of ETaPS vs. DMM response.**

**Figure from reference *(34)*.**

# Chapter 2: Instrumentation

## 2.1 Remote Sensing Detector (RSD)

### 2.1.1 Theory of Operation

The RSD used in these experiments was a commercial Environmental Systems Products (ESP) 4000 series. The RSD uses two light sources and a dichroic beam splitter to make colinear IR and UV radiation. The UV source is a deuterium lamp, and the IR source is a 1W tungsten lamp. The IR source is used to measure absorbance by CO, $CO_2$, hydrocarbons (HC), and reference. The light from this source can then be passed through a movable sample cell upon software command. The measurement of light absorbance from gas inside the sample sell is compared to known sample of cylinder gas in order to calibrate the instrument. The UV source measures absorbance by NO. The light from the sources is reflected off a mirror and travels approximately the length of a single road lane. Here, the beam is reflected back to the instrument for detection. The beam is focused and sent towards a spinning mirror. The spinning mirror reflects light sequentially toward one of a set of five mirrors. This sends the different portions of light to different detectors as the wheel turns. The diverging IR light coming from the spinning mirror is then refocused into one of four, Peltier cooled, PbSe detectors. Each detector measures the absorbance for a portion of the returned light corresponding to CO,

$CO_2$, HC, or REF. If absorbance has occurred from the transmitted light, a signal is recorded. The unfocused UV light is refocused into a fiber optic cable and is measured separately.

A typical setup for the system is shown in **Figure 21**. Absorbance is continuously measured at 100Hz and a 200ms buffer of data is kept in memory. As a vehicle passes, it blocks the beam of radiation. If there is a 10ms or more block, this pre-block buffer is stored and checked for the lowest reference voltage. After unblock, a half second of data is recorded and the zero-offset is subtracted from all points. The least polluted 10ms average over the entire 0.7s is then used to make the Clean Air Reference (CAR) to which the other data are compared.

After all data corrections have been made, the data sets of CO, NO, and HC are set against $CO_2$. Either the slope of the resultant correlation lines or the integration of the resultant data vs. time is used to calculate the ratios $CO/CO_2$, etc. With these ratios, the grams per kilogram fuel for each substance can be directly calculated, given correction for excess oxygen and for water vapor present in exhaust, and using a stoichiometric relationship for combustion the concentrations, which would be monitored by an on-line tail pipe probe.

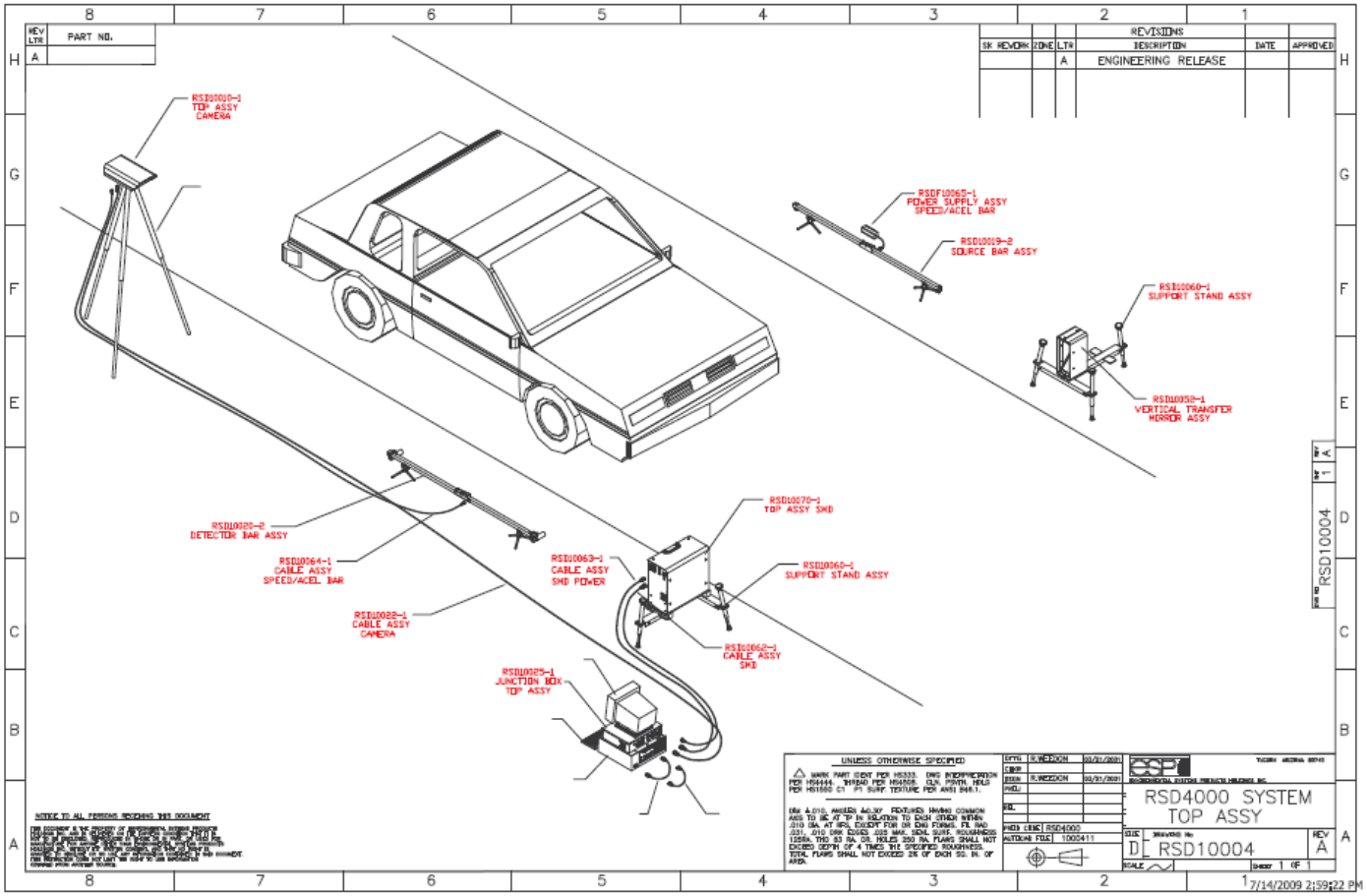


**Figure 21: RSD typical experimental setup. The vehicles to be measured pass in a single lane from left to right between the marked bars.**

**Figure from reference *(44)*.**

### 2.1.2 Calculations

**Stoichiometry Ratio Calculations:** *(35).*

Several assumptions have to be made before the stoichiometry calculation.

1. The fuel's ratio of hydrogen to carbon is 2. (not a large effect)
2. Fuel is not oxygenated i.e. contains no ethanol, MTBE, etc. (not a large effect)
3. Corrected for excess air not involved in combustion.
4. Exhaust hydrocarbons are measured in comparison to the propane calibration gas. ($C_3H_8$ but assumed to have the same C:H ratio as the fuel $C_3H_6$)
5. Equal amounts of detected and undetected hydrocarbons are present in the exhaust when compared on the basis of carbon mass.

A vehicle in normal operation with a proper air/fuel mixture, and assuming a simplified $O_2$:$N_2$ ratio for air, has a stoichiometric combustion equation

$$CH_2 + 1.5(O_2 + 4N_2) \rightarrow CO_2 + H_2O + 6N_2$$

Taking into account formation of nitric oxide from nitrogen in ambient air

$$N_2 + O_2 \leftrightarrow 2NO$$

and unburned hydrocarbons the equation, with a more accurate stoichiometry for air, becomes

$CH_2 + \mathbf{m}(0.21O_2 + 0.79N_2) \rightarrow \mathbf{a}CO + \mathbf{b}H_2O + 2\mathbf{c}C_3H_6 + \mathbf{d}CO_2 + \mathbf{e}NO + (0.79\mathbf{m} - \mathbf{e}/2)N_2$

The factor of 2 before the hydrocarbon term compensates for the fact that the IR calibrated with propane measures about half the carbon mass which would be measured by a flame ionization detector. RSD only detects hydrocarbons within a narrow band at around 2940cm$^{-1}$, the absorption region for alkane C-H stretches. Alkene C-H and aromatic stretches are weak in or fall outside this range. However, using a flame ionization detector for comparison, it has been found that the ratio of detected vs. undetected hydrocarbons is about equal. A factor of 2 to 2.3 is a fair approximation of the total HC in diesel exhaust *(36)*.

The three measured pollutant ratios are then defined as per $CO_2$.

$$Q = \frac{CO}{CO2} = \frac{a}{d} \quad (1)$$

$$Q' = \frac{HC}{CO2} = \frac{c}{d} \quad (2)$$

$$Q'' = \frac{NO}{CO2} = \frac{e}{d} \quad (3)$$

Assuming the ratio of H to C is 2:1 the equation can be rebalanced.

$$a + 6c + d = 1 \textit{ (carbon)} \quad (4)$$

$$2b + 12c = 2 \textit{ (hydrogen)} \quad (5)$$

$$a + b + 2d + e = 0.42m \textit{ (oxygen)} \quad (6)$$

The a term is dropped by rearranging equation 1 and substituting into equation 4

$$a = dQ \quad (7)$$

$$a + 6c + d = 1 \rightarrow dQ + 6c + d = 1 \quad (8)$$

The c term is dropped by rearranging equation 2 and substituting into equation 8

$$c = dQ' \quad (9)$$

$$dQ + 6c + d = 1 \rightarrow dQ + 6dQ^{'} + d = 1 \quad (10)$$

Rearranging in terms of d yields

$$d = \frac{1}{Q + 6Q^{'} + 1} \quad (11)$$

To drop the b term, equation 9 is first substituted into equation 5 and put in terms of b.

$$2b + 12dQ^{'} = 2 \quad (12)$$

$$b = 1 - 6dQ' \quad (13)$$

Equation 3 is rearranged to

$$e = dQ" \quad (14)$$

The a, b, and e terms are then substituted into equation 6 to make

$$dQ + (1 - 6dQ') + 2d + dQ" = 0.42m \quad (15)$$

Dividing by d

$$0.42\frac{m}{d} = Q + \frac{1}{d} - 6Q' + 2 + Q" \quad (16)$$

Substituting d on the right side

$$0.42\frac{m}{d} = Q + (Q + 6Q' + 1) - 6Q' + 2 + Q" \quad (17)$$

Simplifying

$$0.42\frac{m}{d} = Q" + 2Q + 3 \quad (18)$$

The mole fraction of $CO_2$ is calculated by

$$fCO_2 = \frac{d}{a + 2c + d + e + 0.79m - \frac{e}{2}} \quad (19)$$

Multiplying right side by (1/d)/(1/d)

$$fCO_2 = \frac{1}{\frac{a}{d} + \frac{2c}{d} + 1 + \frac{e}{d} + 0.79\frac{m}{d} - \frac{e}{2d}} \quad (20)$$

Substituting in Q, Q', and Q"

$$fCO_2 = \frac{1}{Q + 2Q' + 1 + Q" + 0.79\frac{m}{d} - \frac{Q"}{2}} \quad (21)$$

Multiplying right side by 0.42/0.42

$$fCO_2 = \frac{0.42}{0.42Q + 0.84Q' + 0.42 + 0.21Q" + 0.79(0.42\frac{m}{d})} \quad (22)$$

Substituting 0.42m/d

$$fCO_2 = \frac{0.42}{0.42Q + 0.84Q' + 0.42 + 0.21Q" + 0.79(Q" + 2Q + 3)} \quad (23)$$

Simplifying

$$fCO_2 = \frac{0.42}{2.79 + 2Q + 0.84Q' + Q"} \quad (24)$$

To convert to $\%CO_2$ multiply right side by

$$\frac{100\frac{100}{42}}{100\frac{100}{42}} \quad (25)$$

To yield

$$\%CO_2 = \frac{100}{6.64 + 4.76Q + 2Q' + 2.38Q"} \quad (26)$$

The other pollutants can now be calculated in terms of $\%CO_2$ and the appropriate Q value.

$$\%CO = \%CO_2 * Q \quad (27)$$

$$\%HC = \%CO_2 * Q' \quad (28)$$

$$\%NO = \%CO_2 * Q'' \quad (29)$$

**Calculation for Q Values** *(37).*

As stated previously, values for Q are determined by plotting the 50 points of ½ second post block beam data. Either one of two methods can then be used to pull out the Q values. In method B, three plots are made of CO vs. $CO_2$, HC vs. $CO_2$, and NO vs. $CO_2$. Values Q, Q', and Q", respectively, are determined by the slopes of these plots. Data are considered valid if there is less than 20% uncertainty in the slope. In method A, Q values are calculated by individually integrating the line graph of the data set collected by each channel as a function of time. Ratios of each integration are then taken. This method may give unsuitable data if there is an improper baseline adjustment. It also fails to determine if pollutants detected are from the same vehicle.

**Smoke factor – UV**

The smoke factor of an exhaust stream can be represented as the ratio of the particle mass per unit fuel.

$$\frac{N_P * \left(\frac{grams_{part}}{cm^2}\right)}{N_F * \left(\frac{grams_{fuel}}{cm^2}\right)} \quad 30$$

Along with the other measurements, a beam of UV radiation of wavelength of 230nm is also passed through the exhaust stream. The transmittance is represented by the equation

$$T = e^{k_{UV} N_P} \quad 31$$

Where $k_{UV}$ is the sum of the absorption and scattering coefficients of soot is 230nm. For this parameter a value of $18 \cdot 10^4$ $cm^2/g$ is used *(38)*. $N_P$ is the density in grams/$cm^3$ multiplied by the path length. From this equation $N_P$ can be calculated.

$$N_P = \frac{-ln(T)}{k_{UV}} \quad 32$$

Because carbon containing compounds in the exhaust can only come from fuel, the moles of fuel can be directly compared to the sum of the carbon containing combustion products.

$$N_F = N_{CO} + N_{CO_2} + N_{HC} \quad 33$$

If one mole of fuel is considered to be $CH_2$, then it will have a mass of 14grams. Putting $N_F$ in terms of cross-sectional area gives

$$\frac{N_F(moles) * \left(\frac{14 g_{fuel}}{mole}\right)}{cm^2} = \frac{(N_{CO} + N_{CO_2} + N_{HC}) * (moles) * \left(\frac{14 g_{fuel}}{mole}\right)}{cm^2} \quad 34$$

Therefore the final smoke factor equation can be represented by

$$\left[\left[\left(N_{CO}+N_{CO_2}+N_{HC}\right)*(\%.cm)\right]\left(\frac{1}{100\%}\right)*\frac{\mathrm{N_L}\left(\frac{\text{molecules}}{\text{cm}^3}\right)}{\mathrm{N_{AV}}\left(\frac{\text{molecules}}{\text{mole}}\right)}\right]*\left(\frac{14g_{fuel}}{mole}\right) \quad 35$$

Where

$N_L$ is Loschmidt's Number $2.479*10^{19}$ molecules per $cm^3$ at 1atm and 20°C

$N_{AV}$ is Avogadro's Number $6.023*10^{23}$ molecules per mole

Calculating equation 35

$$\left(N_{CO}+N_{CO_2}+N_{HC}\right)*5.76210^{-6}\left(\frac{14g_{fuel}}{\text{cm}^3}\right) \quad 36$$

Substituting the right side of equation 32 in the numerator and equation 35 in the denominator of equation 30 yields

$$\text{sf}=\frac{\frac{-\ln(T)}{k_{UV}}\left(\frac{g_{\text{part}}}{\text{cm}^3}\right)}{\left(N_{CO}+N_{CO_2}+N_{HC}\right)*5.76210^{-6}\left(\frac{14g_{fuel}}{\text{cm}^3}\right)} \quad 37$$

Calculating equation

$$\text{sf}=\ 0.964*\frac{-\ln(T)\left(\frac{g_{\text{part}}}{\text{cm}^3}\right)}{\left(N_{CO}+N_{CO_2}+N_{HC}\right)\left(\frac{g_{fuel}}{\text{cm}^3}\right)} \quad 38$$

In practice, 0.964 can be treated as 1 and therefore equation 37 becomes

$$\text{sf}=\frac{-\ln(T)}{\left(N_{CO}+N_{CO_2}+N_{HC}\right)}\frac{\left(\frac{g_{\text{part}}}{\text{cm}^3}\right)}{\left(\frac{g_{fuel}}{\text{cm}^3}\right)} \quad 39$$

Smoke factor is reported as SF in 10g/kg. Canceling the $cm^3$ units and converting equation 39 yields

$$\frac{(g_{\text{part}})}{(g_{fuel})} * \frac{100(g_{fuel})}{(100 g_{fuel})} * \frac{10}{10} * \frac{100 g_{fuel}}{\frac{1}{10}(kg_{fuel})} * \frac{(10\text{g}_{\text{part}})}{10(\text{g}_{\text{part}})} = \frac{(10 gram_{\text{ particles }})}{(\text{kg}_{fuel})} \quad 39$$

After conversion equation 39 becomes

$$\text{SF} = \frac{-\ln(T) * 100}{(N_{CO} + N_{CO_2} + N_{HC})} \frac{(10 g_{\text{pa rticles}})}{(kg_{fuel})} \quad 39$$

All RSD data are reported in units SF.

**Error/Uncertainty/Operation Concerns**

The RSD system is inhibited by outside influences. Heavy rain, snow, or dust either in the air or kicked up from the road can cause too much interference. Too much water vapor, in the form of aerosol liquid droplets, can interfere with HC measurement or completely block all channels if all wavelengths are absorbed or scattered. Vibrations affecting optical alignment must be monitored. The REF channel alleviates this problem, though not perfectly.

The effect of instrument noise can measured in real world operating conditions. It is useful to use negative absorbance data sets to measure noise, because negative emissions cannot occur. This will mean that all of these data points must somehow be influenced by noise. Because the RSD can be automated to take measurements throughout the day for lengthy periods of time, a large database (out of a total pool of over 10,000 measurements) of negative values can be tabulated. The emissions points on the negative end of the distribution are binned. The log of the frequency of occurrence is

then plotted against the magnitude of the negative emission. The negative slope of this line is called the Laplace factor and is a measure of the uncertainty. Each pollutant has an associated Laplace factor. Also, the uncertainties in the means caused by this factor become smaller with fleet averaging. For a fleet average of 10,000 the uncertainty is reduced by 100. One study showed individual Laplace factors of 17.1, 7.64, and 0.57g/kg for CO, HC, and NO respectively *(39)*.

Another concern is differences in measurement relative to the operating mode of the vehicle. One study compared RSD measurements of CO an HC between a Fuel Efficiency Automobile Test (FEAT) detector and a GM On-Board (GMOB) sensor developed by General Motors Research Laboratories for different operation modes. Results of these tests showed ±5% CO and ±15% HC variability between instruments. Although the uncertainty for this measurement is high, the total contribution of HC to the total exhaust is very small. Because the HC ratio is added to the CO and $CO_2$ ratios for the smoke factor calculation, its small relative size does not significantly change the results.

## 2.2 ETaPS

The ETaPS is able to detect particles sizes between approximately 10nm and 3μm, and from concentrations of approximately 0.1 to 100mg/$m^3$ (depending on size and flow). The operating limits for the device are flow rates between 3 to 50m/s and exhaust temperatures of less than 500ºC. To remain under the required operating temperature

when connected to a vehicle exhaust pipe, the instrument requires a "sheath" air flow of 50-60lpm. This maintains an air flow isolated from the exhaust flow that cools the casing. The output signal ranges from 0-10V with a reference signal of 0-10V. The power required to maintain the high voltage is 12-18 VDC with 10W maximum (*40*). Diagrams of the inner parts of the ETaPS can be seen in **Figure 22**. The instrument hookup to a tailpipe connector is shown in **Figure 23**.

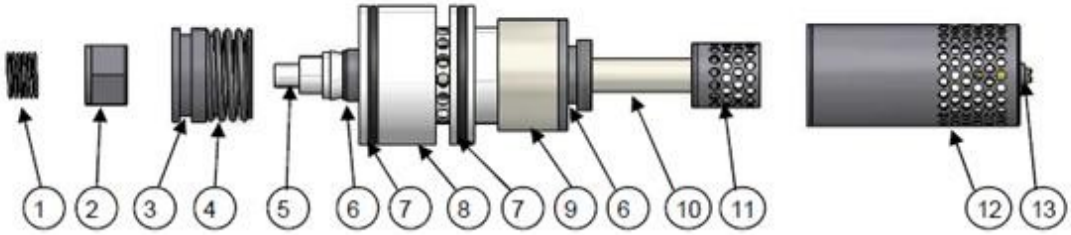


1) Spring contact
2) Svageloc nut
3) Assembly ring
4) Spring
5) Plastic insulator
6) Metal core
7) O-ring
8) Teflon insulator
9) Ceramic insulator
10) Ceramic insulator bar
11) Inner charging chamber
12) Outer charging chamber
13) Corona needle

**Figure 22: Exploded diagram of ETaPS inner parts.**

**Figure from reference *(40).***

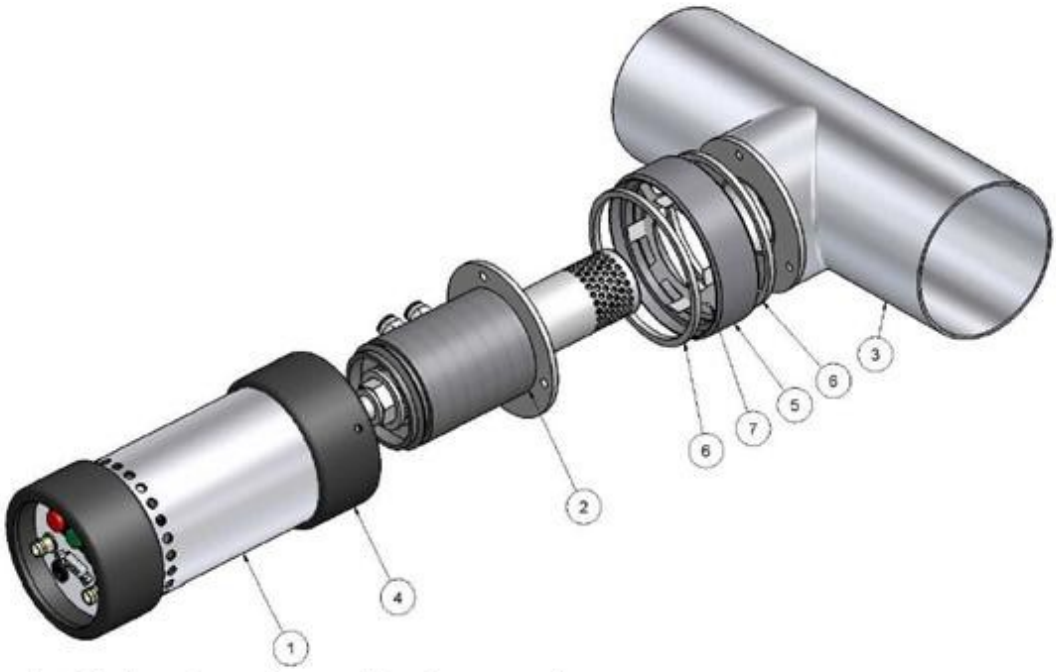


1. Electronics and user interface panel
2. Sensor head, frame and sheath air connectors
3. Tailpipe connection piece
4. Rubber cushion
5. Sleeve
6. Ceramic gaskets
7. Ground contact

**Figure 23: Exploded diagram of ETaPS outer parts.**

**Figure from reference *(40).***

### 2.2.1 Theory of Operation

Theory of operation for the ETaPS is summarized from the user manual version 1.0 *(40)*. The ETaPS works on the principle of charging particles. There are two methods in which to accomplish this: field and diffusion charging. Both methods work on the principle of transferring charge from ionic current to a particle surface, but differ on how these ions flow to the particle. In field charging, an ion is accelerated toward a particle by an external electric field. Charge builds on the particle until the point that new charges are repelled by the charged particle. In diffusion charging, ions move due to their thermal energy. If an ion has high enough thermal energy, it can collide with the particle. A particle charged by diffusion is charged independently of external field strength, and is governed by the field created by the charged particle.

The ETaPS is a type of diffusion charger and a diagram of its basic operation is shown in **Figure 24**. The charger is made up of two electrodes. One electrode is small metal thread on the end of a screw. The other is a needle attached by a thin rod to a metal cup located approximately 5mm away from the wire. The voltage between the two electrodes is 5kV. The wire portion is attached to an outer mesh which is at the potential of virtual ground relative to the instrument chassis. The needle electrode is connected to the inner mesh of the device and is at a negative potential. The resulting field lines created from the electric field between the two electrodes are in the shape of parabolas.

Corona discharge current flows between the two electrodes and is kept constant and thus keeping the ion density constant. The particles flowing through the perforations in the outer and inner mesh acquire charge level from the corona from diffusion charging. The charge level of a particle is the result of three things. First, it is dependent on the ion density of the field. This density is kept constant by adjusting the current. Secondly, it is dependent on the particle's residence time inside the chamber. A longer residence time increases the charging efficiency, and therefore increases the signal. Residence time is dependent on the flow rate. One study showing the effect of flow rate on the ETaPS signal is show in **Figure 25**. The final factor is the active surface area. The surface area is related to particle size, but there is no direct correlation because particles are not perfect spheres. Useful information about particle size can be inferred from signals of particles for which the shape distribution is known.

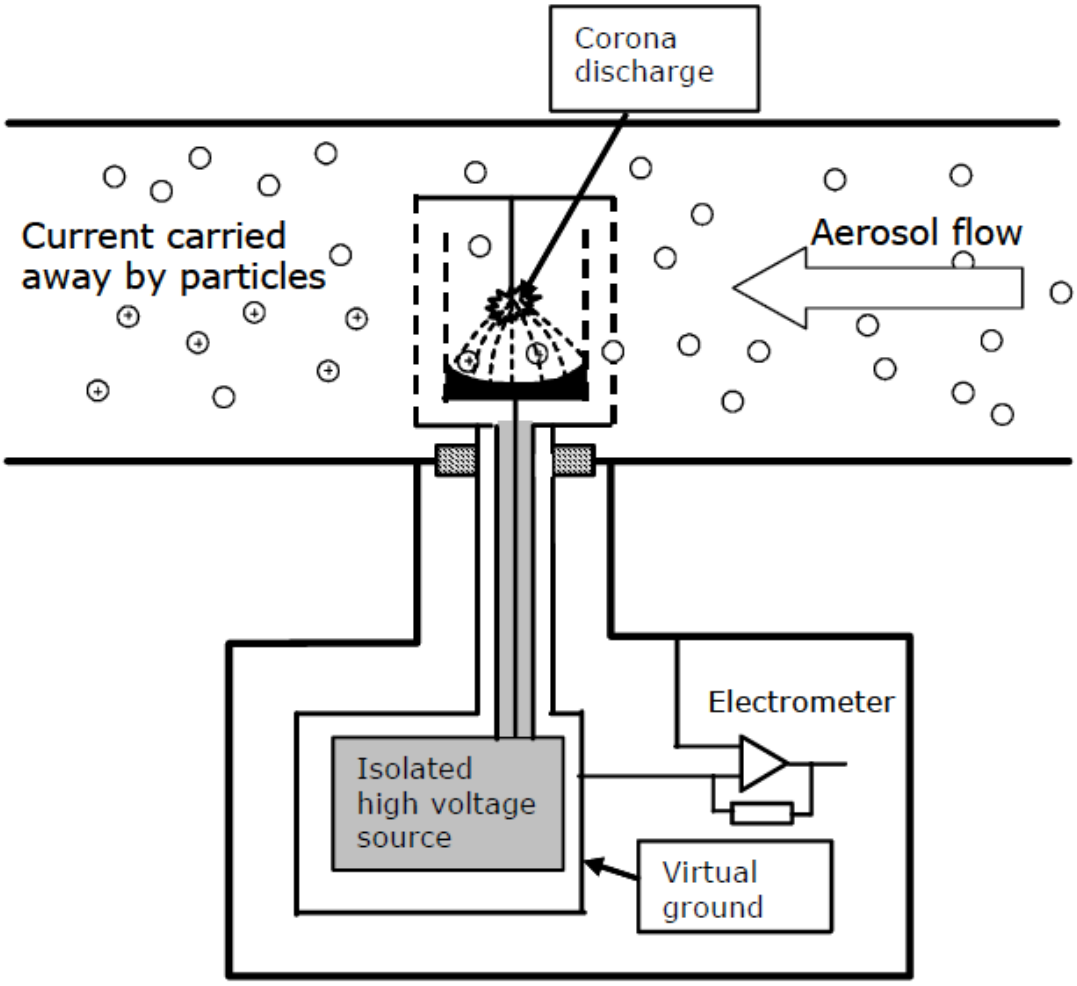


**Figure 24: ETaPS block diagram.**

**Figure from reference *(40)*.**

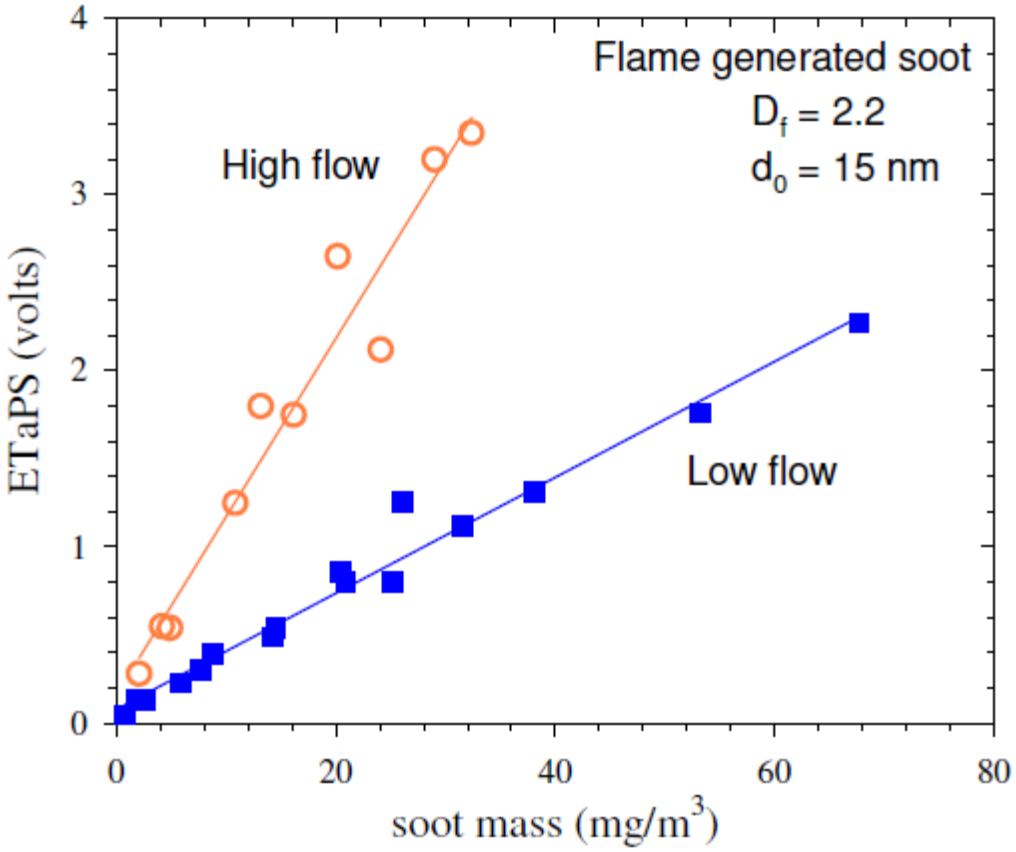


**Figure 25: Ford study of ETaPS signal vs. particle mass calculated from SMPS data at two different flow rates.**

**Figure from reference *(34)*.**

Particles flowing through the corona discharge take on ions due to Brownian motion. A current is required to maintain chassis voltage at zero potential. An electrometer measures this current, which is amplified to a signal in units of volts.

Although the words "particle sensor" appear in the acronym for the title of the instrument, it does not directly measure mass. The ETaPS is dependent on two factors in order to make a mass determination. The first factor is flow rate. Flow rate can affect ETaPS in two separate ways. First, higher flow rate results in higher particle flux through the corona. This raises the signal. This could make it appear as if there was more particle mass than was actually present. The second factor, affecting the signal in the opposite manner, is the residence time of the particle. Higher residence times lead to higher signals. Higher flow rate leads to shorter residence times, and the inverse is also true. The effect is not equally compensating, and therefore may be an influencing factor in the final measurement.

The second factor is the size distribution of the particles measured. The ETaPS signal is proportional to the active surface area of the particles passing the sensor. Because surface area is not proportional to mass, ETaPS measurements cannot be taken as direct mass measurements. Comparisons may be made between the two depending on the composition of the exhaust. Particle size distribution also has an effect on the residence time of a particle. A correlation of the ETaPS signal vs. a direct measure of particle mass for a particular type of exhaust stream would have to be made before a direct comparison could be made. A measurement of this correlation is one goal of this work.

One final concern is particle loss. “Most particle losses in the sensor are caused by turbulent deposition on the sensor surfaces *(41).*” Losses are reported to be negligible in comparison to signal, but no specific numbers are reported on the size of these losses or their proportion to the total signal.

The ETaPS outputs one measurable quantity, volts. This signal can be used, with many assumptions about the exhaust stream passing the ETaPS, to make a mass concentration calculation. The steps in this calculation are detailed in a study done by Tampere University *(41).* Preferably however, a correlation between the ETaPS and another mass measurement device can be made, and assumptions about the sample and complex calculations can be avoided.

# Chapter 3: Experimental Setup

\

Below is a list of make and manufacturer of the specific equipment used in the study. The complete experimental setup of each piece is described in more detail in following sections.

- ETaPS
  - Model A SN#: 53101
  - Model B SN#:53105
  - Manufacturer: Dekati
    - Osuusmyllynkatu 13
      FIN 33700 Tampere
      Finland
- Oxygen sesnor
  - Model: OXY 6200 SN#: 45406236
  - Manufacturer: Engine Control and Monitoring (ECM)
    - Los Altos, California
- DAQ
  - Model USB6009 SN#: 13C7C04
  - Manufacturer: National Instruments
    - Austin, Texas
- Airpump
  - SN#:
  - Manufacturer - K N F Neuberger
    - 2 Black Forest Rd.
      Trenton, NJ 08691
- Honda 1KW generator
- RSD 4600
  - SN#: 4639
  - Manufacturer – Environmental Systems Products (ESP)
    - Tuscon, AZ
- Gravimetric
  - West Virginia University's Transportable Heavy Duty Vehicle Emissions Testing Laboratory (THDVETL) *(42)*.

## 3.1 ETaPS

Two ETaPS models were provided by Dekati for use in testing. Both acted with similar response and carried a reference voltage between 3-6V *(40)*. The ETaPS is equipped with two inputs and four digital and two analog outputs. One input turns the corona on and off, the other toggles between high and low range. Switching between high and low range changes the sensitivity by a factor of 10. High range measures with lower sensitivity and low range measures with higher sensitivity. Digital outputs indicate whether the corona charger is on or off, if range is high or low, if the instrument is operating properly, and if the instrument is in "over range". If overheated, the operating light will blink and eventually shut off. If the ETaPS measures more than 10V the "over range" light will come on. The two analog outputs are the signal and reference and are measured as volts. The model A ETaPS does not appear to have a working high/low toggle or "over range" indicator. The model B ETaPS high/low toggle functions properly, but also does not have a working "over range" indicator. The ETaPS instrument does not come equipped with data collection capabilities and must be setup by the user. Provided with the ETaPS is a 14 pin cable connection a shown in **Figure 26**. Below is a description of the function of connectors to the ETaPS system and wiring scheme to a data acquisition system.

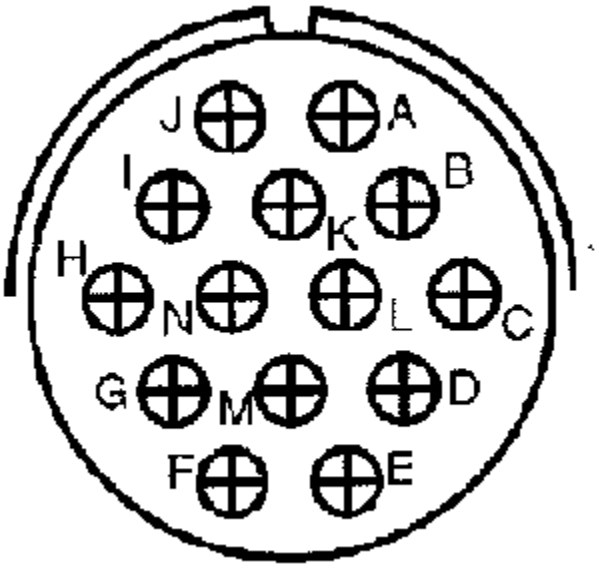


**Figure 26: Cable junction letter assignment.**

### 3.1.1 Connector Pins

A – Charger ON (Input)

Controls a digital switch (0/+5V logical level) that turns the corona charger on and off when the instrument is powered.

B – High Range ON (Input)

Toggles the high/low range by a digital switch (0/+5V logical level)

C – Digital Ground

D – High Range ON (Output)

Digital output (0/+5V). A reading of +5V indicates high range is active.

E – Charger ON (Output)

Digital output (0/+5V). A reading of +5V indicates corona charger is on.

F – Input Voltage OK (Output)

Digital output (0/+5V). A reading of +5V indicates operational voltage is OK

G – Over range (Output)

Digital output (0/+5V). A reading of +5V indicates measurement exceeds the 10V detection limit. This feature does not seem present on our model.

H – Chassis ground

Ground wire connected to instrument chassis. Wire terminal was found to be empty on our model.

I – Power input +

12-18 VDC, 0.5 A

J – Power input –

K – Reference voltage +

L – Reference voltage –

M – Signal output +

0-10V signal output

N – Signal output –

### 3.1.2 Oxygen Sensor

Manufacture: Engine Control and Monitoring (ECM)

Model: OXY6200

Range: 0.0 to 25.0 $\%O_2$

Accuracy: < ±0.1 $\%O_2$

Response Time: < 150ms

Output: 1 – 5.5V linearized with $\%O_2$

The oxygen sensor is calibrated to report a voltage equivalent to the $\%O_2$ measured. For direct measurements, the instrument should undergo an initial calibration, and the final $\%O_2$ reported is adjusted by the relationship of the reported voltage to the original calibration voltage give in the equation

$$\%O_2 m = \left[\frac{Vout - 1.0}{Vcal - 1.0}\right] * \%O_2 cal$$

Where

$\%O_2$cal = 20.95

The $\%O_2$ can then be further corrected for pressure change after calibration. However, the pressure change in the exhaust stream is unknown.

$$\%O_2a = \% \frac{O_2m}{[1.000 + 6.459 * 10^{-4}(P - Pcal) - 1.054 * 10^{-7}(P - Pcal)^2]}$$

Examing the equation reveals that the effect of pressure changes on the signal are very minor and below the round off point of the data collection.

**Calculating %$CO_2$ from %$O_2$**

Given the combustion equation

$$CH_2 + \mathbf{m}(0.21O_2 + 0.79N_2) \rightarrow H_2O + CO_2 + \mathbf{a}O_2 + \mathbf{b}N2$$

$$fO_2 = \frac{a}{2 + a + b} \quad (1)$$

$$fCO_2 = \frac{1}{2 + a + b} \quad (2)$$

Therefore

$$fCO_2 = \frac{\%O_2}{a} \quad (3)$$

Given

$$0.42n = 3 + 2a\ (oxygen) \quad (4)$$

$$0.79n = b\ (nitrogen) \quad (5)$$

%$CO_2$ can be solved for.

Rearranging equation 4

$$n = \frac{3 + 2a}{0.42} \quad (6)$$

Substituting n into equation 5

$$b = \frac{0.79(3 + 2a)}{0.42} \quad (7)$$

Substituting b into equation 1

$$fO_2 = \frac{a}{2 + a + \frac{0.79(3 + 2a)}{0.42}} \quad (8)$$

Solving for a

$$a = \frac{3.21(\%O_2)}{0.42 - 2(\%O_2)} \quad (9)$$

Substituting into equation 2

$$fCO_2 = \frac{fO_2}{\frac{3.21(f\%O_2)}{0.42 - 2(fO_2)}} = \frac{(0.42 - 2(fO_2))}{3.21} \quad (10)$$

$$\%CO_2 = fCO_2 = \frac{(42 - 2(\%O_2))}{3.21} \quad (11)$$

### 3.1.3 O2 Cable interface

$O_2$ sensor was purchased prewired to a proprietary DAQ box. The four relevant output wires, power +, -, and signal +, -, were connected to the fabricated housing box. Power lines were connected to a 15 V power supply. Signal lines were connected to a separate National Instruments DAQ box.

### 3.1.4 Digital Acquisition (DAQ)

All ETaPS I/O communication was performed through a third party digital acquisition box. The DAQ used was a B-Series National Instruments USB-6009. The analog input channels have a 48kS/s sampling rate, 14 bit resolution, and a measurement range of -10 to 10V.

NI USB – 6009 terminal assignments in the downloadable pdf from National Instruments website are from the 6008 model and do not match up. The proper diagram is as follows.

| | |
|---|---|
| 1. GND | 17. P0.0 |
| 2. AI0 | 18. P0.1 |
| 3. AI4 | 19. P0.2 |
| 4. GND | 20. P0.3 |
| 5. AI1 | 21. P0.4 |
| 6. AI5 | 22. P0.5 |
| 7. GND | 23. P0.6 |
| 8. AI2 | 24. P0.7 |
| 9. AI6 | 25. P1.0 |
| 10. GND | 26. P1.1 |
| 11. AI3 | 27. P1.2 |
| 12. AI7 | 28. P1.3 |
| 13. GND | 29. PFI0 |
| 14. AO0 | 30. +2.5V |
| 15. AO1 | 31. +5V |
| 16. GND | 32. GND |

### 3.1.5 Wiring Assignment

2. AI0 : $O_2$ Signal Output +

3. AI4 : $O_2$ Signal Output -

5. AI1 : M – Signal Output +

6. AI5 : N – Signal Output –

8. AI2 : K – Reference +

9. AI6 : L – Reference –

14. AO0 : A - Charger ON (Input)

15. AO1 : B - High Range ON (Input)

17. P0.0 : E - Charger ON (Output)

18. P0.1 : D - High Range ON (Output)

19. P0.2 : F – Input Voltage OK (Output)

20. P0.3 : G – Over Range (Output)

All ground wires were bolted to the instrument case.

## 3.2 Proof of Concept

Before road and dynamometer tests were to be done in West Virginia, the ETaPS was run through some basic setups to test its operating ability. The first studies in this program were carried out in Denver and showed that the ETaPS, oxygen sensor, power supplies, laptop data acquisition system, and generator could be successfully mounted and removed from different types of trucks in various configurations. The second part of these studies was to test the ETaPS in real world driving situations.

### 3.2.1 Mounting an ETaPS on a Modern Truck

The first step in truck measurements was mounting the ETaPS securely to an exhaust pipe. For this, the ETaPS was attached to a telescoping pole. The pole could be attached to piping by two hose clamps with metal bars welded to them. The hose clamps could be placed over various sizes of exhaust piping. The metal bars from the hose clamps could then be attached to the pole on the ETaPS. In this manner, the ETaPS could be attached to an exhaust pipe in 5-10min. The ETaPS is connected to its support pole by a rotatable hinge allowing a full range of motion from completely vertical to horizontal. This allows the ETaPS to be aligned with the various types of exhaust shapes.

**Figure 27** shows the ETaPS connected to a 5 inch diameter exhaust pipe curved back and to the right side of the cab of the truck. The padding is a vest put between the

hose clamps and the exhaust pipe to protect it from scratches. For on road use, insulation from any auto parts store would be suitable protection.

**Figure 28** shows the ETaPS connected to a 7 inch diameter straight exhaust pipe. The ETaPS here has been adjusted to sit horizontally over the pipe.

**Figure 27: ETaPS mounted on the 5” tailpipe of a 2000 MY Peterbilt tractor. The cloth was used to protect the vehicle (for sale in a dealer lot) from scratches.**

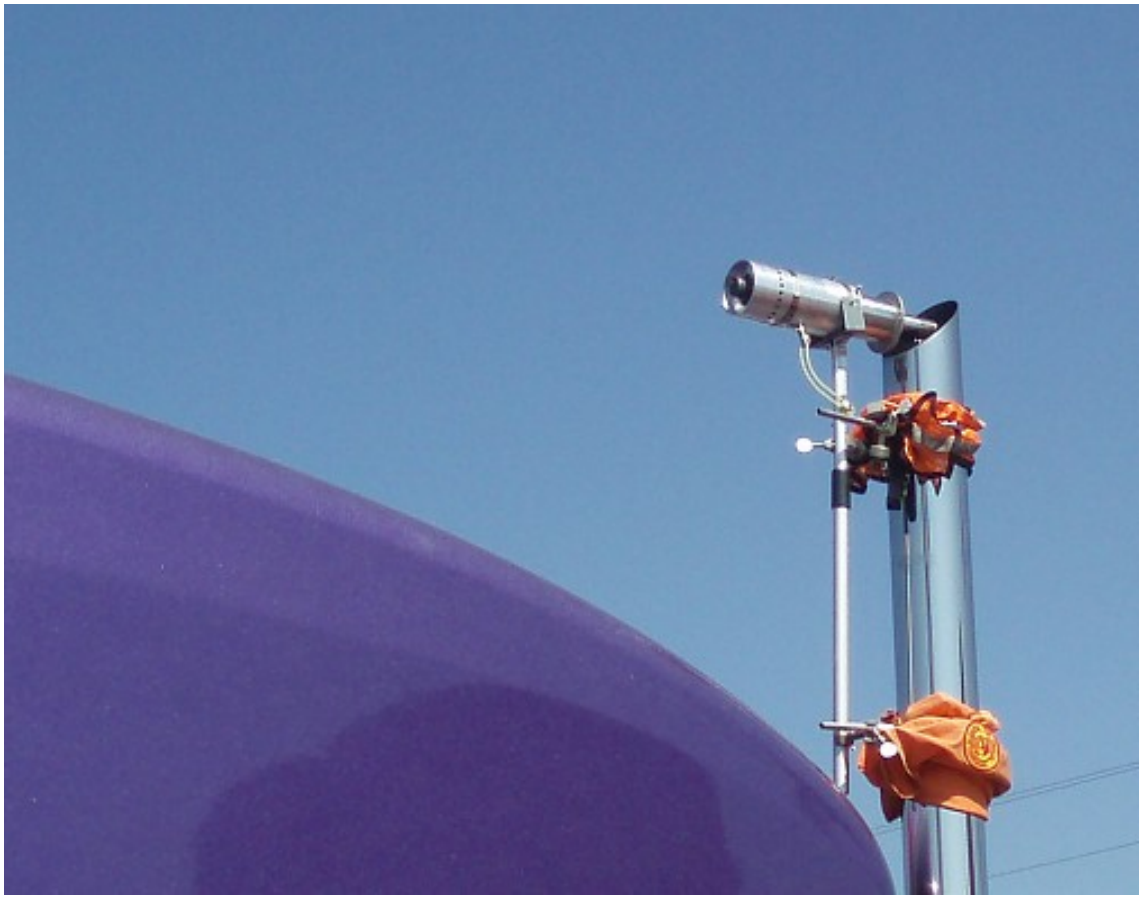

**Figure 28: ETaPS on a 7” exhaust stack from a DPF equipped 2006 MY Peterbilt tractor.**

### 3.2.2 Preliminary ETaPS Results from Denver

Prior to the trip to Westover, West Virginia the ETaPS was attached to a Caterpillar Diesel front loader and gasoline powered Winnebago to verify functionality and test the data acquisition system.

The Caterpillar was measured before the data recording program was finalized. Samples were taken every second but they were the final value for a data stream acquired at 100Hz. All supplemental equipment was strapped atop the vehicle. The Caterpillar was driven for a few passes around a building for a few minutes. **Figure 29** shows the mounting and **Figure 30** shows the ETaPS data from the run.

The Winnebago and all later results were again monitored at 100Hz but stored the average every second. All recording equipment was stored inside the vehicle with connecting wires run through the back door. The vehicle was driven in a variety of conditions from stop and go city traffic to highway speeds. **Figure 31**and **Figure 32** show different angles of the mounting to the low level exhaust, and **Figure 33** shows the ETaPS data from the run.

Both tests, as expected, demonstrate the ETaPS measuring at zero volts when there were few particles in the exhaust, and increased signal when accelerating, therefore demonstrating that simply placing the ETaPS where it intercepts the exhaust did not eliminate its potential usefulness. Vibrations from all but very heavy jarring did not contribute to signal in any noticeable way. The results showed a reasonable expectation

that the outdoor mounting of the ETaPS could provide useful particle information upon exposure to realisic truck exhaust in Westover.


**Figure 29: ETaPS mounted on a diesel Caterpillar front loader. As in all installations power was provided from an on-board 110V generator grounded to the vehicle**

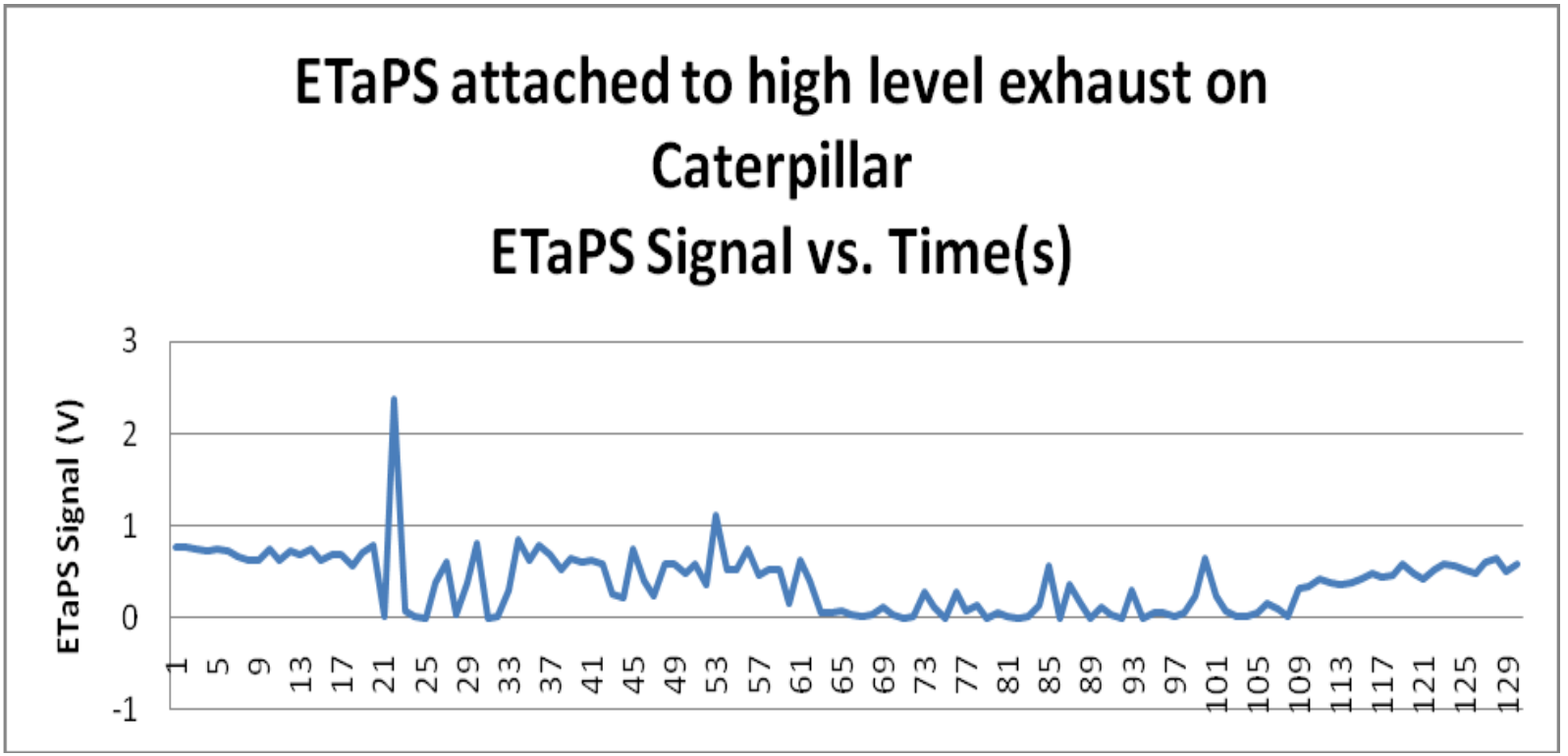


**Figure 30: ETaPS signal results versus time showing the expected particle response upon startup and upon higher power towards the end with closer to zero when the engine was warmed up and under low load in the 60-85 second time frame.**

**Figure 31: ETaPS mounted analyze the particles exiting the exhaust of a gasoline powerd 1996 Winnebago Itasca motor home powered by a GM 454 cu.in. V8 engine.**


**Figure 32: Alternate view of Winnebago ETaPS mounting.**

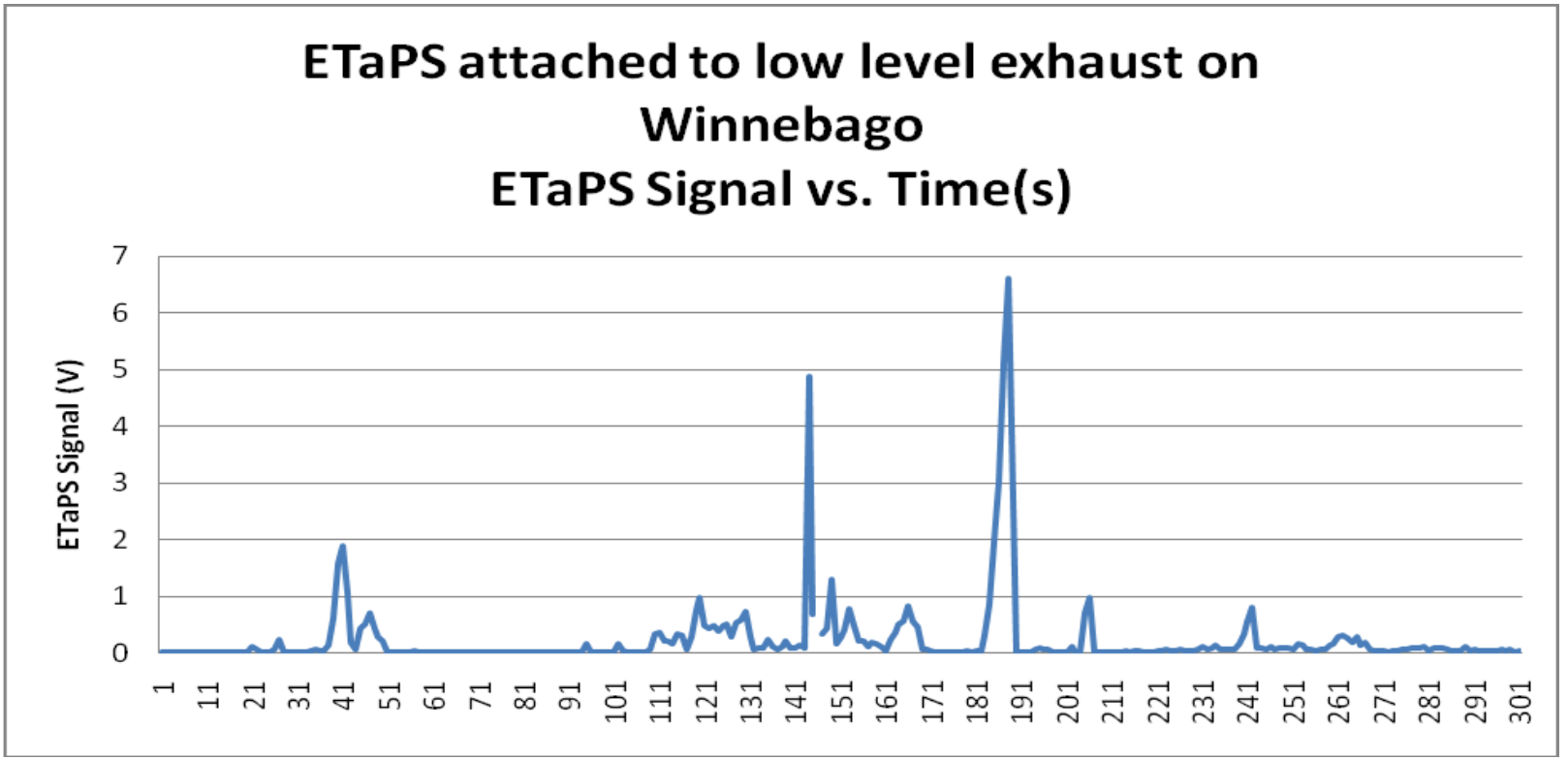


**Figure 33: Typical on-road ETaPS trace versus time for the gasoline powered motor home showing peaks for each acceleration event and readings indistinguishable from zero under cruise conditions.**

## 3.3 Experiments at the WVU facility in WV

The major experimental aspect of this project was to compare RSD and ETaPS readings to gravimetric readings obtained using the West Virginia University HDDV dynamometer facility in Westover WV. The experimental design was a two step process. In the first step, a tractor/trailer combination was to be equipped with an ETaPS and driven at various speeds and loads past the outdoor RSD system. In the second step the same truck was to be taken into the facility and subjected to various cycles at a comparable load while simultaneously the ETaPS signals and the pollutant gas concentrations and gravimetric filter data were obtained.

This study focused on the emissions evaluation of 44 heavy-duty vehicle configurations. Each vehicle configuration was tested on-road concurrently with RSD and ETaPS, as well as on WVU's chassis dynamometer, with simultaneous ETaPS measurements, in order to correlate PM mass emissions. Per WVU's telecom with ESP (Niranjan Vescio), California Air Resources Board (CARB) (John Collins), and University of Denver (Don Stedman) the following test vehicle configurations were selected.

1. Five vehicles (pre-2007 model year) without diesel particulate filters (DPFs) were tested in the initial phase of the study.
2. An additional five vehicles (post-2007 model year) that were equipped with a DPF and/or an oxidation catalyst were tested during the second phase of the study.

3. For each of the post-2007 vehicles (five), the exhaust system was modified by installing a bypass loop around the aftertreatment system. The amount of bypass was controlled to alter the exhaust stream PM concentration downstream of the aftertreatment system in order to simulate a DPF failure, as well as attempt to quantify the low-level sensitivity/performance of the ETaPs.

### 3.3.1 Facility

Testing was done at the Westover WVU facility. A satellite picture of the testing site is shown in **Figure 34**.


**Figure 34: Satellite photo of Westover WVU facility and surroundings. The building at the top right, with visible trucks parked on the east side, is the dynamometer facility. The RSD scaffolding and measurement system were set up at the black dot located at in the center south end of the parking lot of the testing facility. RSD measurements were taken across industrial park road. All readings were taken with truck traveling on an uphill slope westbound. Frequently the repeat measurements were made by looping around the small rectangle of roadways starting with a left turn down the center of the picture.**

**Figure from reference *(43).***

### 3.3.2 Test Vehicles

Ten trucks were tested total. Five of these were pre-2007 trucks and were considered likely high emitters. The five other trucks, model years 2007 and later, were Diesel Particle Filter (DPF) equipped and considered low emitters. The newer trucks were then tested again with modified exhausts bypassing the DPF's. Some vehicles were equipped with low level exhausts and were modified with extra piping to raise the exhaust to a height measurable by the RSD on the scaffolding. With the exclusion of the two buses and Penske boxt truck, when tested for the RSD the vehicles were measured unloaded and loaded with weighted trailers in order to increase engine load.

| Test Vehicle | Gross Vehicle Weight Rating (GVWR) | Measured Vehicle Curb Weight (lbs.) | Vehicle Test Weights | |
|---|---|---|---|---|
| | | | ETaPS/RSD | ETaPS/WVU THDVETL |
| 1995 Mack | 52,000 | 17,360 | 39,080 | 42,352 |
| 1996 Peterbilt | 46,000 | 20,340 | 42,160 | 42,352 |
| 1995 Freightliner | 51,954 | 19,160 | 40,900 | 42,352 |
| 1999 Peterbilt | 33,000 | 14,900 | 33,580 | 30,000 |
| 2005 Thomas Bus | 36,200 | 22,860 | 22,860 | 35,000 |
| 2009 Thomas Bus* | 36,200 | 22,220 | 22,220 | 35,000 |
| 2008 Volvo Tractor* | | 18,160 | 37,060 | 42,000 |
| 2008 International Box Truck* | 25,500 | 15,260 | 15,260 | 25,600 |
| 2008 Volvo Day Cab* | 50,350 | 16,600 | 35,080 | 42,000 |
| 2007 International* | 52,000 | | | 42,000 |

Note: The GVWR of a tractor is not the same as the Combined GVWR of tractor and trailer (typically 80,000 lbs.)

* DPF equipped

**Table 1 Vehicle Test Weights**

### 3.3.3 ETaPS vs. RSD

The experimental setup is shown in **Figure 35**. The majority of truck exhaust pipes, and for all of the trucks used in this study, are high level. The RSD was placed on scaffolding to raise the detection beam approximately 14ft from the ground in order to measure this high level exhuast. Because of the sensitive nature of RSD to vibrations, the scaffolding was secured with guy wires. Contact with the scaffolding was limited to alignment performed before the start of each day's measurements.

In normal operation, vehicles block the RSD which initiates measurement. The RSD in the scaffolding setup is never physically blocked. A second repositionable beam is used for this purpose. This beam was sometimes setup to pass across the path of the truck. When the truck blocked the beam, an RSD measurement was taken. However, placement of the beam to have a beam block occur where the RSD was aligned with the exhaust was not always practical. Often, the beam was artificially blocked by hand to be timed with the exhaust pipe passing by the RSD.

**Figure 35: RSD setup outside WVU testing facility. To the rear of the rear scaffolding is the Mobile laboratory (Itasca) which housed the computer for the RSD.**

#### *3.3.3.1 ETaPS Setup*

The ETaPS setup as described in the Dekati manual is shown in **Figure 36**. The ETaPS is mounted to a metal tailpipe connector piece, and tubing connects it to the exhaust. Exhaust flows through the tubing, through the connector piece, across the corona discharge, and out the open end of the connector piece.

The setup used in this study is shown in **Figure 37** and **Figure 38**. The tailpipe connector piece was not used, and instead the tip of the ETaPS with the corona discharge was placed directly in the exhaust stream, 1-3" from the tailpipe opening. The angle of the ETaPS was adjustable and the instrument was angled to be parallel to the exhaust pipe opening face.

The oxygen sensor was mounted directly in the exhaust stream at the opening of a vehicle tailpipe. The sensor comes equipped with a 5/8" threading designed to fit engine exhaust or air intake. A strip of metal was bolted to the sensor using this fitting and used as a surface to clamp the instrument to the exhaust pipe. The airpump supplying sheath air and data aquistion system were either secured to metal gratings located between the truck cabins and trailer hitches, or placed inside the truck cabins. The Honda 1KW generator was secured to the outside of the truck. Setup of the system could be accomplished in approximately 10-15 minutes.


**Figure 36: Dekati's experimental setup for measuring on-road vehicle emissions.**

**Figure from reference *(40).***


**Figure 37: ETaPS mounted on left side of elevated exhaust pipe. $O_2$ sensor mounted on right side of elevated exhaust. Data acquisition equipment, air pump, and generator are visible on the metal platform behind the cabin. Of note is the overhead power line on the upper right later shown to cause interference with the ETaPS signal.**

**Figure 38: Three angles of an ETaPS mounting. ETaPS and $O_2$ sensor are attached to the exhaust pipe. Data acquisition equipment, air pump, and generator are secured to metal platform behind the cabin.**

#### *3.3.3.2 Testing Procedure*

Before each day of testing began, the time on the computer recording ETaPS data and the time on the computer recording RSD data were synchronized. This was necessary in order to match up the continuous ETaPS data to the snapshot RSD data.

Testing in West Virginia was performed in two segments, from November 30, 2008 to December 20, 2008 and from January 19, 2009 to February 6, 2009. Each segment employed a different testing procedure. In each test, the ETaPS was mounted to the vehicle tailpipe and set to continuously measure. The vehicle would then pass the RSD detector and the RSD would make a single record.

During the first trip each truck made six runs past the RSD detector. Four runs would be performed at approximately 5, 10, 15, and 20mph. The next two runs would be made by starting from full stop in third or fifth gear and accelerating past the detector.

After the first trip, adjustments were made to this procedure. After reviewing the initial data it became a concern that because the ETaPS signal for an exhaust stream may occur at a slightly different time than the RSD snapshot of that same stream, the correlation may be skewed. A new method was developed to compensate for this. If the ETaPS signal did not vary over a stretch of time around the RSD snapshot, the signal could be averaged and correlated with the RSD data. The Labview program was modified to display a green light to the instrument monitor if the ETaPS signal stayed under a standard deviation of 0.5, for five seconds of measurement and red light if not.

A second modification to the testing procedure was to set up a system wherein data from separate runs could be compared and checked for large outliers. To do this, runs at the same speed were repeated several times so the variance between runs could be compared.

The testing procedure for the second segment was performed with 9 runs past the RSD detector for each truck. Three runs were done at 5mph, three runs were done between 10 and 15mph, and three runs were done at 20mph.

### 3.3.4 ETaPS vs. Dynamometer Chassis Gravimetric Filter

In this setup the ETaPS measured HDDV exhaust continuously while a gravimetric filter collected particles during the course of the dynamometer cycle. The ETaPS set up is described in more detail below. Exact specifications of the facility are available from West Virginia University's testing center (*42*). The dynamometer setup is shown in **Figure 39**.


**Figure 39: ’08 Volvo day cab on dynamometer with insulated pipe leading to ETaPS and CVS dilution tunnel.**

#### *3.3.3.1 ETaPS setup*

The ETaPS was positioned directly in the exhaust flow as close as possible to the dilution system. As shown in **Figure 40**, the exhaust connector piece was attached to the end of the truck's exhaust pipe extension and the piping leading into the dilution system. The exhaust stream in this setup would regularly climb above the operating temperature of the ETaPS. Placement of a fan a few feet away, as well as repositioning the ETaPS in a horizontal instead of vertical position, was enough to alleviate this problem. Originally the OXY6200 oxygen sensor was used. This was inserted in the exhaust stream by means of a small bore into the piping near the ETaPS. This was discontinued in favor of a direct measurement from the dilution system's on board $CO_2$ sensor.

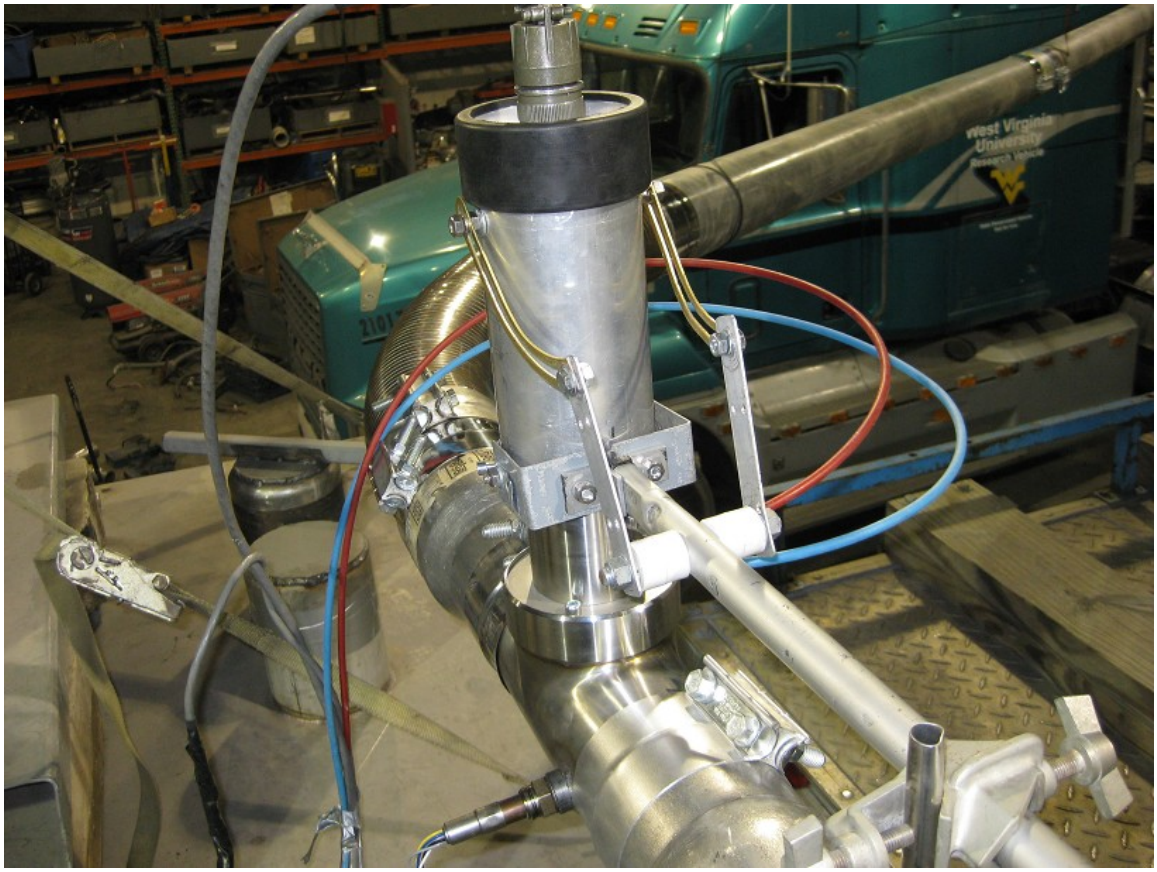

**Figure 40: ETaPS in hot, raw exhaust before CVS dilution tunnel. In this setup the ETaPS is placed above the exhaust piping and the $O_2$ sensor can be seen connected to a small port exiting the bottom left side of the exhaust piping just below the ETaPS. This setup was later changed to have the ETaPS coming in from the side, and the $O_2$ sensor removed in favor of the facility's sensor.**

#### *3.3.3.2 Testing Procedure*

Each truck was subjected to three different test cycles, two of which were performed three times, for a total of nine tests. For each cycle the ETaPS collected continuous data directly in the exhaust stream. Directly after ETaPS measurement, the exhaust stream was diluted and measured by TEOM, as well as collected on a filter for gravimetric analysis. The three tests are as follows.

1. UDDS (Test D):

   The USEPA Urban Dynamometer Driving Schedule (UDDS), often referred to as "Test D" with an average speed of 18.8 mph and a maximum speed of 58 mph, was used as the primary chassis test schedule The cycle is shown in **Figure 41**.

2. Steady-State Cruise Cycle (ETAPS_40):

   A steady-state cycle, at a sustained cruise speed at 40mph, was created to simulate steady highway operation. In addition, stability of signal and, more importantly, inference of aerosol concentration from the ETaPS signal could be more directly made. The cycle is shown in **Figure 42**.

3. Acceleration Ramps (ETAPS_acc):

   A test cycle, derived from the WVU 5-mile schedule, was utilized to evaluate correlation of ETaPS signal with gravimetric PM during vehicle acceleration. **Figure 43.**

   A chart tabulating all dynamometer measurement cycles is shown in **Table 2**.

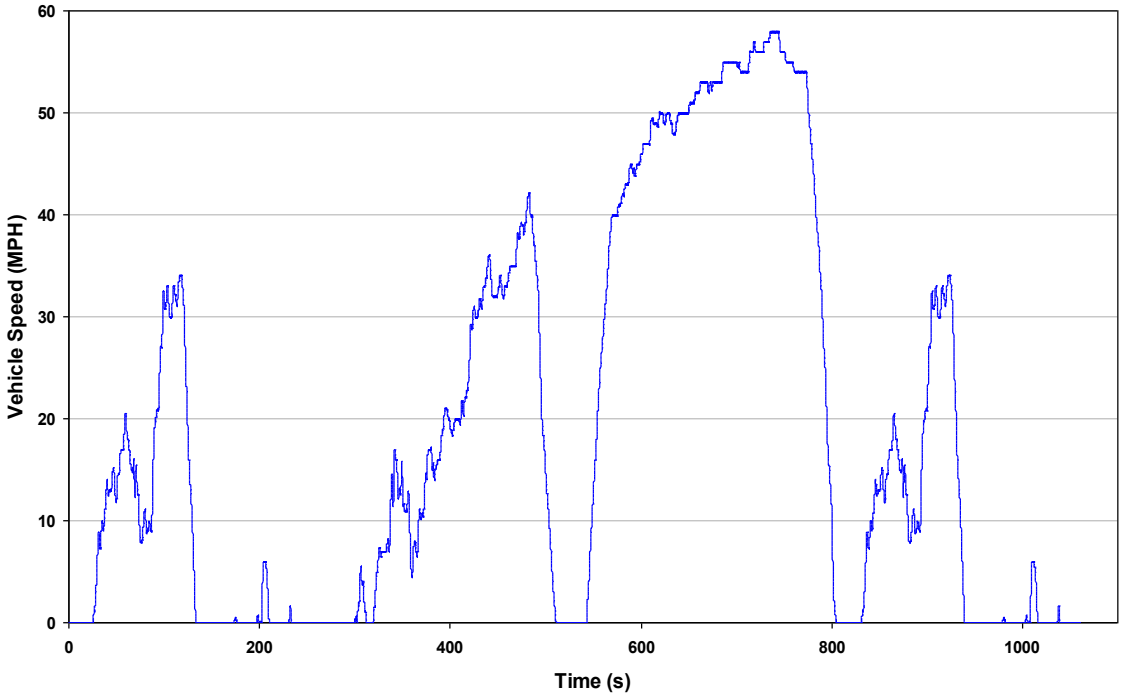


**Figure 41 UDDS Chassis Dynamometer Test Cycle.**

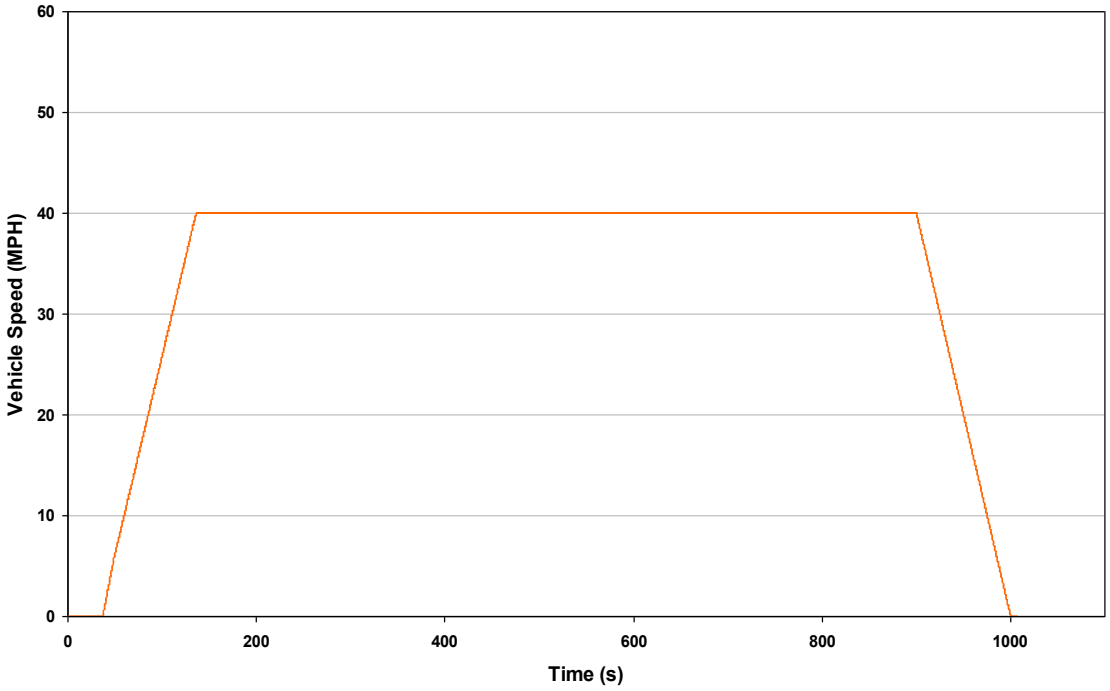


**Figure 42 Steady-state Cruise Chassis Dynamometer Test Cycle (ETAPS_40).**

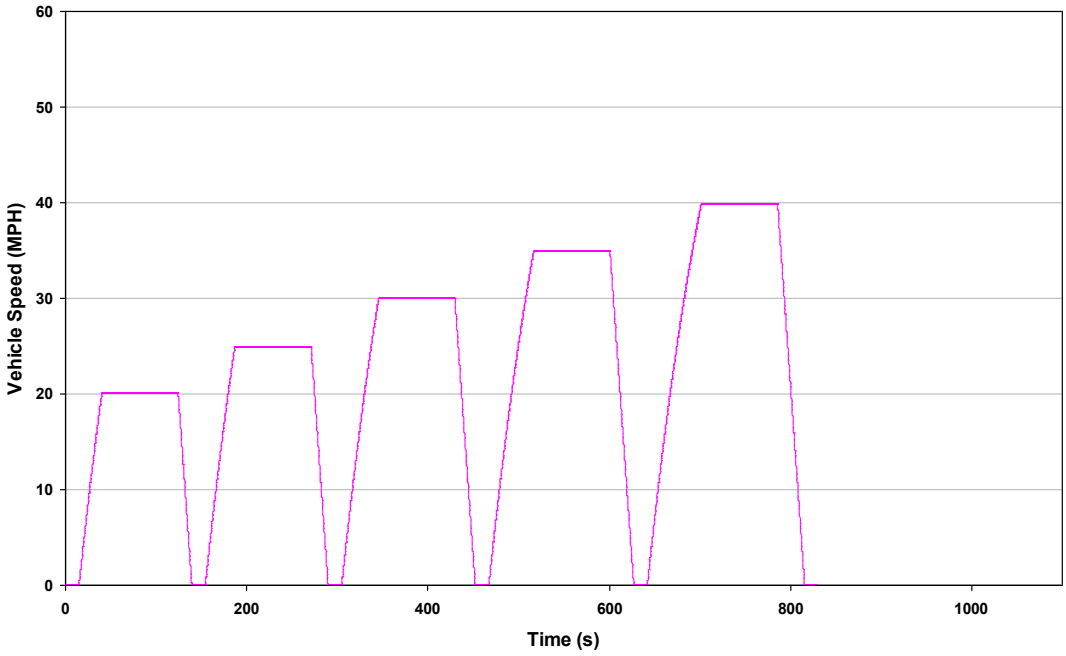


**Figure 43 ETaPS_acc Chassis Dynamometer Test Cycle**.

| Test | Test Cycle | Measurement Systems | Tests Completed | Test Description | Vehicle Model Year |
|---|---|---|---|---|---|
| 1 | UDDS (Test D) | WVU THDVETL/ETaPs | 3 | Pre 2007 Exhaust Concentration | 1995 |
| 2 | UDDS (Test D) | WVU THDVETL/ETaPs | 3 | Pre 2007 Exhaust Concentration | 1996 |
| 3 | UDDS (Test D) | WVU THDVETL/ETaPs | 3 | Pre 2007 Exhaust Concentration | 1995 |
| 4 | UDDS (Test D) | WVU THDVETL/ETaPs | 3 | Pre 2007 Exhaust Concentration | 1999 |
| 5 | UDDS (Test D) | WVU THDVETL/ETaPs | 3 | Pre 2007 Exhaust Concentration | 2005 |
| 6 | UDDS (Test D) | WVU THDVETL/ETaPs | 3 | Post 2007 Exhaust Concentration (DPF-Equipped) | 2009 |
| 7 | UDDS (Test D) | WVU THDVETL/ETaPs | 3 | Post 2007 Exhaust Concentration (DPF-Equipped) | 2008 |
| 8 | UDDS (Test D) | WVU THDVETL/ETaPs | 3 | Post 2007 Exhaust Concentration (DPF-Equipped) | 2008 |
| 9 | UDDS (Test D) | WVU THDVETL/ETaPs | 3 | Post 2007 Exhaust Concentration (DPF-Equipped) | 2008 |
| 10 | UDDS (Test D) | WVU THDVETL/ETaPs | 3 | Post 2007 Exhaust Concentration (DPF-Equipped) | 2007 |
| 11 | UDDS (Test D) | WVU THDVETL/ETaPs | 3 | Simulated DPF Failure (DPF-Bypass) | 2009 |
| 12 | UDDS (Test D) | WVU THDVETL/ETaPs | 3 | Simulated DPF Failure (DPF-Bypass) | 2008 |
| 13 | UDDS (Test D) | WVU THDVETL/ETaPs | 3 | Simulated DPF Failure (DPF-Bypass) | 2008 |
| 14 | UDDS (Test D) | WVU THDVETL/ETaPs | 3 | Simulated DPF Failure (DPF-Bypass) | 2008 |
| 15 | UDDS (Test D) | WVU THDVETL/ETaPs | 3 | Simulated DPF Failure (DPF-Bypass) | 2007 |
| 16 | ETAPS_40 | WVU THDVETL/ETaPs | 3 | Pre 2007 Exhaust Concentration | 1995 |
| 17 | ETAPS_40 | WVU THDVETL/ETaPs | 3 | Pre 2007 Exhaust Concentration | 1996 |
| 18 | ETAPS_40 | WVU THDVETL/ETaPs | 3 | Pre 2007 Exhaust Concentration | 1995 |
| 19 | ETAPS_40 | WVU THDVETL/ETaPs | 3 | Pre 2007 Exhaust Concentration | 1999 |
| 20 | ETAPS_40 | WVU THDVETL/ETaPs | 3 | Pre 2007 Exhaust Concentration | 2005 |
| 21 | ETAPS_40 | WVU THDVETL/ETaPs | 3 | Post 2007 Exhaust Concentration (DPF-Equipped) | 2009 |
| 22 | ETAPS_40 | WVU THDVETL/ETaPs | 3 | Post 2007 Exhaust Concentration (DPF-Equipped) | 2008 |
| 23 | ETAPS_40 | WVU THDVETL/ETaPs | 3 | Post 2007 Exhaust Concentration (DPF-Equipped) | 2008 |
| 24 | ETAPS_40 | WVU THDVETL/ETaPs | 3 | Post 2007 Exhaust Concentration (DPF-Equipped) | 2008 |
| 25 | ETAPS_40 | WVU THDVETL/ETaPs | 3 | Post 2007 Exhaust Concentration (DPF-Equipped) | 2007 |
| 26 | ETAPS_40 | WVU THDVETL/ETaPs | 3 | Simulated DPF Failure (DPF-Bypass) | 2009 |
| 27 | ETAPS_40 | WVU THDVETL/ETaPs | 3 | Simulated DPF Failure (DPF-Bypass) | 2008 |
| 28 | ETAPS_40 | WVU THDVETL/ETaPs | 3 | Simulated DPF Failure (DPF-Bypass) | 2008 |
| 29 | ETAPS_40 | WVU THDVETL/ETaPs | 3 | Simulated DPF Failure (DPF-Bypass) | 2008 |
| 30 | ETAPS_40 | WVU THDVETL/ETaPs | 3 | Simulated DPF Failure (DPF-Bypass) | 2007 |
| 31 | ETAPS_acc | WVU THDVETL/ETaPs | 1 | Pre 2007 Exhaust Concentration | 1995 |
| 32 | ETAPS_acc | WVU THDVETL/ETaPs | 1 | Pre 2007 Exhaust Concentration | 1996 |
| 33 | ETAPS_acc | WVU THDVETL/ETaPs | 1 | Pre 2007 Exhaust Concentration | 1995 |
| 34 | ETAPS_acc | WVU THDVETL/ETaPs | 1 | Pre 2007 Exhaust Concentration | 1999 |
| 35 | ETAPS_acc | WVU THDVETL/ETaPs | 1 | Post 2007 Exhaust Concentration (DPF-Equipped) | 2009 |
| 36 | ETAPS_acc | WVU THDVETL/ETaPs | 1 | Post 2007 Exhaust Concentration (DPF-Equipped) | 2008 |
| 37 | ETAPS_acc | WVU THDVETL/ETaPs | 1 | Post 2007 Exhaust Concentration (DPF-Equipped) | 2008 |
| 38 | ETAPS_acc | WVU THDVETL/ETaPs | 1 | Post 2007 Exhaust Concentration (DPF-Equipped) | 2008 |
| 39 | ETAPS_acc | WVU THDVETL/ETaPs | 1 | Post 2007 Exhaust Concentration (DPF-Equipped) | 2007 |
| 40 | ETAPS_acc | WVU THDVETL/ETaPs | 1 | Simulated DPF Failure (DPF-Bypass) | 2009 |
| 41 | ETAPS_acc | WVU THDVETL/ETaPs | 1 | Simulated DPF Failure (DPF-Bypass) | 2008 |
| 42 | ETAPS_acc | WVU THDVETL/ETaPs | 1 | Simulated DPF Failure (DPF-Bypass) | 2008 |
| 43 | ETAPS_acc | WVU THDVETL/ETaPs | 1 | Simulated DPF Failure (DPF-Bypass) | 2008 |
| 44 | ETAPS_acc | WVU THDVETL/ETaPs | 1 | Simulated DPF Failure (DPF-Bypass) | 2007 |

**Table 2: Tabulation of testing done by all vehicles.**

# Chapter 4: Results

### 4.1 ETaPS vs. $CO_2$

A wide-range oxygen sensor was placed near the ETaPS corona in raw exhaust to infer $CO_2$ and was compared to ETaPS response as well as the $CO_2$ measurements in the dilution chamber. **Figure 44** shows good agreement between the wide-range oxygen sensor and the $CO_2$ measurements in the dilution chamber for the 1999 Peterbilt during a cruise cycle. **Figure 45** shows the inferred $CO_2$ from the wide-range oxygen sensor versus the $CO_2$ measurements from the dilution chamber from 200 -875 seconds of the 1000 second cycle. **Figure 46** shows the ETaPS response versus the inferred $CO_2$ readings from 200-1000 seconds of the 1999 Peterbilt cruise cycle. A good correlation was reached within a certain operating range. Correlation appears to deviate at ETaPS measurements of less than 0.1V. A correlation is expected because as engine load increases more fuel is being burned, resulting in greater loss of $O_2$ coupled with greater production of $CO_2$. It should also be noted that for older vehicles, increase in particle emissions with increased load is expected.

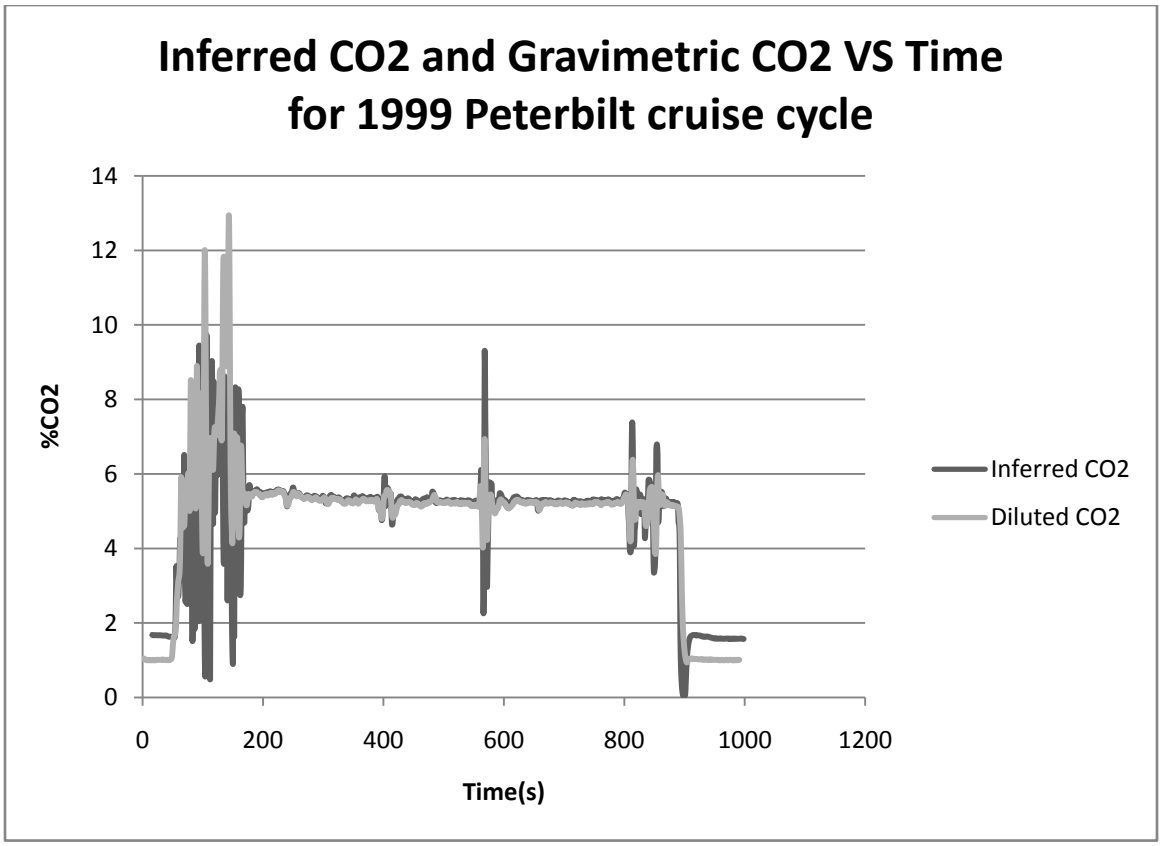


**Figure 44: Inferred $CO_2$ and $CO_2$ from the dilution chamber vs time. The diluted $CO_2$ readings have been adjusted by the chambers dilution factor and adjusted for the delay time it takes the exhaust around the ETaPS to reach the dilution chamber.**

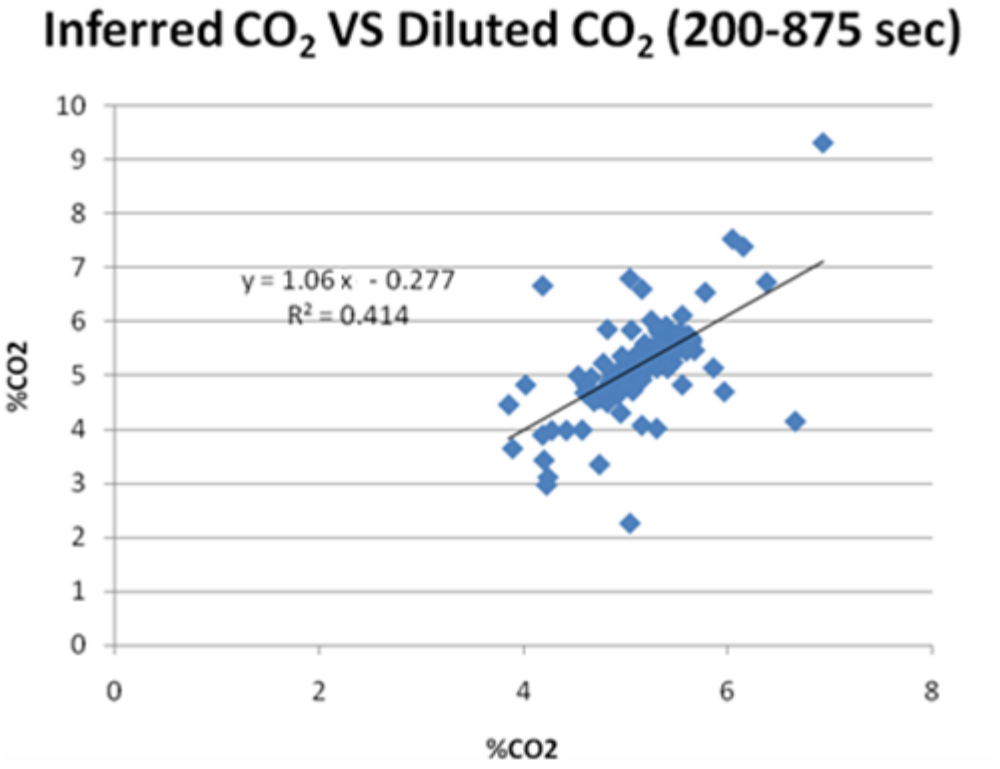


**Figure 45: Two ends of the cycle were discarded because of "jerky" accelerations and slowdowns that may have caused "coughs" in the system. Data were taken from the 1999 Peterbilt cruise cycle. It should also be noted that both instruments consistently read 0% $CO_2$ when the engine is shut off.**

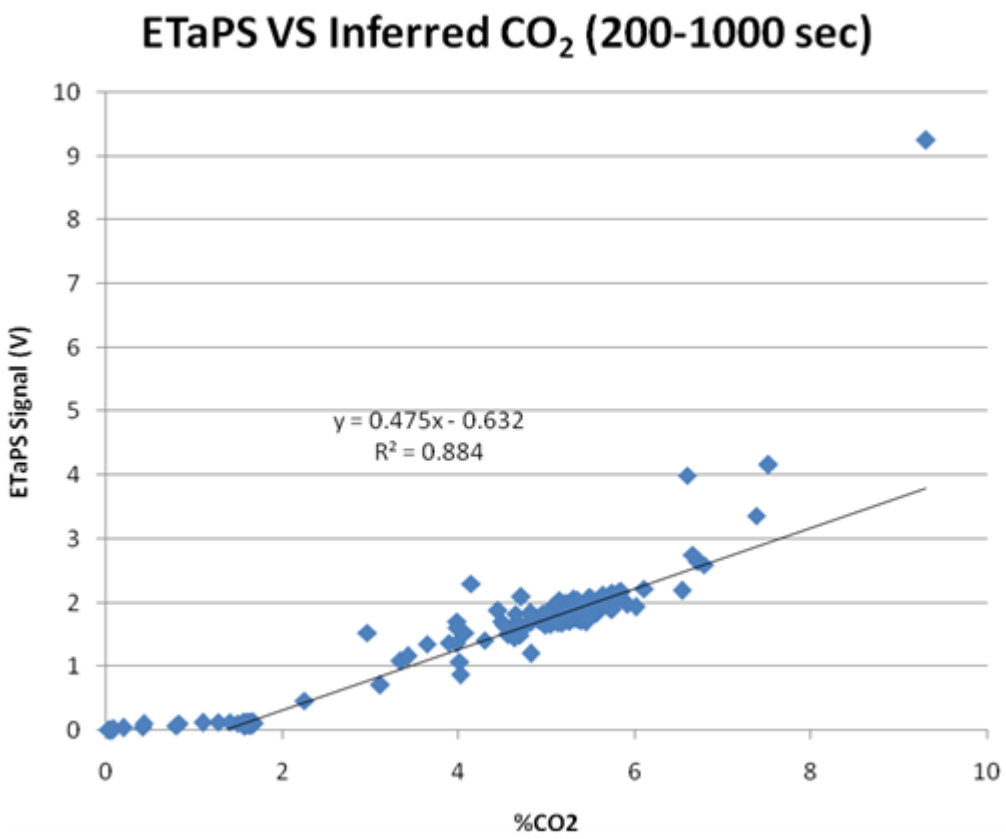


**Figure 46: 1999 Peterbilt cruise cycle from 200-1000 seconds. The first 200 seconds were discarded also because of "jerky" accelerations causing "coughs."**

## 4.2 RSD vs. ETaPS

### 4.2.1 Power line Interference

Before reporting the results of the RSD vs. ETaPS study, the effect of power line interference on the ETaPS is detailed. After the first round of tests in West Virginia, a correlation between the five older truck exhaust ETaPS measurements and their RSD results was attempted. This effort was based on the successful preliminary observations in Denver and also based on the observation that when the ETaPS was placed on the trucks close to the dynamometer facility and the trucks were not operating, the ETaPS signal was essentially zero. When passing the RSD, all trucks showed significant readings. This was expected due to the age of the trucks and lack of pollution controls.

An effort was made to correct for any time difference between the ETaPS and RSD measurements. ETaPS data points from a five second timeframe around the RSD measurement time were checked for large deviations. Data with too large of a deviation over the five second time frame were discarded. An effort was made on the second trip to West Virginia to make sure runs were repeated until this condition was satisfied. This was done so that no runs would have to be discarded. This deviation was originally chosen arbitrarily. On the second trip, the deviation was tested while driving on back roads around the facility. The deviation was then lowered as far as possible to still allow measurements.

Carrying out these later runs, it was discovered that an unexpected and undesirable repeatable pattern appeared for every run. A DPF equipped bus, which is expected to show zero ETaPS signal, was used to map out this pattern. The bus was stopped 200ft away from the RSD platform. For every ten feet, the bus was allowed to idle and ten seconds of data were recorded. Each point on the graph, **Figure 47**, represents the average of the ten data points at each ten foot stop. The peak corresponds to the point directly beneath a power line crossing over the street. These are large signals compared to the zeros which we expected based upon our preliminary measurements in Denver.

Three same speed runs for a DPF equipped and DPF bypassed vehicle taken within minutes of each other are graphed in **Figure 48** and **Figure 49**. The x-axis shows a time window of 15 seconds around the time of measurement. Both graphs show a consistent pattern matching the power line interference. It should also be noted in this case that when the vehicle is DPF bypassed, there is approximately a 0.25V increase from the non-bypassed runs. Unfortunately, this expected increase is also within the differences seen between various runs with the DPF installed and operating. These differences were interpreted as arising from different values of the current in the overhead power lines. The power lines were apparently at least at several thousand volts because they are equipped with about 15 cm long insulators.

Because power line interference with the ETaPS may vary over time, due to varying current over the day, measurement signals from all DPF equipped modern trucks were compared over time in **Figure 50**. This was done to see how much the ETaPS

signal varied on the road compared to on the dynamometer. The tightest cluster of points belonged to the DPF equipped Penske truck. This set of data is shown expanded versus time in **Figure 51**. The observed signal had a range of about 0.25V.

The dynamometer testing, presumably having no power line interference, only showed a signal range of about 0.0275V for approximately 2000 one-second data points for both the cruise and step test. These results are shown in **Figure 52** and **Figure 53**. In the best case scenario, the variability with time of ETaPS signals under the power line is an order of magnitude larger than the variability on the dynamometer. The observed variability is also equal in magnitude to the signal difference between a DPF bypassed and non-bypassed Volvo truck. In the worst case scenario, the fluctuation of ETaPS signals under the power line ranged from 0 to 3V in a single day. Not only is this variability a problem but also the average ETaPS signal is over 1V while it should be less than 0.01 V.

In retrospect, the ETaPS readings were looked at from the later round of vehicle testing when the truck engine was turned off. These readings varied from the expected zero to as high as 3.7V, presumably depending on where the driver chose to park the tractor relative to the overhead power lines.

Further testing was done after returning from West Virginia. Four tests were performed. The ETaPS was attached to the top of the Winnebago used in the preliminary studies. The Winnebago has low level exhaust, and the ETaPS was not exposed to it.

Everything was connected as if conducting a real test with the air pump running and the $O_2$ sensor taking measurements.

Four tests were performed in total. Two tests were done at around 2.5ft from a power line, and two tests were done at around 90ft from the same power line. At each of these distances, a test was done by measuring the ETaPS signal at 1Hz for one minute, one test with the tailpipe connector off, and one test with the tailpipe connector on. The tailpipe connector was used as an EM radiation shield. The results of these tests are shown in **Figure 54**. The results show clear interference in the unshielded measurements. The ETaPS measures a signal of 1.5V at 9ft and .5V at 90ft. The results demonstrate a very strong interference that spans a very large distance. Both shielded measurements show a signal an order of magnitude below signals recorded for the DPF equipped truck on the dynamometer.

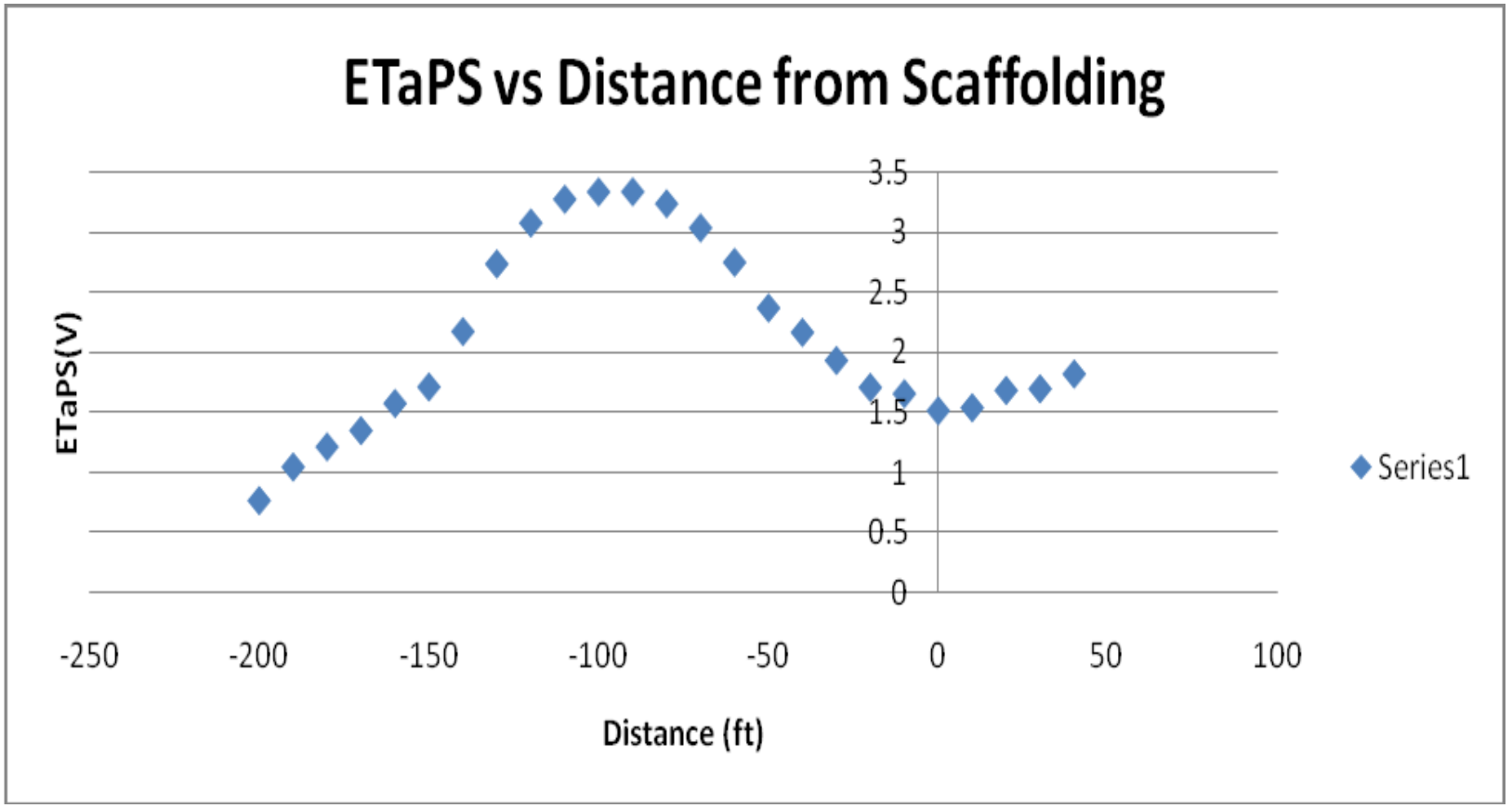


**Figure 47: ETaPS readings as a function of distance from the RSD location showing a large signal peak when the ETaPS was under the power line crossing the roadway.**

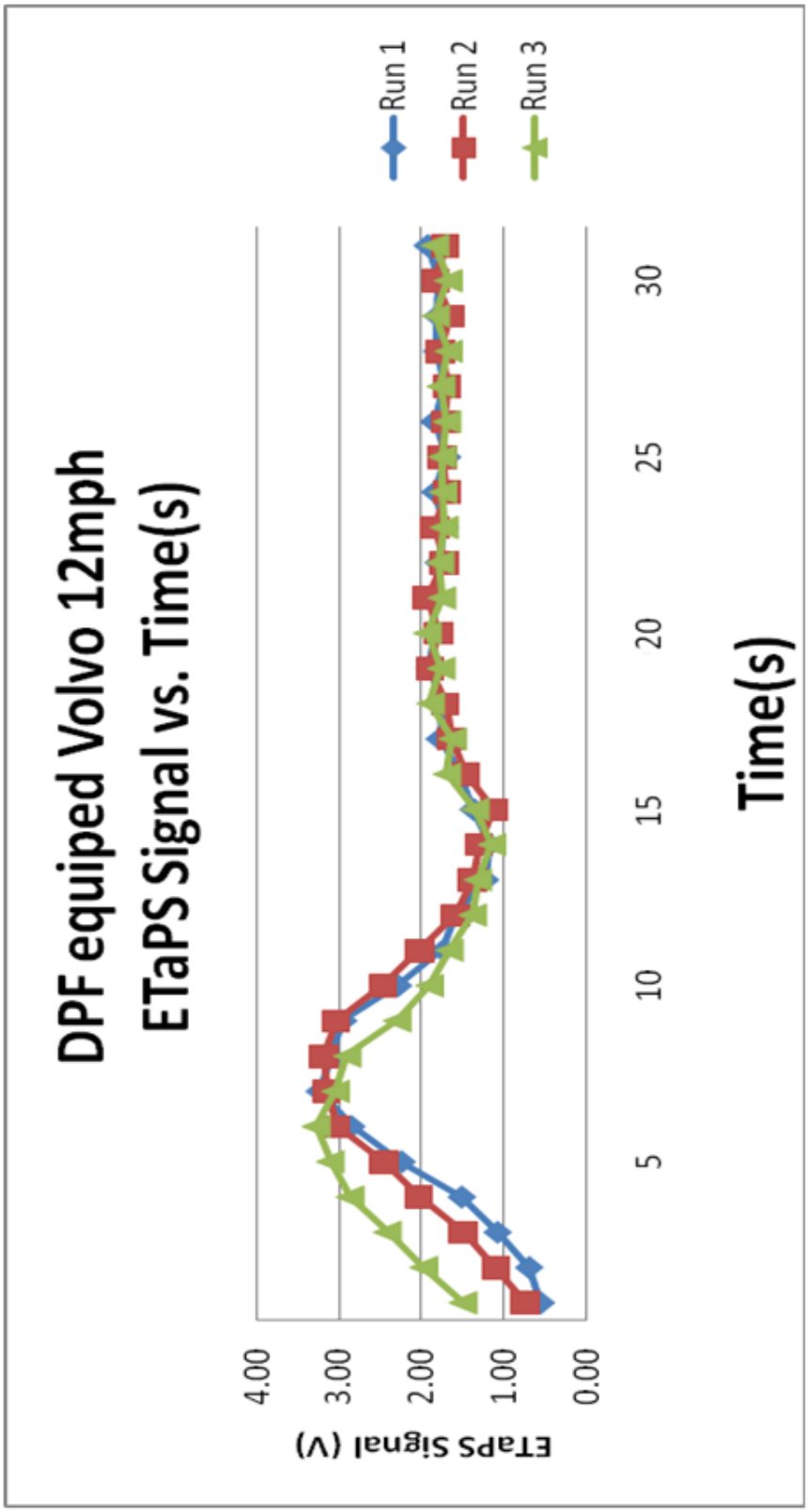


**Figure 48: ETaPS signals versus time in seconds for three runs of a DPF equipped Volvo.**

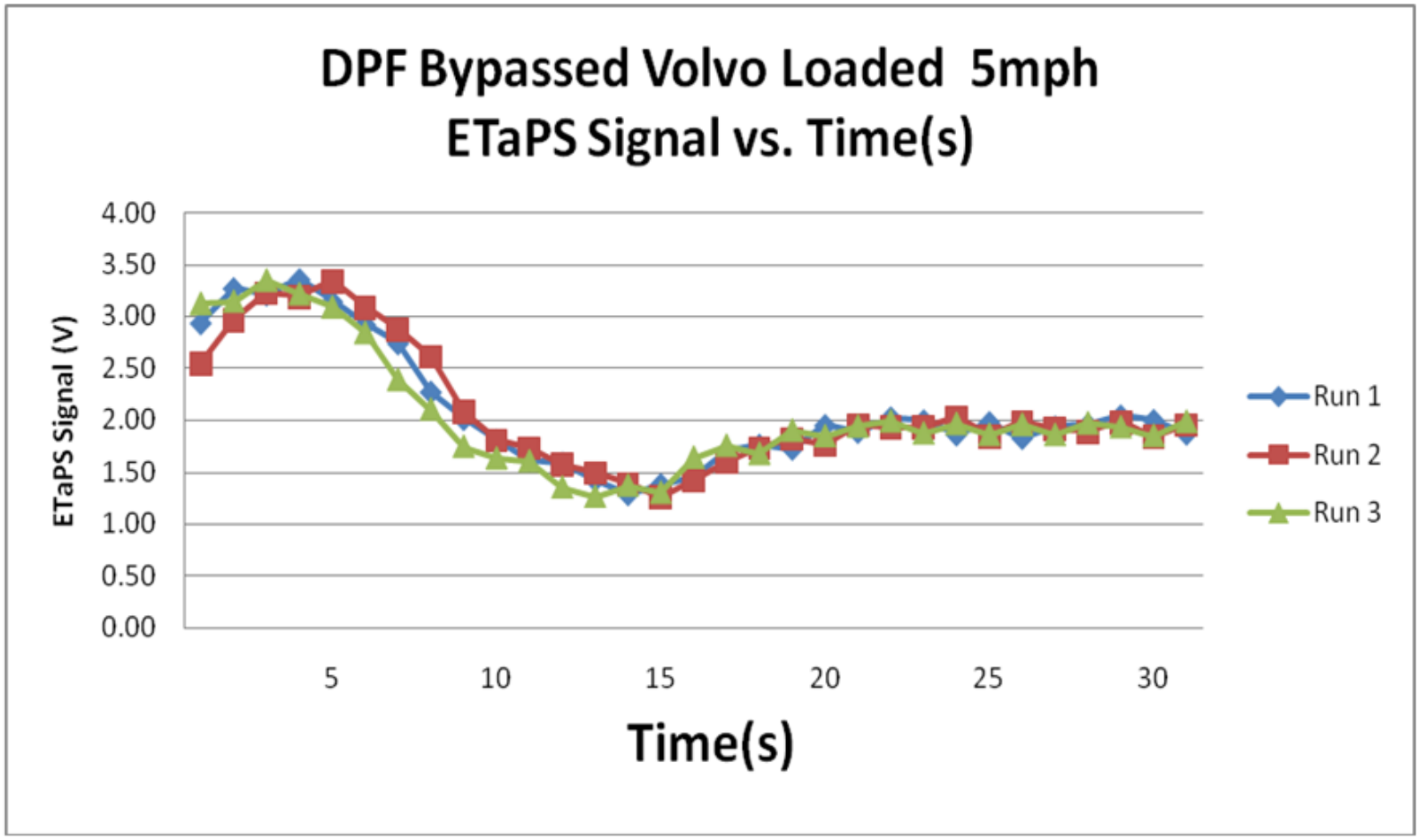


**Figure 49: ETaPS signals versus time in seconds for three runs of the Volvo shown in Figure with the DPF bypassed.**

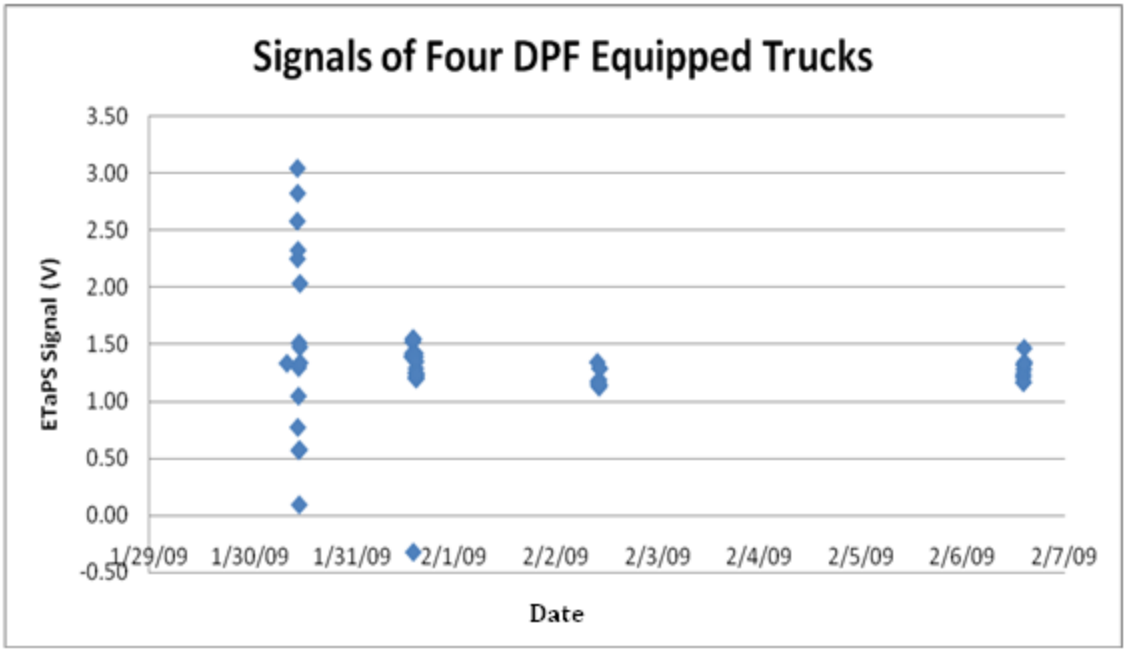


**Figure 50: Two second average ETaPS readings from four DPF equipped trucks as they passed the RSD location.**

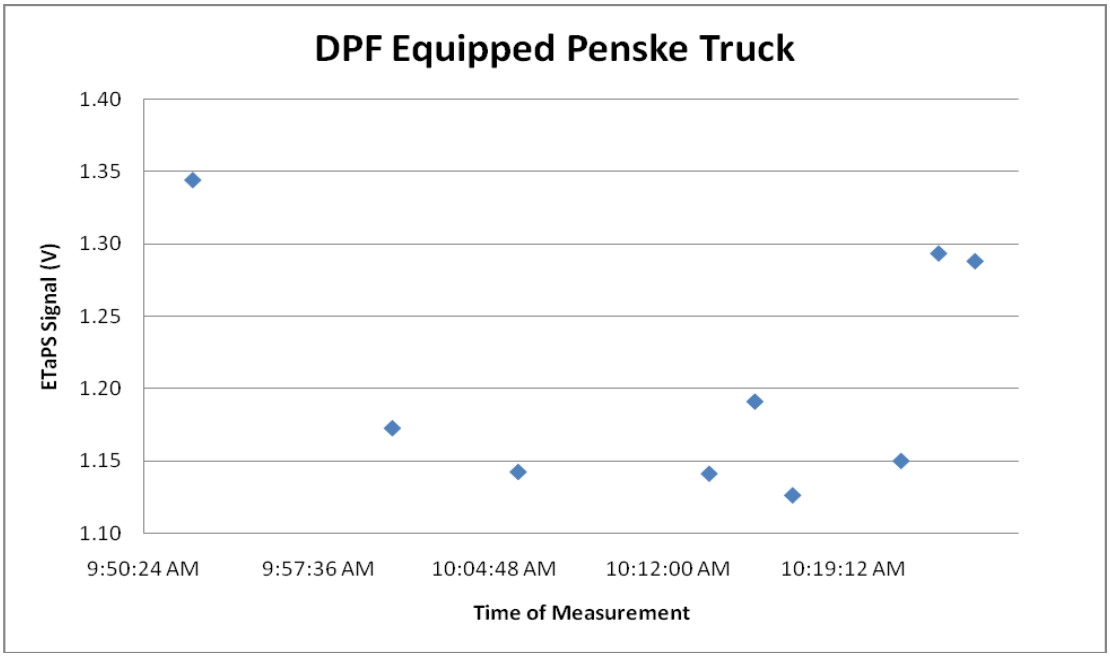


**Figure 51: Two second average ETaPS voltage readings graphed versus the time at which this vehicle passed the RSD location for the least variable DPF equipped vehicle monitored at Westover.**

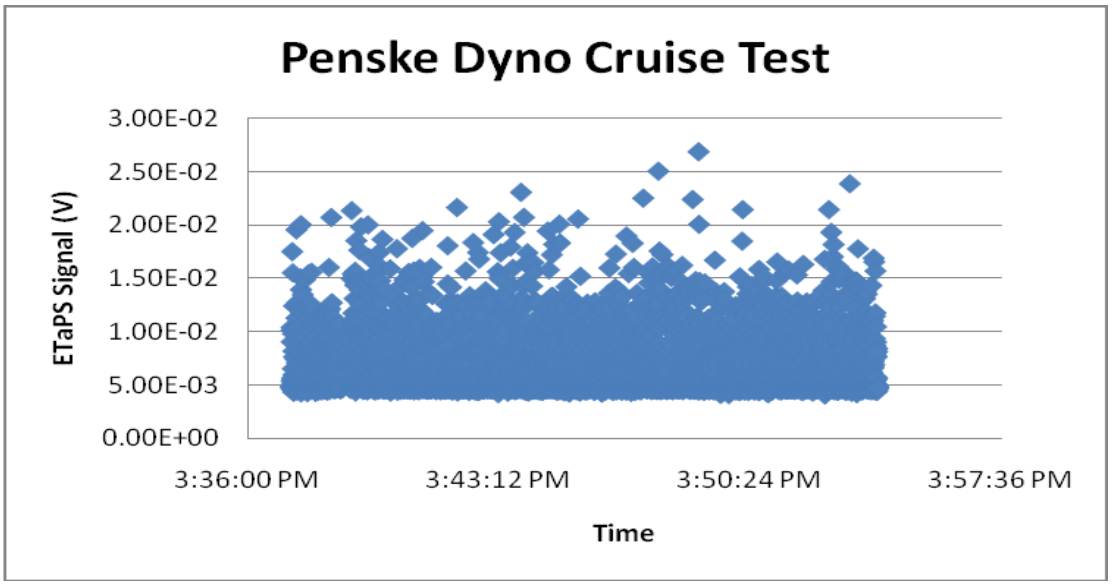


**Figure 52: More than 2000, one second ETaPS readings from a DPF vehicle on the dynamometer.**

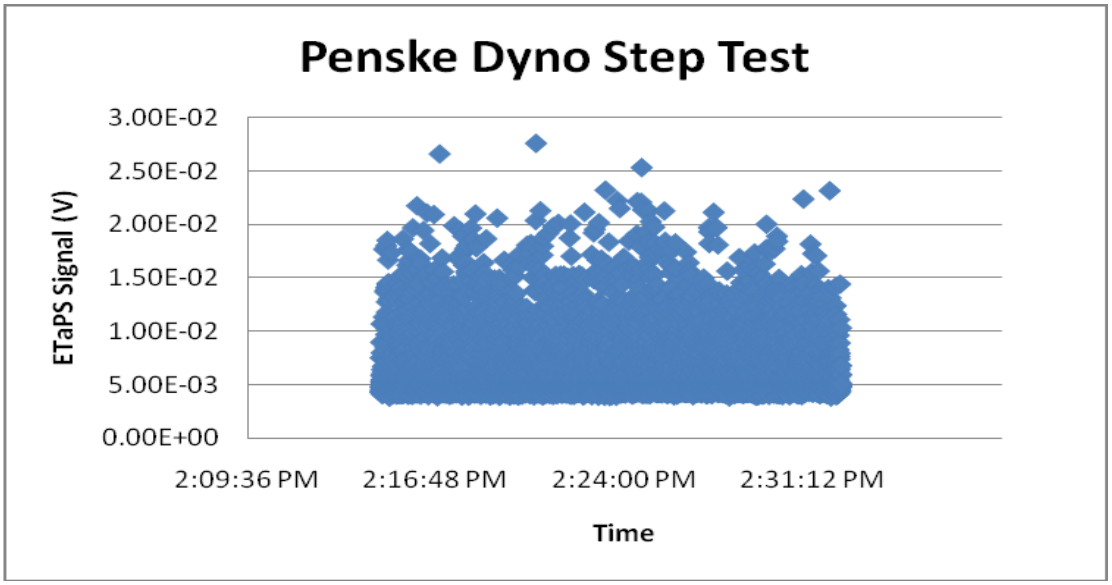


**Figure 53: More than 2000, one second ETaPS readings from a DPF vehicle on the dynamometer.**

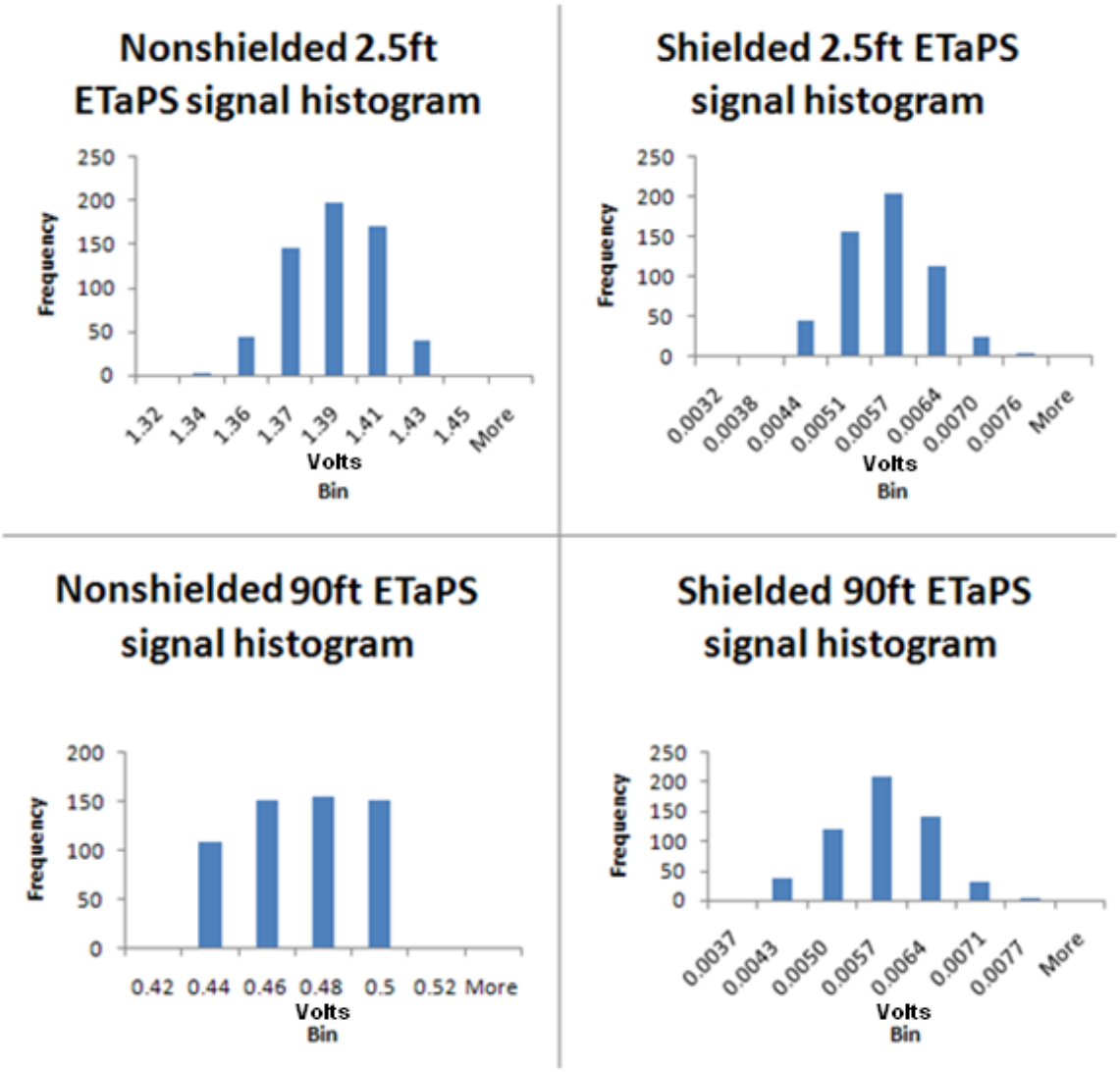


**Figure 54: Histograms of ETaPS signal in four scenarios; 2.5ft from power line unshielded, 2.5ft from power line shielded, 90ft from power line unshielded, and 90ft from power line shielded. (Data provided by Brent Schuchmann)**

### 4.2.2 ETaPS versus RSD Data

As discussed in the previous section, the ETaPS data in Westover are compromised by the effect of the local overhead power lines. We did not originally know if this interference was with the ETaPS corona itself or with the data lines which bring the data to the data acquisition system. We have now confirmed the former, because the same data lines were used in all studies in Denver in which the ETaPS baseline readings were reasonably close to zero volts.

In case there was any useful residual information in the outdoors ETaPS readings, PM measurement by ETaPS was calculated in ratio to $CO_2$ to compare to the RSD readings which are all ratio to $CO_2$. The ETaPS readings were averaged over two seconds when the vehicle was passing the RSD unit. $CO_2$ was determined by calculation from the measurement of percent $O_2$ in the exhaust stream averaged over the two seconds when the vehicle was passing the RSD unit. This ETaPS ratio was plotted vs. UV smoke signal from the RSD 4600 in **Figure 55**.

There is significant scatter in the data, although there does appear to be a large clump of data close to zero (mostly provided by the DPF equipped vehicles) and a general tendency of the ETaPS/$CO_2$ readings to increase as the UV smoke reading increases. This correlation was not studied further in view of the conclusions above regarding the unreliability of the Westover ETaPS readings. Based on the consistent ETaPS results in Denver, we expected reliable ETaPS readings at Westover.

We now know that successful results would have been obtained had there been no overhead power lines or had we mounted the ETaPS in its shield.

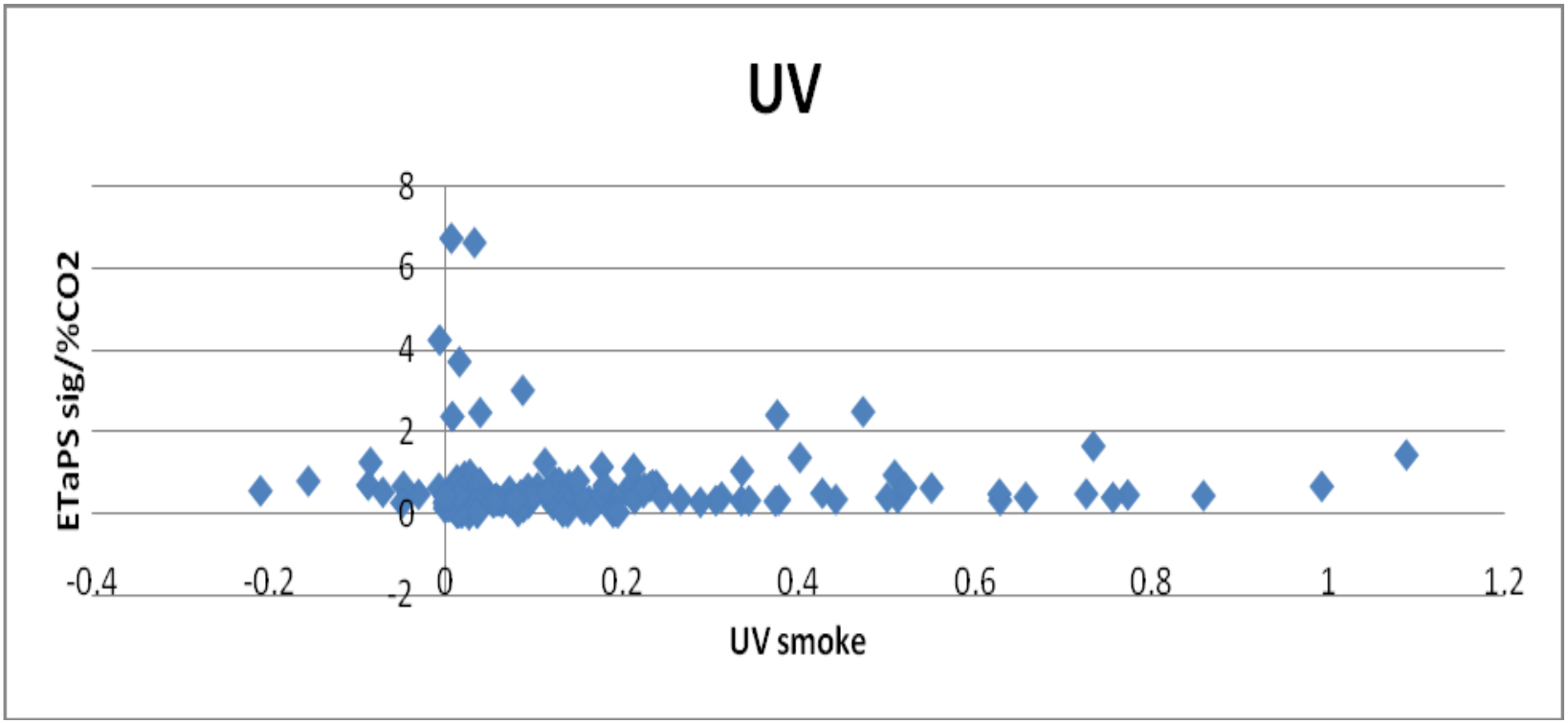


**Figure 55: ETaPS divided by CO2 versus UV smoke reading.**

## 4.3 ETaPS vs. Dynamometer

Data were collected from fifteen trucks; five pre 2007 trucks, five post 2007 trucks equipped with a functioning DPF and simulated failed DPF. Each "truck" underwent three different cycles (UDDS-Test D, ETaPS40-cruise, and Acc) on the dynamometer chassis. One bus was not tested for the Acc cycle due to time constraints. This made for a total of 44 tests. Correlations were also analyzed between ETaPS and inferred $CO_2$ measurements using a wide-range oxygen sensor in the raw exhaust as well as $CO_2$ measurements inside the dilution chamber and integrated ETaPS measurements against integrated TEOM measurements.

Each truck also underwent at least three runs, sometimes more, at three different speeds (5mph, 10-15mph, and ~20mph) through the RSD 4600 for a total of 90 tests. RSD was graphed against the gravimetric results to see if RSD can be a reasonable detector of high PM emitting trucks.

Correlations were plotted as ETaPS signal vs. grams collected on the filter per mile of dynamometer testing. ETaPS signal was recorded as integral volts and correlated to total grams. Because dynamometer gravimetric data are typically reported as g/mile, the ETaPS integral signal was converted to integrated signal per mile to preserve literature standards.

### 4.3.1 ETaPS versus Gravimetric Data

Combining all points/trucks, categorized by vehicle and averaged for each cycle, shows a decent correlation between a wide variety of vehicles. Error bars in all graphs show the standard deviation for filter weight and integrated ETaPS signal for a given cycle. Because only one Acc cycle was performed for each vehicle, no standard deviation calculation was made, and no error bars are present for those points in the graphs. **Figure 56** shows all points from the beginning of testing. With the exception of the ’08 Volvo, there is an apparent correlation among the rest of the points.

The ’08 Volvo data in this outlier set was from the DPF bypassed measurement. The lack of ETaPS response for the '08 Volvo could be from hot semi-volatiles in the exhaust. The ETaPS would have a hard time “seeing” these hot semi-volatiles compared to the gravimetric filter which weighs the diluted/cooler exhaust. This seems likely due to the high content of hydrocarbons detected in the exhaust. As measured by WVU’s testing facility, hydrocarbon levels for all other vehicles were below 0.5g/mi. The exhaust for the bypassed ’08 Volvo, however, ranged from 2 to 10g/mi for every test. In the interest of examining the rest of the data, the ’08 Volvo data will be excluded from some charts. It can be concluded, however, that the ’08 Volvo DPF equipped and the ’08 Volvo DPF bypassed each act as two different trucks.

Once the ’08 Volvo was removed there are a total of 51 data points plotted in **Figure 57**. Many of these points are located within the box outlined near the origin. This box is enlarged in **Figure 58** to show where any functional DPF equipped truck would fall compared to a non-equipped DPF truck or a failing DPF.

Every truck with a DPF system tested under functioning conditions totaled less than 10 volts on the ETaPS over a 5 mile test and less than 25mg/mile on the gravimetric scale. The cleanest bypassed trucks (’08 Volvo day cab and ’09 Penske), according to the gravimetric readings, were just as clean as the functioning DPF systems but had at least a 5 times higher reading on the ETaPS. This alone demonstrates that ETaPS can detect DPF failures before they appear in a gravimetric response.

**Figure 59** separates the data by cycle. It is worth noting that even though the data set was divided into smaller groups, by each test, there is a better $R^2$ value for each group than the overall trend line. This suggests a dependency of correlation to driving cycle.

The data indicate that when the ETaPS is placed in a shielded environment it very accurately determines high PM emitting trucks whose exhaust does not contain large amounts of semi-volatiles. Semi-volatiles in the hot, raw exhaust are in the gas phase and cannot be seen by the ETaPS and alternate means of detection (gravimetric filters) are needed for semi-volatiles.

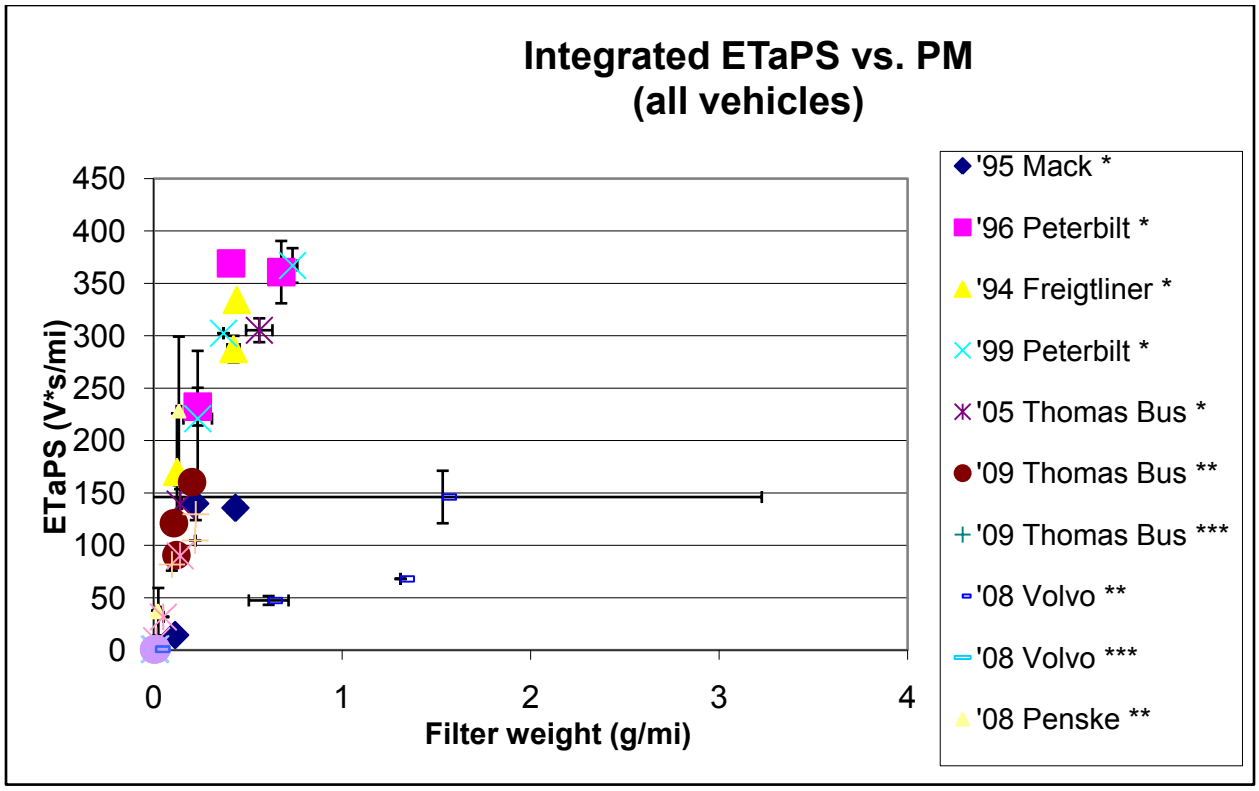


**Figure 56: ETaPS vs. PM for all vehicles categorized by individual truck. Integrated volts on the y-axis are the summation of 1Hz measurements for the duration of a gravimetric test.**

*** No DPF equipped**
**** DPF bypassed**
***** DPF equipped**

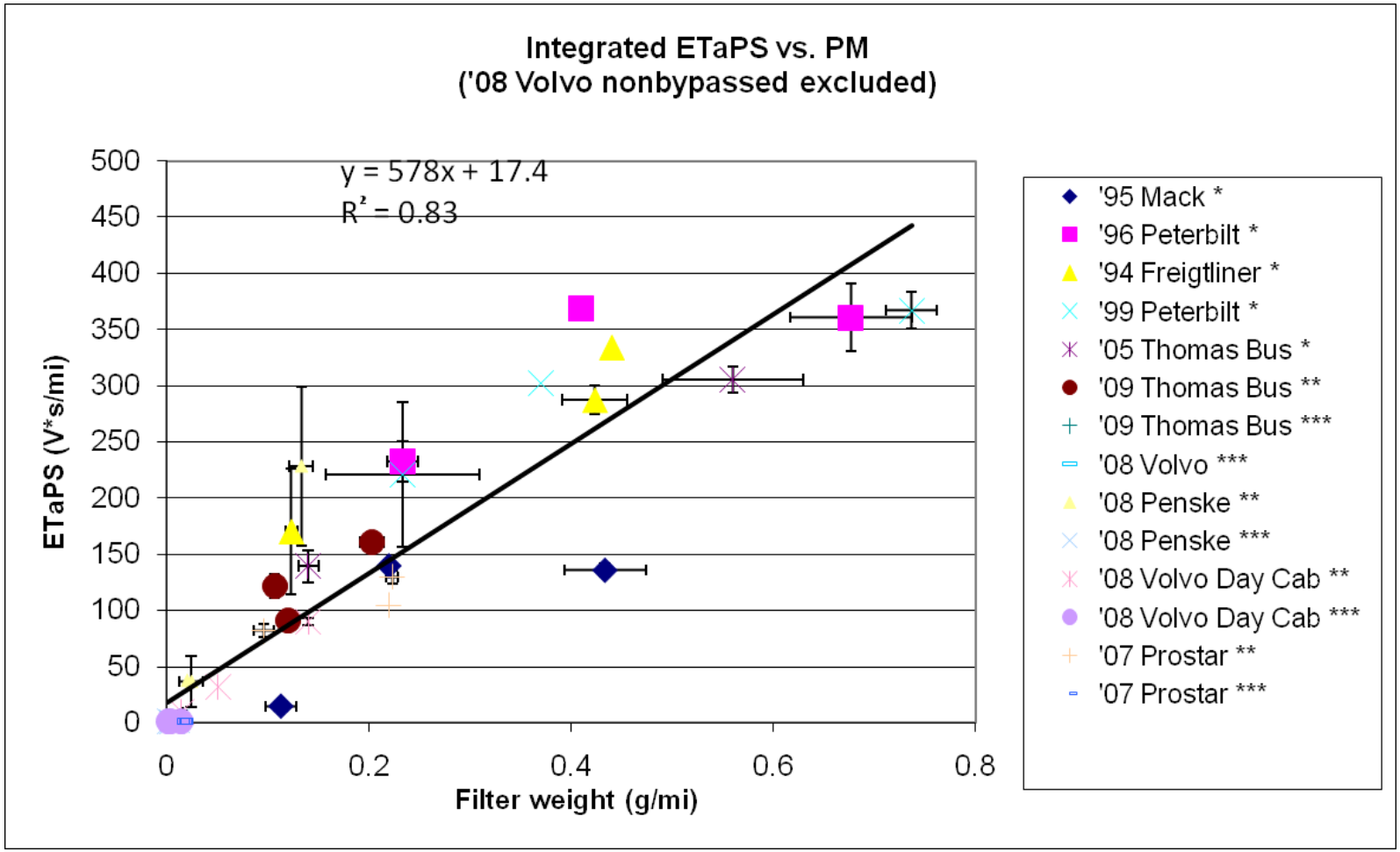


**Figure 57: ETaPS vs. PM showing correlation after excluding the '08 Volvo. Low emitting trucks are binned in the box. ETaPS instrument noise is ≤ 15mV*s. An exploded view of this region is shown in Figure.**

*** No DPF equipped, ** DPF bypassed, *** DPF equipped**

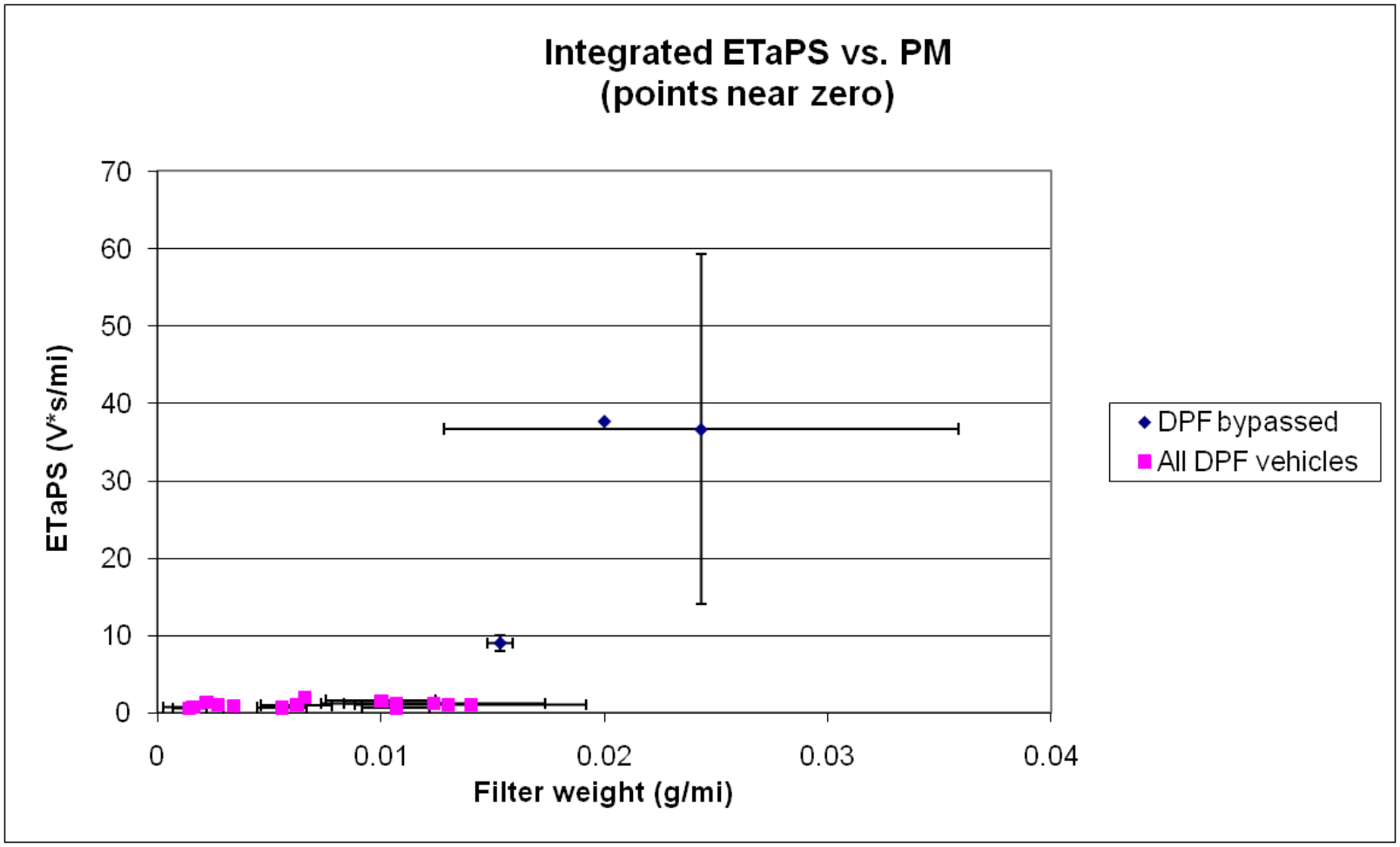


**Figure 58: A closer view of points around the origin. Total noise for all DPF equipped vehicles is ≤ 160mV*s**

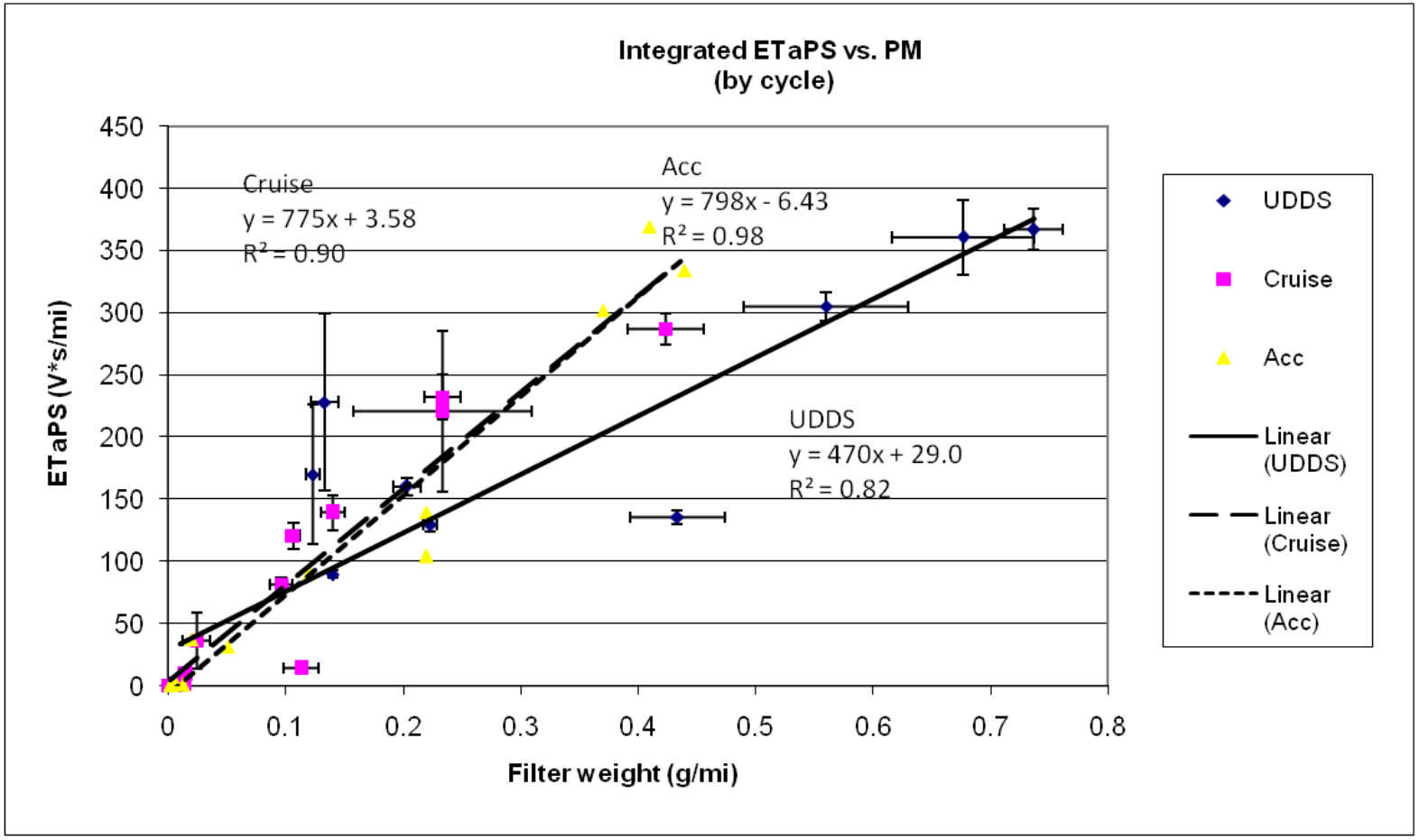


**Figure 59: ETaPS vs. PM after excluding the '08 Volvo. Vehicles are grouped by cycle. Linear regression is performed on each cycle.**

## 4.4 Integral ETaPS VS Integral TEOM

Comparing between the integrated ETaPS signal and the integrated TEOM mass shows results similar to the integral ETaPS VS PM mass filters with only a few negative TEOM values. Error bars in all graphs show the standard deviation for integrated TEOM and integrated ETaPS signal for a given cycle. Because only one Acc cycle was performed for each vehicle, no standard deviation calculation was made, and no error bars are present for those points in the graphs. **Figure 60** shows each truck by DPF equipped and with a failing (bypass) DPF. **Figure 61** separates each test by the cycle driven. Integrated ETaPS and integrated TEOM data did not correlate as well as gravimetric did. More problems arose with the TEOM's dependence on humidity and temperature. While the $R^2$ values were only slightly less for the ETaPS/TEOM analysis, large negative and large positive values were thrown out due to temperature/humidity control problems that either added weight or reduced weight in the TEOM results.

Comparison of real time ETaPS signal vs. real time TEOM mass does not demonstrate strong correlation. **Figure 62** shows the plot of the continuous overlay of data points from the two instruments vs. time. One issue in comparing these two sets of data is finding the timing of ETaPS measurements that match up to the relevant diluted exhaust stream measured by the TEOM. However, it should be possible by inspection to match up signal peaks and low signal areas. But when looking at the plot, there does not seem to be any significant overlap. Plotting ETaPS vs. TEOM also shows a poor correlation. This is most likely due to the nature of the TEOM to temporarily pick up semi volatiles and water vapor causing positive and negative signal fluctuations that are

not registered by the ETaPS. This would allow the real time data to be poorly matched, but the integrated data to still hold a correlation.

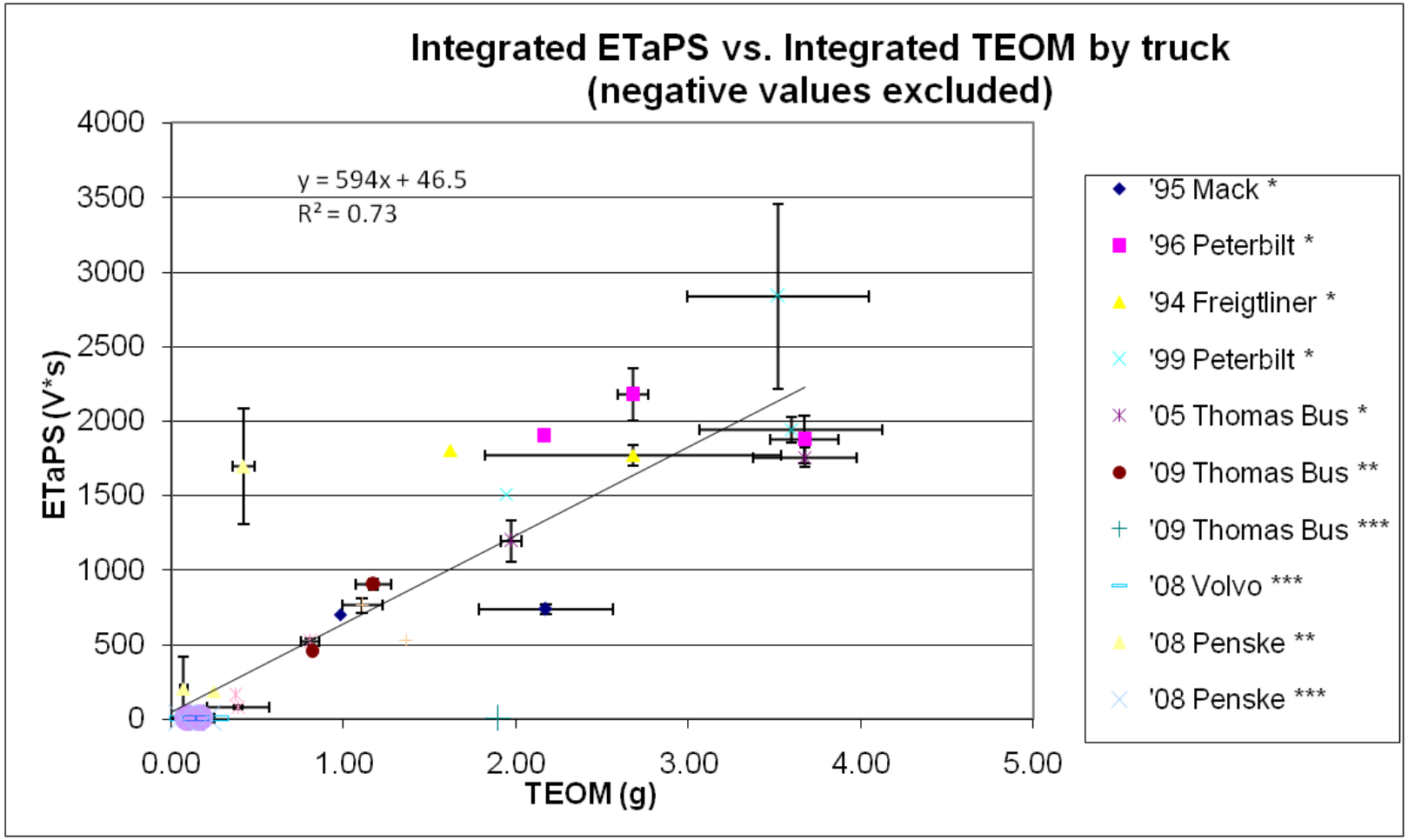


**Figure 60: Excludes points < 0 for integrated TEOM and excludes the '08 Volvo Bypass tests. Data are grouped by vehicle type.**

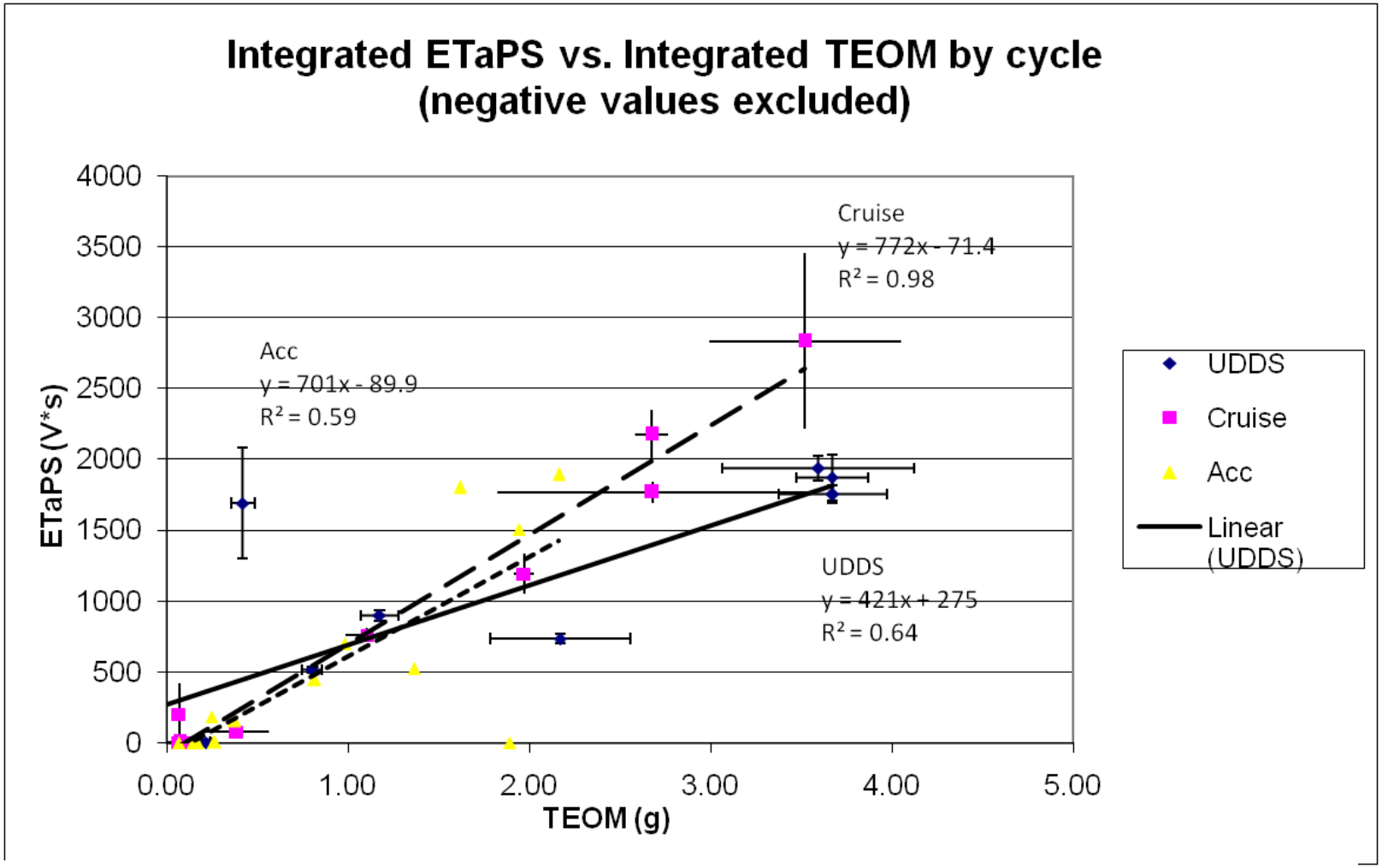


**Figure 61: Excludes negative values for integrated TEOM and excludes the '08 Volvo Bypass tests. Data are grouped by driving cycle.**

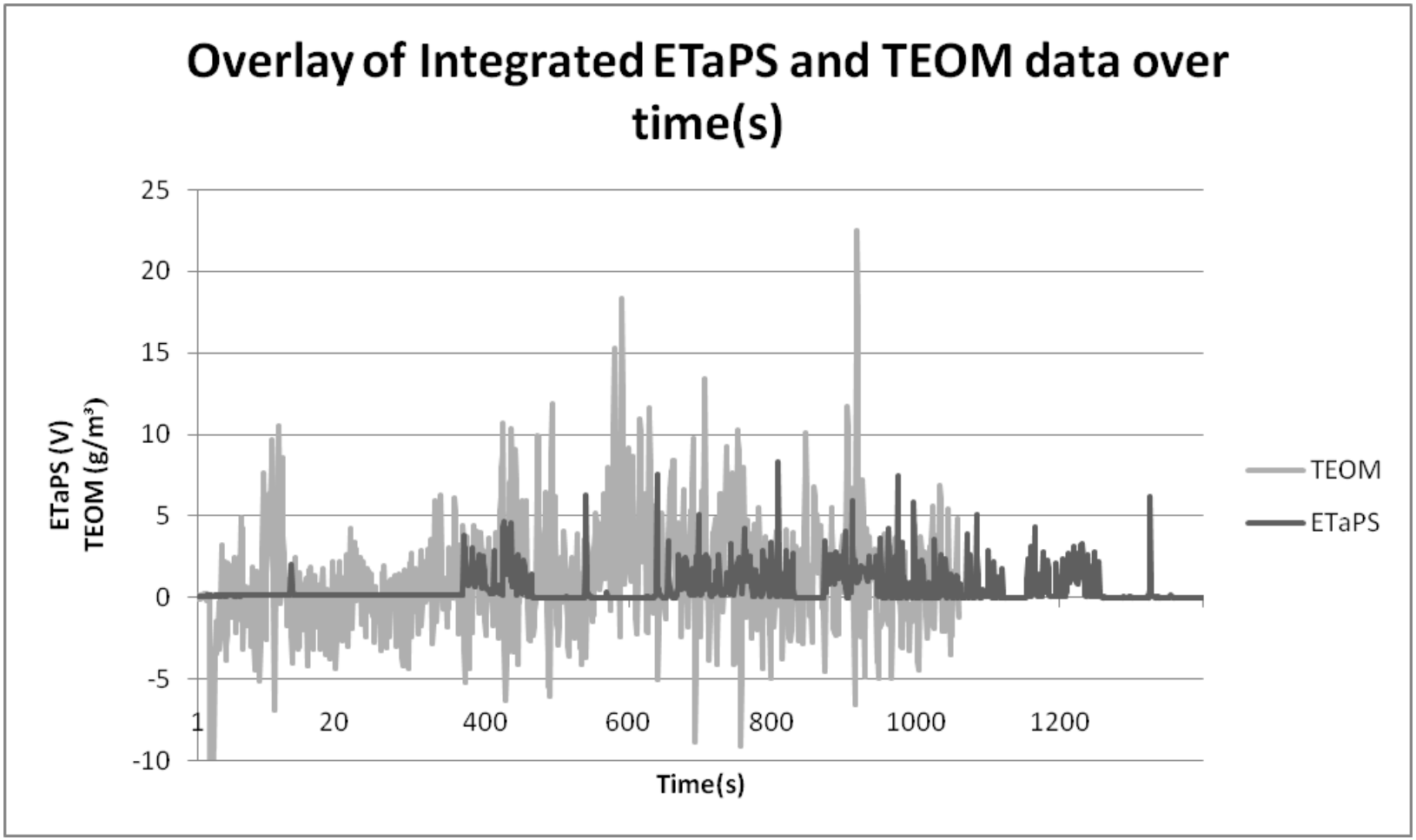


**Figure 62: Line graph of the ETaPS signal overlaid on the TEOM data. Time shift of data may not be correct, but visual inspection shows no clear correlation.**

## 4.5 RSD vs. Gravimetric

This study was originally designed to compare two paired sets of data: ETaPS and gravimetric, and ETaPS and RSD. ETaPS and gravimetric comparisons were successful, but ETaPS and RSD correlations could not be determined due to the previously mentioned power line interference.

As an alternative, an attempt was made to find a correlation between RSD and gravimetric data. Because these tests were not measured in a simultaneous manner, a direct correlation cannot be made. However, because the same trucks were used between the tests, some trends may be apparent when graphing averaged data.

RSD averages of either bypassed, non-bypassed, or non-DPF equipped trucks were plotted against averages of their gravimetric results. RSD averages are made from all speed and acceleration from stop smoke data for one truck averaged for either UV or IR measurements. This is plotted vs. the gravimetric data averaged for all cycles for each truck. Standard deviation was calculated for each average and is represented by the error bars on the graphs.

The average RSD IR smoke vs. the averaged gravimetric data did not have much utility. **Figure 63** shows a plot of all the data points. No correlation is seen, there is little separation between DPF types, and error is large. **Figure 64** shows a close up of the area around the origin of **Figure 63**. With such large error, no distinction can be made from DPF equipped and DPF bypassed vehicles. **Figure 65** shows a normalized histogram of

all un-averaged RSD IR smoke measurements for DPF equipped and DPF bypassed vehicles. There is very little separation between the two groups.

The average RSD UV smoke vs. the average gravimetric data showed much more promise. **Figure 66** shows a plot of all the data points. Again, little correlation is seen. However, viewing a close up of the origin in **Figure 67** shows a separation between DPF equipped and DPF bypassed vehicles with very small error. **Figure 68** shows a normalized histogram of all un-averaged RSD-UV smoke measurements for DPF equipped and DPF bypassed vehicles. This figure shows that if a cutoff point of 0.1 were chosen, 5% of DPF equipped vehicles would give a false positive for high emissions and 20% of DPF bypassed and DPF non equipped vehicles would give false negatives. This separation would allow the RSD to serve as a screening device for vehicles with no DPF or DPF failures for further testing.

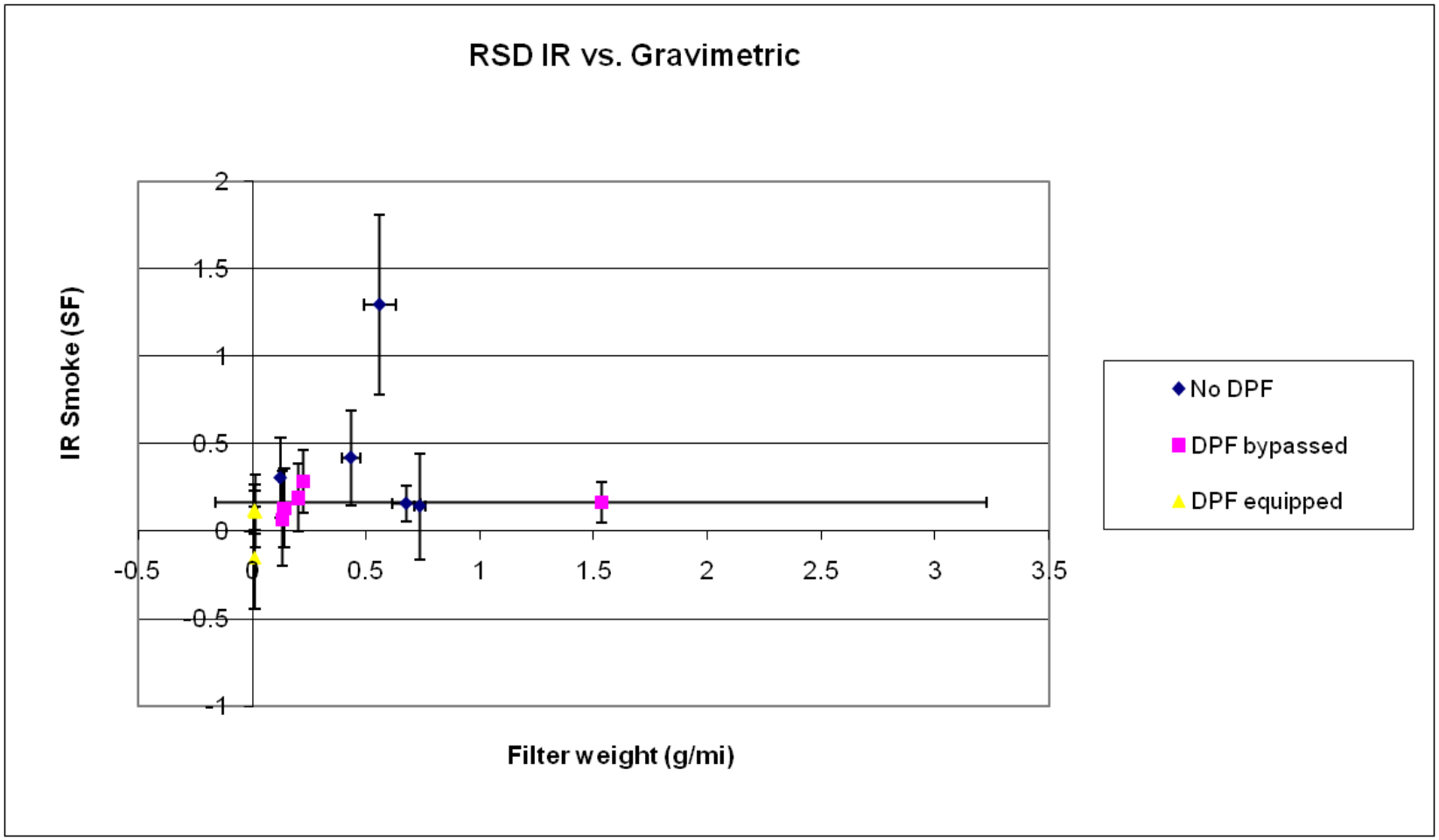


**Figure 63: Averaged data of IR smoke plotted against gravimetric grouped by DPF type. The instrument noise for the IR smoke factor channel of the RSD is ≤ 0.10 SF.**

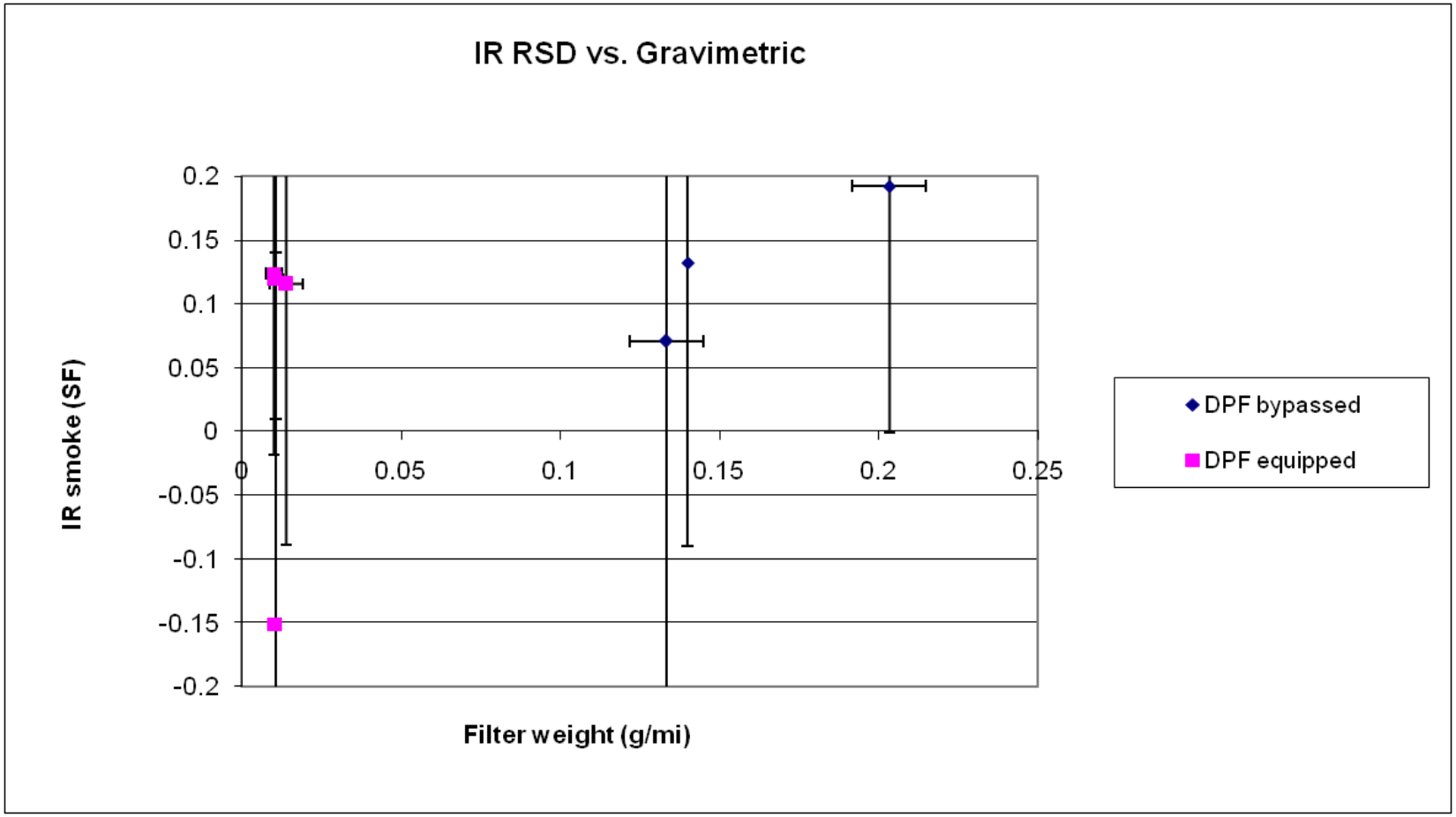


**Figure 64: Close up of area around the origin of Figure.**

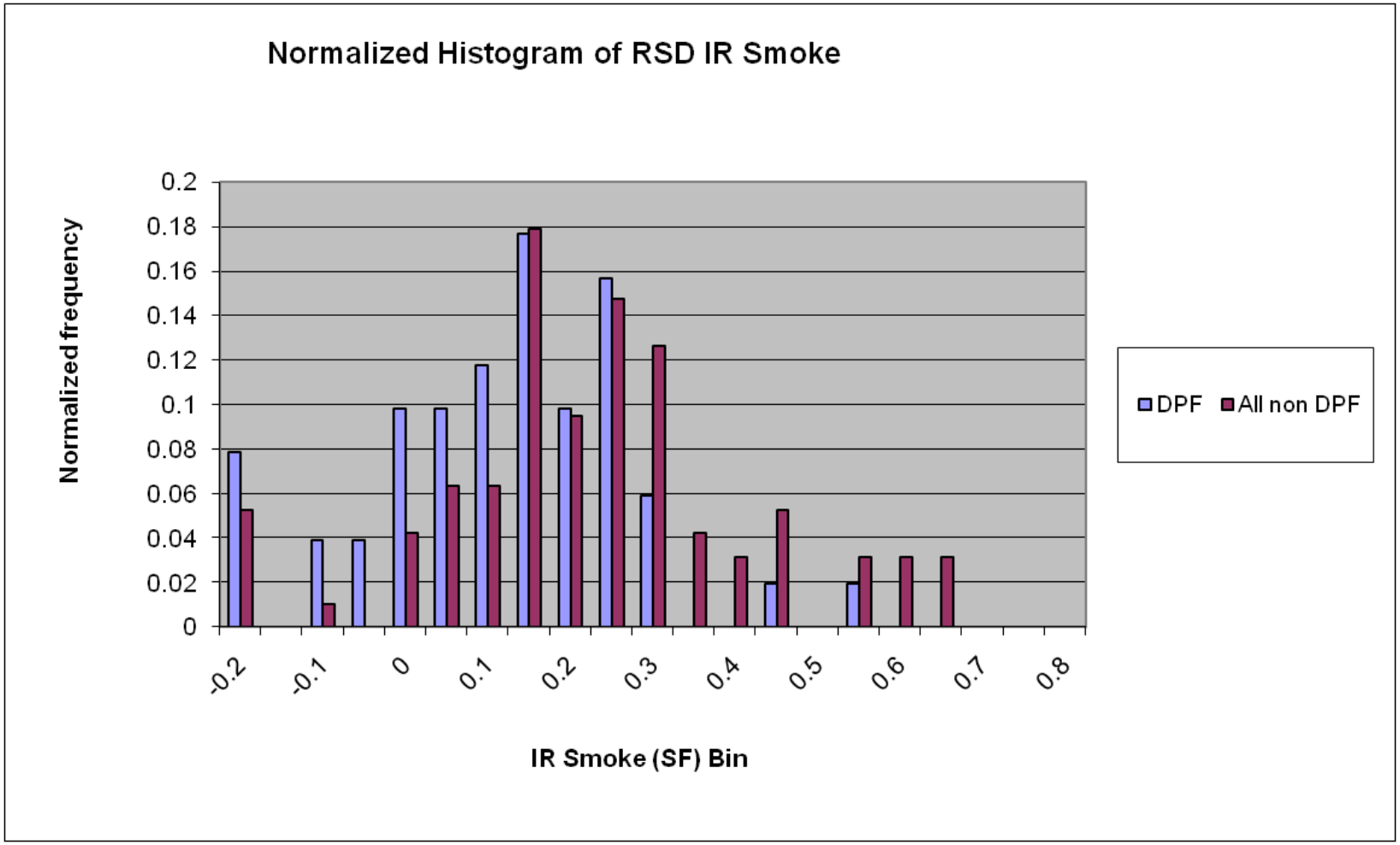


**Figure 65 Distribution histogram of IR smoke readings of DPF equipped, DPF bypassed, and non-DPF equipped vehicles.**

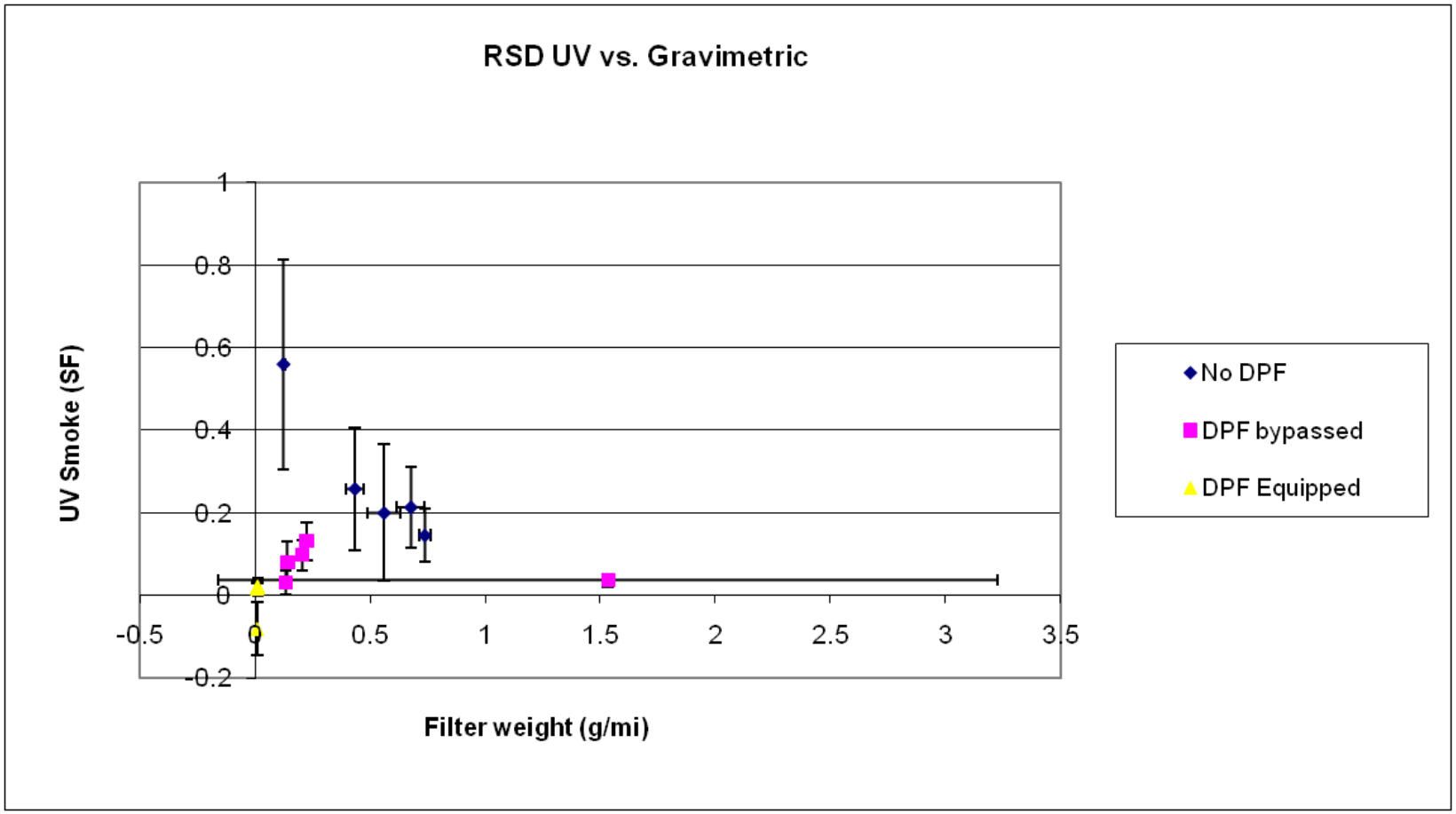


**Figure 66: Averaged data of RSD UV smoke plotted against gravimetric grouped by DPF type. The instrument noise for the UV smoke factor channel of the RSD is ≤ 0.012 SF.**

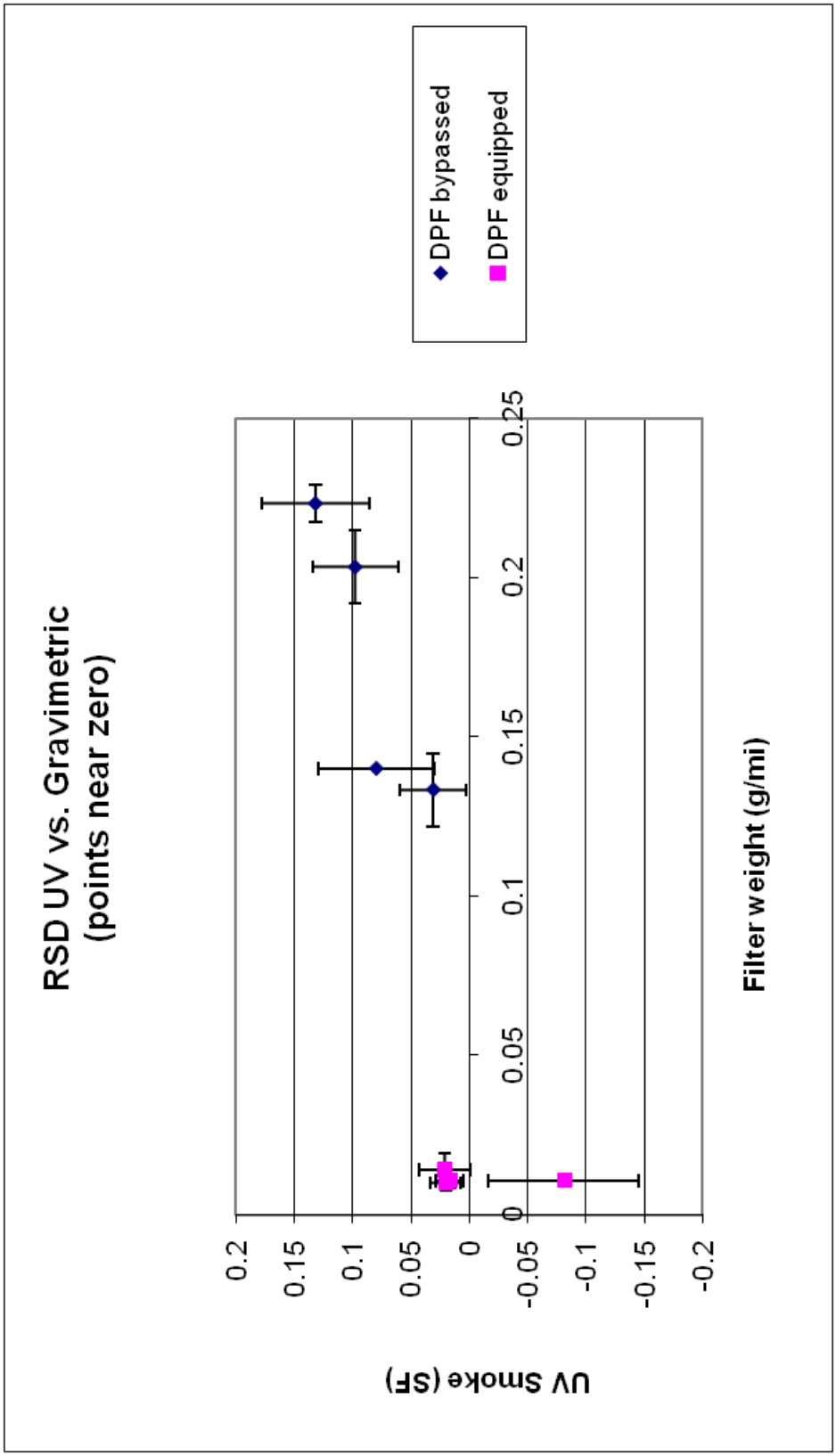


**Figure 67: Close up of area around the origin of Figure.**

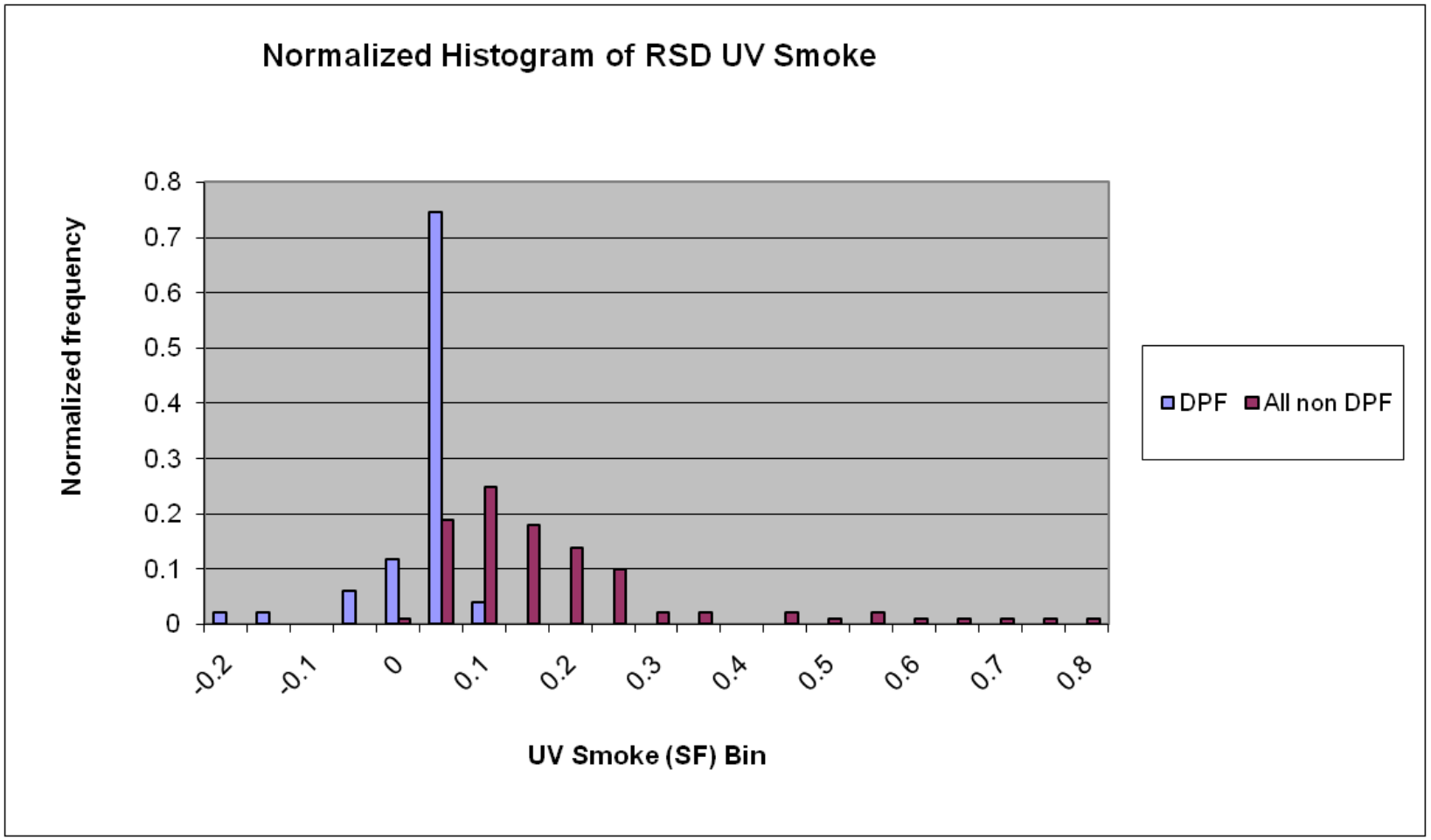


**Figure 68: Distribution histogram of UV smoke readings of DPF equipped, DPF bypassed, and non-DPF equipped**

# Chapter 5: Conclusion

One goal of this study was testing the ability of the ETaPS to effectively measure particle mass of exhaust, because there is currently little literature available on the subject. This goal was achieved by correlating the ETaPS to the gravimetric filter data from the dynamometer tests. ETaPS showed a linear response to particle mass in all but one case. This exception is most likely due to the collection of cooled semi-volatiles that were measured on the filter, but bypassed the ETaPS as gas.

Another goal of the study was to see if a good correlation between RSD and ETaPS could be achieved in real world conditions. This study did not yield any usable results due to power line interference. With the RSD vs. ETaPS study invalidated, another method to tie RSD opacity readings to particle mass was employed through the already collected data. RSD readings were compared to gravimetric readings. This is possible because the same trucks were measured in the ETaPS vs. RSD study and the ETaPS vs. Gravimetric Analysis study. By comparing averages of all RSD runs and all dynamometer cycles it was shown that there exists a clear threshold for opacity readings between DPF equipped vehicles with very low gravimetric filter weight and non DPF equipped/DPF bypassed vehicles with higher gravimetric filter weights.

While RSD could not detect particle mass for on-road measurements, it could be used to identify likely candidates for further testing. It would be much more cost effective to test a group of vehicles that are likely to have DPF failures, than to randomly select vehicles for dynamometer testing. Random selection would test fewer vehicles, and given that most vehicles on the road would pass emissions testing, random selection would needlessly test mostly passing vehicles. RSD would be able to screen many vehicles per day and ensure that vehicles flagged for the more expensive and time consuming dynamometer test are likely candidates for DPF failures.

## 5.1 Future Work

### 5.1.1 ETaPS vs. RSD – EM Shielded

It was shown in later testing that the standard ETaPS tailpipe connector was a suitable shield to EM radiation coming from power lines. It has been shown herein that the ETaPS has reasonable correlation versus dynamometer gravimetric testing. However, realistic correlation between the ETaPS vs. RSD would need to be performed. If a screening threshold could be determined, as with the RSD vs. gravimetric analysis, then RSD could be used to screen likely HDDV's with DPF failures for on-road testing with the ETaPS as long as the ETaPS is mounted with shielding attached.

### 5.1.2 ETaPS vs. Continuous RSD

Testing the ETaPS vs. RSD in real world driving conditions involves the recruitment of several HDDV's, many man hours, and return of only a few data points per vehicle at a high cost. While a real world test should ultimately be performed, it would make sense to first start with a more controlled lab test. Failure to find meaningful correlations in lab testing may indicate that more expensive tests are not justified.

One small scale test may be to find a correlation between RSD opacity and ETaPS. It would be useful to record as many data points as possible to determine if there is any relationship. To do this, RSD could be setup to continuously record opacity. Testing could then be done by continuously measuring exhaust stream by ETaPS and by RSD.

A variety of experimental set ups could be imagined from here. The easiest to perform would be to measure candle soot leaving a long tube. After that, light duty vehicles could easily be measured. A preliminary slow to fast idle test could be made. From there, different simulated driving modes may be measured from light duty vehicles on small dynamometers, or driving around a parking lot. In this manner, it would be possible to collect many data points at low cost.

These tests could give a better picture of the correlation between RSD opacity and ETaPS, but they still have some limitations. And even if the end result showed poor

overall correlation, it would also be of interest to see the groupings of DPF equipped vs. non DPF equipped/DPF bypassed HHDVs. This would not be seen until a variety of trucks were actually measured. Continuous measurement of these vehicles in non-idle conditions would require expensive dynamometer tests.

# References


1. California Air Resources Board Research Division. *Full Proposal for Particulate Measurement Devices;* Proposal; Environmental Systems Products Holdings Inc. (ESP): Tuscon, June 2006.

2. Van Houtte, J.; Niemeier, D. A Critical Review of the Effectiveness of I/M Programs. *Environ. Sci. Technol.* **2008,** 7856-7865.

3. EPA, U. E. P. A. *Health Assessment Document for Diesel Engine Exhaust;* Assessment; EPA: Springfield, May 2002.

4. Energy and Environmental Analysis, Inc. *State Diesel Emission Inspection Programs:Trends and Outcomes;* Diesel Technology Forum Report; Energy and Environmental Analysis, Inc.: Arlington, 2004.

5. Gautam, M. R.; Byrd, R. L.; Carder, D. K. R.; Banks, P. D.; Lyons, D. W. R. Particulate matter emissions and smoke opacity from in-use heavy-duty vehicles. *J. Environ. Sci. Health, Part A: Toxic/Hazard. Subst. Environ. Eng.* **2000,** 557.

6. Weaver, C.; Klausmeier, R. *Radian Corporation, Heavy Duty Diesel Vehicle Inspection and Maintenance Study Final Report;* California Air Resources Board: Sacremento, 1988.

7. McCormick, R. L.; Graboski, M. S.; Alleman, T. L.; Alvarez, J. R.; Duleep, K. G. Quantifying the Emission Benefits of Opacity Testing and Repair of Heavy-Duty Diesel Vehicles. *Environ. Sci. Technol.* **2009,** 630-637.

8. Jacobs, P. E.; Chernich, D. J.; Miller, E. F.; Cabrera, R. P.; Baker, M.; Ianni, R. E.; Gaslan, D. P.; Duleep, K. G.; Meszler, D. California's revised heavy-duty vehicle smoke and tampering inspection program. *SAE Tech. Pap. Ser.* **1998**.

9. Society of Automotive Engineers (SAE). *Snap Acceleration Smoke Test Procedure for Heavy-Duty Powered Vehicles;* Technical Paper; Warrendale, 1996.

10. Brodrick, C. J.; Sperling, D.; Weaver, C. S. http://www.uctc.net/papers/421.pdf. UC Transportation Center. http://www.uctc.net/papers/421.pdf (accessed March 21, 2009).

11. Yanowitz, J.; Graboski, M. S.; Ryan, L. B. A.; Alleman, T. L.; L., M. R. Chassis Dynamometer Study of Emissions from 21 In-Use Heavy-Duty Diesel Vehicles. *Environ. Sci. Technol.* **1999,** 209-216.

12. Norris, J. Vosacorp repository. Vosacorp. http://www.vosa.gov.uk/vosacorp/repository/Low%20Emission%20Diesel%20Research.pdf (accessed May 21, 2009).

13. St. Denis, M.; Lindner, J. Review of light-duty diesel and heavy-duty diesel gasoline inspection programs. *J. Air Waste Manage. Assoc.* **2005,** 1876-1884.

14. Energy and Environmental Analysis Inc. (EEA). Costs of the HDVIP and PSIP. http://www.arb.ca.gov/msprog/hdvip/TSD6.pdf (accessed March 21, 2009).

15. Moosmuller, H.; Arnott, W. P.; Rogers, C. F.; Bowen, J. L.; Gillies, J. A.; Pierson, W. R. Time Resolved Characterization of Diesel Particle Emissions. 1. Instruments for Particle Mass Measurements. *Environ. Sci. Technol.* **2001,** 781-787.

16. GRIMM. GRIMM Aerosol. http://www.grimm-aerosol.com/Nano-Particle-Instruments/mobile-condensation-particle-counter.html (accessed July 4, 2009).

17. Clark, N. N.; Gautam, M. *Evaluation of Technology to Support A Heavy-Duty Diesel Vehicle Inspection And Maintenance Program;* Department of Mechanical & Aerospace Engineering College of Engineering and Mineral Resources West Virginia University: Morgantown, 2001.

18. BPA Air Quality Solutions LLC. Cyclone Dust Collector: Guide to Inertial Separators. http://www.dustcollectorexperts.com/cyclone/ (accessed July 4, 2009).

19. Pagels, J.; Gudmundsson, A.; Gustavsson, E.; Asking, L.; Bohgard, M. Evaluation of Aerodynamic Particle Sizer and Electrical Low-Pressure Impactor for Unimodal and Bimodal Mass-Weighted Size Distributions. *Aerosol Science and Technology* **2005,** 871–887.

20. TSI Inc. Model 3070A Electrical Aerosol Detector. http://www.tsi.com/uploadedFiles/Product_Information/Literature/Spec_Sheets/3070A.pdf (accessed July 4, 2009).

21. Kaufman S.L., e. a. An Electrical Aerosol Detector Based on the Corona-Jet Charger. *Abstracts of 2002 AAAR*, Charlotte, 2002; p 223.

22. Hewitt, G. W. The charging of small particles for electrostatic precipitation. *Communications and Electronics* **1957,** 300–306.

23. TSI Inc. Scanning Mobility Particle Sizer Spectrometers. http://www.tsi.com/uploadedFiles/Product_Information/Literature/Spec_Sheets/SMPS3936-3034.pdf (accessed July 4, 2009).

24. TSI Inc. Model 3090 Engine Exhaust Particle Sizer Spectrometer. http://www.tsi.com/uploadedFiles/Product_Information/Literature/Spec_Sheets/3090_2980244A.pdf (accessed July 4, 2009).

25. Dankers, S.; Leipertz, A. Determination of primary particle size distributions from time-resolved laser-induced incandescence measurements. *APPLIED OPTICS* **2004,** 3731.

26. Lamda Photometrics. LII: Laser Induced Photometrics. http://www.lambdaphoto.co.uk/applications/100.230 (accessed July 4, 2009).

27. Zielinska, W. P. B.; Rogers, C. F.; Sagebiel, J.; Park, K.; Chow, J.; Mossmuller, H.; Watson, J. G. Evaluation of 1047-nm Photoacoustic Instruments and Photoelectric Aerosol Sensors in Source-Sampling of Black Carbon Aerosol and Particle-Bound PAHs from Gasoline and Diesel Powered Vehicles. *Environ. Sci. Technol.* **2005,** 5398-5406.

28. Kramer, L.; Bozoki, Z.; Niessner, R. SETUP, CALIBRATION AND CHARACTERIZATION OF A MOBILE. *J. Aerosol Sci.* **2000,** 872-873.

29. Macias, E. S.; Husar, R. B. Atmospheric Particulate Mass Measurement with Beta Attenuation Mass Monitor. *Envrion. Sci. Tech.* **2002,** 904-907.

30. Lu, C.; Czanderna, A. W. *Applications of Piezoelectric Quartz Crystal Microbalances;* Elsevier Scientific Publishing Company, 1984.

31. Sager, T. M.; Castranova, V. Surface area of particle administered versus mass in determining the pulmonary toxicity of ultrafine and fine carbon black: comparison to ultrafine titanium dioxide. *Particle and Fibre Toxicology* **2009,** 15.

32. Niemelä, V.; Janka, K.; Kekki, A.; Tikkanen, J.; Rostedt, A.; Marjamäki, M.; Keskinen, J.; Davis, M.; Giechaskiel, B.; Ntziachristos, L.; Samaras, Z., 2006. http://ec.europa.eu/enterprise/automotive/pems_meetings/dekati.pdf (accessed July 04, 2009).

33. Tikkanen, J. OBS/ITM Sensor for Raw Exhaust PM Measurements: ETaPS. *Automotive Testign Expo*, Stuttgart, 2006.

34. Maricq, M. M.; Xu, N.; Chase, R. E.; Shah, S. D. *Evaluation of a prototype tailpipe PM sensor;* Technical Paper.

35. Geunther, P. L. *Contributions to On Road Remote Sensing;* MSc Thesis; Denver University: Denver, 1992.

36. Singer, B. C.; Harely, R. A.; Littlejohn, D.; Ho, J.; Vo, T. Scaling of Infrared Remote Sensor Hydrocarbon Measurements for Motor Vehicle Emission Inventory Calculations. *ENVIRONMENTAL SCIENCE & TECHNOLOGY* **1998,** *32* (21).

37. Full, G. *Smoke Factor Theory;* White Paper; ESPH.

38. Schnaiter, M.; Horvath, H.; Mohler, O.; Naumann, K. H.; Saathoff, H.; Schock, O. w. UV-VIS-NIR spectral optical properties of soot and soot-containing aerosols. *Aerosol Science* **2003,** 1421-1444.

39. Burgard, D. A.; Bishop, G. A.; Stadtmuller, R.; Dalton, T. R.; Stedman, D. H. Spectroscopy Applied to On-Road Mobile Source Emissions. *Applied Spectroscopy* **2006,** 136-148.

40. Dekati. Dekati Instruments: ETaPS, 2008. Dekati. http://www.dekati.com/cms/files/File/PDF/ETaPSbrochure.pdf (accessed July 4, 2009).

41. Lemmetty, M. *Modelling the ETaPS;* White Paper; Tampere University of Technology, 2006.

42. Carder, D. *WVU translab;* White Paper; West Virginia University.

43. Mapquest Inc. Map of Westover, WV. http://www.mapquest.com/maps?city=Westover&state=WV#a/maps/l:Westover:WV:US:39.634399:-79.970001:city:Monongalia+County:1/m:hyb:14:39.606555:-79.975123:0:1:1:1:/io:0:f:EN:M:/e (accessed July 19, 2009).

44. Parker, B. *RSD diagram;* Private Communication; ESP, 2009.

# APPENDIX A

Labview Block Diagrams

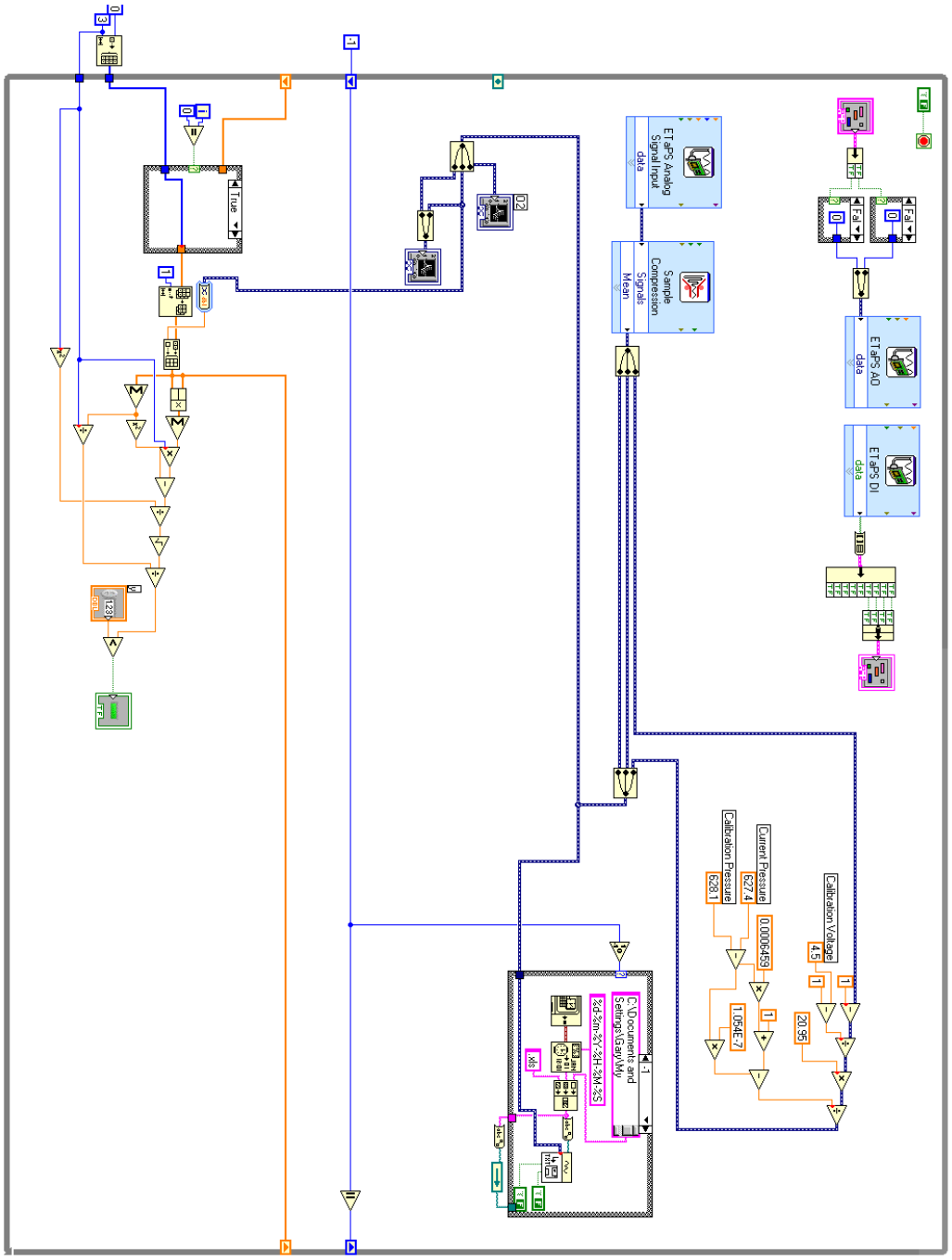
True
ETaPS Analog Signal Input data
Sample Compression Signals Mean
ETaPS AO data
ETaPS DI data
Calibration Pressure
628.1
Current Pressure
627.4
0.0006459
1.054E-7
Calibration Voltage
4.5
20.95
C:\Documents and Settings\Gary\My
%d-%m-%Y_%H-%M-%S

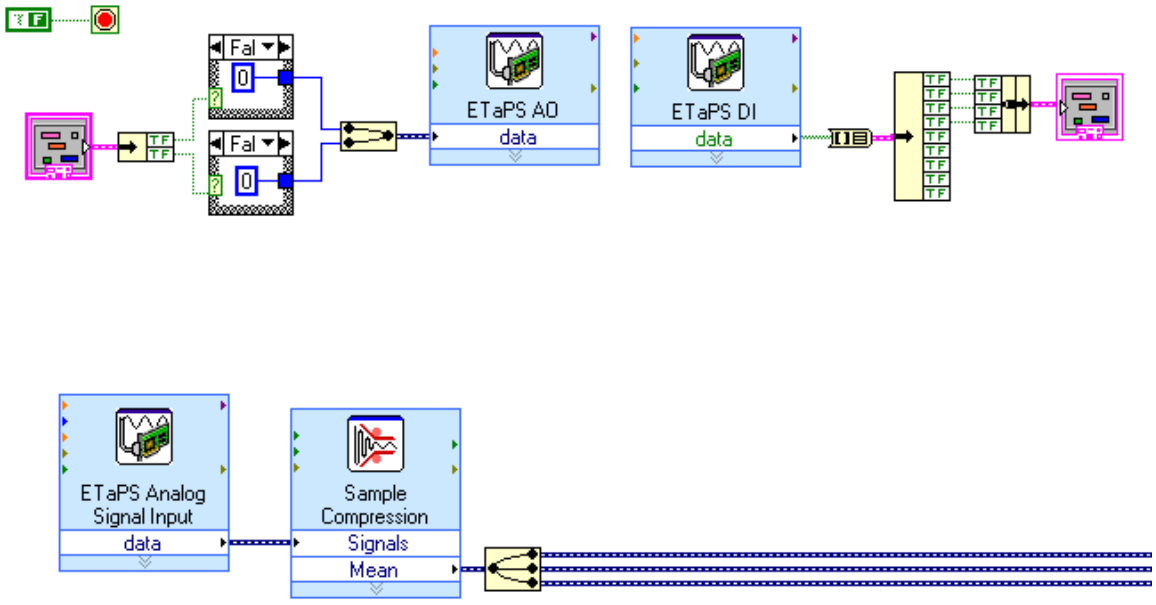


DAQ Assistant “ETaPS AO”

In the upper left portion of the block diagram is the analog output to the ETaPS. The two outputs hold values of either 0 or 5V depending if the control switch on the front panel is off or on respectively. The outputs control whether the corona charger is on or off, or if the hi/lo is on or off.

DAQ Assistant “ETaPS DI”

In the upper right portion of the block diagram is the digital input from the ETaPS. The input returns a 0 or 5V depending on whether the corona charger is off or on, the ETaPS is non-functioning or functioning, the range is set to high or low, or if the ETaPS is under or over the over range limit respectively.

DAQ Assistant “Analog Signal Input”

In the lower portion of the block diagram is the signal input from the ETaPS signal, the ETaPS reference, and $O_2$ sensor signal. The DAQ assistant symbol controls the sample rate and is set at 100Hz. The sample compression symbol averages the signals to 1Hz.

All input and output signals for the DAQ assistant symbols are labeled and can be found by right clicking the symbols and viewing the properties.

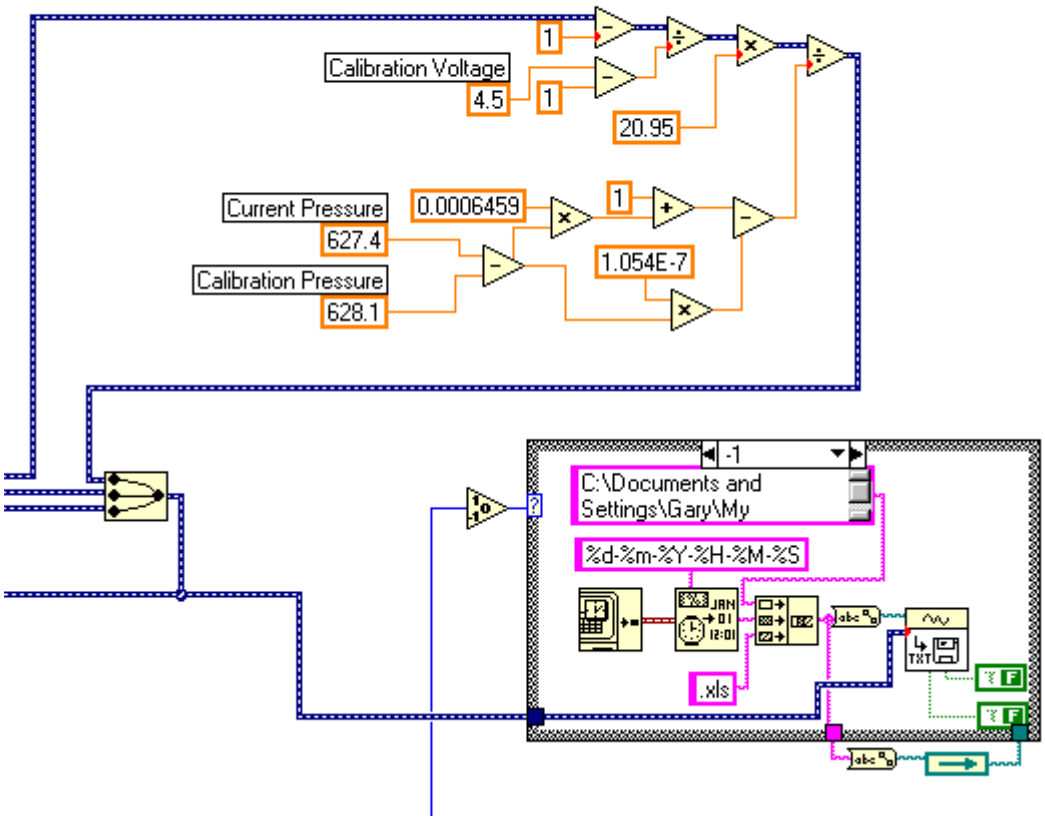


The top portion of the block diagram performs the calculation to convert the voltage of the $O_2$ sensor to a percent $O_2$.

The bottom right portion of the block diagram shows the save function. The function is enclosed in a case diagram. On starting the program an value of -1 is initialized. Upon reaching the case function, the -1 case is performed. This case creates a file named after the current time and date and saves the first measurement of all the signals into separated time stamped columns in a txt file. During this initial program loop the absolute value of the -1 value is taken and passed to the next loop iteration. On the

next iteration the 1 case is performed. In this case, the previous filename is used and the next line of data is stored. The 1 case is used until program stop. Upon next execution of the program, the -1 case is restored, and a new file with a new time stamp is created. The save path can be changed by editing the string field in the -1 case.

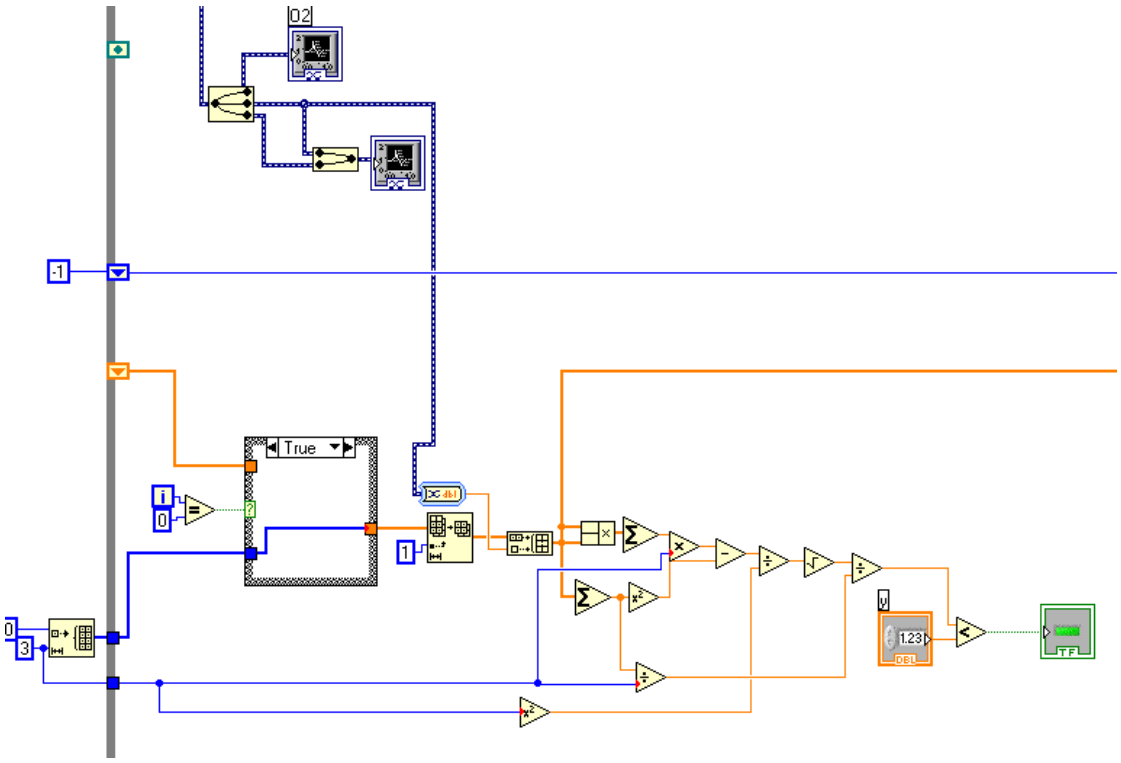


The upper left portion of the block diagram shows the graph symbols. The signal has been split into its three components. The first component, the $O_2$ signal has been sent to one graph symbol. This plots the $O_2$ signal on the front panel. The second and third signals, the ETaPS signal and reference, are merged and sent to another graph symbol. Again, these are plotted on the front panel.

The bottom portion of the block diagram shows the programming responsible for determining if a sequence of ETaPS signal readings are within a user defined standard deviation of each other. The program initializes a 3 element array to store the current and previous two readings. It then performs a standard deviation of the values in this array. If this value is below the number entered into the control box on the front panel, the large led indicator will turn green. If not, the indicator will be red.

# APPENDIX B

Table of Acronyms

| | |
|---|---|
| AI | Analog Input |
| AO | Analog Output |
| APS | Aerodynamic Particle Sizer |
| CAR | Clean Air Reference |
| CARB | California Air Resources Board |
| CBD | Central Business District |
| CPC | Condensation Particle Counter |
| DAQ | Data Acquisition |
| DE | Diesel Exhaust |
| DI | Digital Input |
| DMA | Differential Mobility Analyzer |
| DMM | Dekati Mass Monitor |
| DO | Digital Output |
| DPF | Diesel Particle Filter |
| DPM | Diesel Particulate Matter |
| EAD | Electrical Aerosol Detector |
| ECM | Engine Control and Monitoring |
| EEPS | Engine Exhaust Particle Sizer |
| ELPI | Electric Low Pressure Impactor |
| ESP | Environmental Systems Products |
| ETaPS | Electronic Tailpipe Sensor |
| FAS | Free Acceleration Smoke |
| FEAT | Fuel Efficiency Automobile Test |
| GFM | Gravimetric Filter Method |
| GMOBS | General Motors On-Board Sensor |
| GND | Ground |
| HDDV | Heavy Duty Diesel Vehicle |
| LII | Laser Induced Incandescence |
| MTBE | Methyl-t-Butyl-Ether |

| | |
|---|---|
| HDT | Heavy Duty Transient |
| HDV | Heavy Duty Vehicle |
| ICAT | Innovative Clean Air Technologies |
| I/M | Inspection / Maintenance |
| NESCAUM | North Eastern States for Coordinated Air Use Management |
| NI | National Instruments |
| PAH | Polycyclic Aromatic Hydrocarbon |
| PAS | Photoelectric Aerosol Sensor |
| PASS | Photo Acoustic Soot Sensor |
| PM | Particle Matter |
| RSD | Remote Sensing Device |
| SAE | Society of Automotive Engineers |
| SIP | State Implementation Program |
| SMPS | Scanning Mobility Particle Sizer |
| TE | Tapered Element |
| TEOM | Tapered Element Oscillating Microbalance |
| THDVETL | Transportable Heavy Duty Vehicle Emissions Testing Laboratory |
| TSP | Total Suspended Particles |
| UDDS | Urban Dynamometer Driving Cycle |
| VOC | Volatile Organic Compound |
| WVT | West Virginia Transient |
| WVU | West Virginia University |